DISSERTATION

Antenna Selection for Compact Multiple Antenna Communication Systems

ausgeführt zum Zwecke der Erlangung des akademischen Grades eines
Doktors der technischen Wissenschaften

unter der Leitung von
Univ. -Prof. Dipl. -Ing. Dr. techn. Markus Rupp
Institute of Telecommunications

eingereicht an der Technischen Universität Wien
Fakultät für Elektrotechnik

von

Aamir Habib
1, Islamabad Highway
44000 Islamabad

geboren am 7. Oktober 1973 in Rawalpindi
Matrikelnummer: 0727904

Wien, im June 2012

Die Begutachtung dieser Arbeit erfolgte durch:

1. Univ. -Prof. Dipl. -Ing. Dr. techn. Markus Rupp

   Institute of Telecommunications
   Technische Universität Wien

2. Prof. Dr. C. Oestges

   ICTEAM Institute
   Université catholique de Louvain

Abstract

Multiple-Input Multiple-Output (MIMO) communications is a very promising technology for next-generation wireless systems that have an increased demand for data rate, quality of service, and bandwidth efficiency. This thesis deals with multiple polarized antennas for MIMO transmissions, an important issue for the practical deployment of multiple antenna systems. The MIMO architecture has the potential to dramatically improve the performance of wireless systems. Much of the focus of research has been on uni-polarized spatial MIMO configurations, the performance of which, is a strong function of the inter-element spacing. Thus the current trend of miniaturization, seems to be at odds with the implementation of spatial configurations in portable hand held devices. In this regard, dual-polarized and triple-polarized antennas present an attractive alternative for realizing MIMO architectures in compact devices. Unlike spatial channels, in the presence of polarization diversity, the sub channels of the MIMO channel matrix are not identically distributed. They differ in terms of average received power, envelope distributions, and correlation properties.

The main drawback of the MIMO architecture is that the gain in capacity comes at a cost of increased hardware complexity. Antenna selection is a technique by which we can alleviate this cost. We emphasize that this strategy is all the more relevant for compact devices, which are often constrained by complexity, power and cost. Using theoretical analysis and measurement results, this thesis investigates the performance of antenna selection in dual-polarized and triple-polarized antennas for MIMO transmissions.

In this thesis we combined the benefits of compact antenna structures with antenna selection, effectively reducing the size of the complete user device. The reduction is both in the size of antenna arrays and in the Radio Frequency (RF) domain. The reduction in array size is achieved by using multi-polarized antenna systems. The reduction of complexity and size in the RF domain is achieved by using fewer RF chains than the actual number of antenna elements available by implementing antenna selection techniques. We analyze the performance of N-spoke arrays in terms of channel gains and compare this with the spatial structures, with and without antenna selection. We address the practical issue of mutual coupling and derive capacity bounds as a performance measure.

In our thesis we also incorporate many other compact antenna structures having both polarization and pattern diversity with and without antenna selection. We then compare their performances in terms of capacity. From two dimensional array structures we move on to three dimensional arrays namely triple-polarized systems. We use a probabilistic approach to derive the selection gains of such

systems with antenna selection at both ends. This is further used to calculate the outages of such systems. Performance of such systems in terms of spatially multiplexed data and Space Time Block Coding (STBC) data is also analyzed for various channel scenarios. Convex optimization techniques are applied for calculating the best possible antennas selected to reduce the complexity for multi-polarized systems.

Kurzfassung

Mehrfachantennen-Kommunikation (MIMO) ist eine sehr vielversprechende Technologie für die nächste Generation drahtloser Übertragungssysteme, die eine erhöhte Nachfrage nach Datenrate, Dienstqualität und Bandbreiten-Effizienz haben. Diese Arbeit beschäftigt sich mit mehrfach polarisierten Antennen zur Signalübertragung, ein wichtiges Thema für den praktischen Einsatz von Mehrfachantennen-Systemen. Die MIMO-Architektur hat das Potenzial, die Leistungsfähigkeit von Funksystemen deutlich zu verbessern. Ein Schwerpunkt der Forschung hat sich auf uni-polarisierte räumliche MIMO-Konfigurationen fokussiert, deren Leistungsfähigkeit stark vom Abstand der Einzelelemente abhängt. Daher scheint der aktuelle Trend der Miniaturisierung im Widerspruch mit der Umsetzung in kompakte, tragbare Handgeräte zu stehen. In diesem Zusammenhang stellen dual-polarisierte und dreifach-polarisierte Antennen eine attraktive Alternative für die Realisierung von kompakten MIMO-Architekturen dar. Im Gegensatz zu räumlicher Diversität sind die Unterkanäle des MIMO Kanals bei Polarisationsdiversität nicht identisch verteilt. Sie unterscheiden sich in Bezug auf die durchschnittliche Empfangsleistung, Verteilungsfunktion der Einhüllenden sowie ihrer Korrelationseigenschaften. Der Hauptnachteil der MIMO-Architektur ist, dass die Erhöhung der Kapazität zum Preis von erhöhter Hardware Komplexität kommt. Antennenauswahl ist eine Technik, mit deren Hilfe diese Kosten verringert werden können. Wir betonen, dass diese Strategie umso relevanter für kompakte Geräte ist, die oft durch Komplexität, Leistung und Kosten begrenzt sind. Mit der theoretischen Analyse untersucht diese Arbeit die Leistung der Antennenauswahl in dual-polarisierte und dreifach-polarisierten Antennen zur MIMO Übertragung. Unsere Ergebnisse zeigen, dass Antennenauswahl, wenn sie mit Mehrfach-polarisierten Antennen kombiniert wird, eine effektive Lösung geringer Komplexität darstellt, welche für die Realisierung von MIMO-Architekturen in kompakten Geräten geeignet ist. In dieser Arbeit werden die Vorteile kompakter Antennen-Strukturen mit Antennen Auswahl kombiniert, wodurch eine Verringerung der Größe des Endgeräts erreicht wird. Die Größenreduktion wirkt sowohl im Antennen-Bereich als auch im RF-Schaltungsbereich. Die Größenreduktion der Antennenfelder erreicht man durch mehrfach polarisierte Antennen, während die Schaltungsreduktion dadurch erreicht wird, dass durch Antennenauswahl nun weniger RF-Anteile benötigt werden. Wir analysieren die Leistungsfähigkeit von so-genannten N-Spoke Antennenanordnungen hinsichtlich der Kanal-Gewinne und Kapaziät und vergleichen diese mit räumlich verteilten Strukturen, mit und ohne Antennenauswahl.

In unserer Arbeit betrachten wir ebenso andere kompakte Antennenstrukturen mit Polarisationseffekten jeweils mit und ohne Antennauswahl. Ausgehend von zweidimensionalen Antennenfeldern gehen

wir auf dreidimensionale Felder mit dreifacher Polarisation über. Zur Herleitung der Auswahlgewinne solcher Systeme verwenden wir probabilistische Ansätze, die es uns ermöglichen Ausfallwahrscheinlichkeiten zu berechnen. Ebenso untersuchen wir die Leistungsfähigkeit im Hinblick auf räumlich gemultiplexte Daten und blockkodierte (STBC) Daten in verschiedenen Kanal-Szenarien. Konvexe Optimierungstechniken wurden für die optimale Auswahl eingeführt und so die Komplexität in mehrfach polarisierten Antennanordnungen reduziert.

Acknowledgments

First, I would like to thank my advisor Markus Rupp for his continuous support and excellent guidance over the last several years. Due to his careful proofreading, technical content and presentation of this thesis have been improved significantly. It is also my pleasure to express my thanks to Claude Oesteges, who kindly agreed to act as an external referee and examiner.

Very special thanks go to Bujar Krasniqi, Jesús Gutiérrez and Philipp Gentner. The close collaboration with them has been (and still is) very important for me. In fact, their patient support has been essential for my professional development. Their technical contributions to this thesis are also gratefully acknowledged. I would also like to thank Rizwan Bulbul whose company has always been a source of great inspiration and motivation.

I would also like to thank a lot to my very close friends Rehan Mahmood, Khurram Khurshid, Tariq Masood and Hayat Muhammad Khan for their constant encouragement in writing my thesis.

Contents

7 Conclusions and Future Work 84

Bibliography 88

List of Figures

List of Acronyms

AMC   Adaptive Modulation and Coding

AS   Antenna Selection

AWGN   Additive White Gaussian Noise

BER   Bit Error Ratio

CDF   Cummulative Distribution Function

CPR   Co Polar Ratio

CSI   Channel State Information

DP   Dual Polarized

EM   Electro Magnetic

FDD   Frequency Division Duplex

LNA   Low Noise Amplifier

LOS   Line Of Sight

LTE   Long Term Evolution

MIMO   Multiple-Input Multiple-Output

MISO   Multiple-Input Single-Output

ML   Maximum Likelihood

MMEM   Maximum Minimum Eigenvalue Method

MMSE   Minimum Mean Square Error

MRC   Maximum Ratio Combining

MREM   Maximum Ratio Eigenvalue Method

MRT   Maximum Ratio Transmission

NAS   Non Antenna Selection

NLOS   Non Line Of Sight

OFDM   Orthogonal Frequency Division Multiplexing

OSTBC   Orthogonal Space-Time Block Coding

PDF   Probability Density Function

PD   Polarization Diverse

Q-OSTBC Quasi-Orthogonal Space-Time Block Coding

RAS Receive Antenna Selection

RF Radio Frequency

SCM Spatial Channel Model

SIMO Single-Input Multiple-Output

SISO Single-Input Single-Output

SM Spatial Multiplexing

SNR Signal-to-Noise Ratio

SSDP Spatially Separated Dual Polarized

SSTP Spatially Separated Triple Polarized

STBC Space Time Block Coding

STTC Space-Time Trellis Codes

TAS Transmit Antenna Selection

TDD Time Division Duplex

TD Transmit Diversity

TPD True Polarization Diversity

TP Triple Polarized

TRAS Transmit Receive Antenna Selection

UE User Equipment

ULA Uniform Linear Array

XPD Cross Polarization Discrimination

XPR Cross Polar Ratio

ZF Zero Forcing

List of Important Variables

Variable	Description
α	power leakage from antenna in Rayleigh fading
α_f	power leakage from antenna in Fixed Ricean fading
B_R	number of antenna combinations
$\mathbf{C}$	antenna array coupling matrix
C	mutual information of channel
D	distance between transmitter and receiver
d_r	inter antenna spatial separation
$\mathbb{E}$	electric field vector
$\mathbf{G}$	antenna gain matrix
$G_C(\phi)$	co-polar gain pattern
$G_X(\phi)$	cross-polar gain pattern
$\mathbf{H}$	channel matrix
$\mathbb{H}$	magnetic field vector
$\mathbf{I}$	identity matrix
I_m	maximum current in antenna
K	Ricean factor
k	wave number
$\mathbf{\Lambda}_r$	diagonal matrix
λ	carrier wavelength
λ_i	ith eigen value
L_r	receive side aperture length
L_t	transmit side aperture length
l_r	number of selected receive antennas
l_t	number of selected transmit antennas
l	length of dipole
M_R	number of total receive antennas
N	number of sub-carriers
N_T	number of total transmit antennas
$\mathbf{P}$	antenna array rotation matrix
P	transmit power
$\mathbf{P}_r$	unitary matrix
ϕ	azimuth angle
φ	angular difference between two antennas
φ_n	orientation of arbitrary antenna element
$\mathbf{R}$	normalized correlation matrix
r	radius of dipole
ρ	signal to noise ratio
θ_p	orientation of antenna element
θ_r	inter antenna angular separation
$\mathbf{V}_r$	unitary matrix
$\mathbf{v}$	received AWGN vector
$\mathbf{X}$	XPD matrix
$\mathbf{x}$	transmit signal vector
$\mathbf{y}$	received signal vector
Z_A	impedance of antenna element in isolation
$\mathbf{Z}_r$	mutual impedance matrix

Notation

Notation	Description
$(\cdot)^T$	Matrix or vector transpose.
$(\cdot)^*$	Complex conjugate.
$(\cdot)^H$	Matrix or vector conjugate transpose.
$(\cdot)^{1/2}$	Hermitian square root of the positive semidefinite matrix.
$\odot$	Element-wise scalar multiplication.
$\otimes$	Kronecker product.
$\det(\cdot)$	Determinant of a matrix.
$(\cdot)^{-1}$	Inverse of matrix.
$\mathrm{E}(\cdot)$	Expectation of random variables.
$\lVert\cdot\rVert_F^2$	Squared Frobenius norm for matrices.
$\lvert(\cdot)\rvert$	Modulus of a scalar.
$\log_2$	the base-2 logarithm.
$\mathrm{trace}(\cdot)$	the trace of a matrix.
$\mathrm{diag}(\cdot)$	Vector constructed with the elements in the diagonal of a matrix.
$\max, \min$	Maximum and minimum.
$\Re(\cdot)$	Real part.
$\Im(\cdot)$	Imaginary part.
$\lim$	Limit.
$\log(\cdot)$	Natural logarithm.
$\triangleq$	Defined as.
$\simeq$	Approximately equal.
$\sim$	Distributed according to.
$\Pr(\cdot)$	Probability.
$F(\cdot)$	Cumulative Distribution Function.
$f(\cdot)$	Probability Density Function.
$\mathcal{X}_n^2$	Chi-square distribution with n degrees of freedom.

1

Introduction

1.1 Motivation

Communication schemes with multiple antennas at the transmit and/or receive edges are known to provide remarkable capacity improvements with respect to single-antenna configurations. Due to limitations in the radio spectrum available for wireless systems, multi-antenna approaches have been considered as promising techniques to increase the capacity of future wireless systems. In a multiple-antenna context, the channel capacity can be approached by conducting pre-processing on the transmit side. Unless reciprocity between the forward and reverse links can be assumed, a feedback channel is required to convey Channel State Information (CSI) to the transmitter. However, the amount of information allowed over feedback channels is limited. As a result, perfect and instantaneous CSI is rarely available at the transmitter, specially in those scenarios with fast fading and/or a high number of antennas. An effective solution with low feedback requirements is transmit antenna selection. By selecting the best sub-set of transmit antennas, most of the gain provided by multi-antenna schemes can be obtained, while only a few bits must be fed back. As for the selection criteria, it is common practice to select the subset of transmit antennas that maximize some metric at the physical layer. Within this framework, this PhD dissertation provides a contribution to the study of antenna selection algorithms from a physical layer perspective. More precisely, by focusing our attention on the geometry of antenna arrays, we study antenna selection algorithms aimed at maximizing performance at the physical layer.
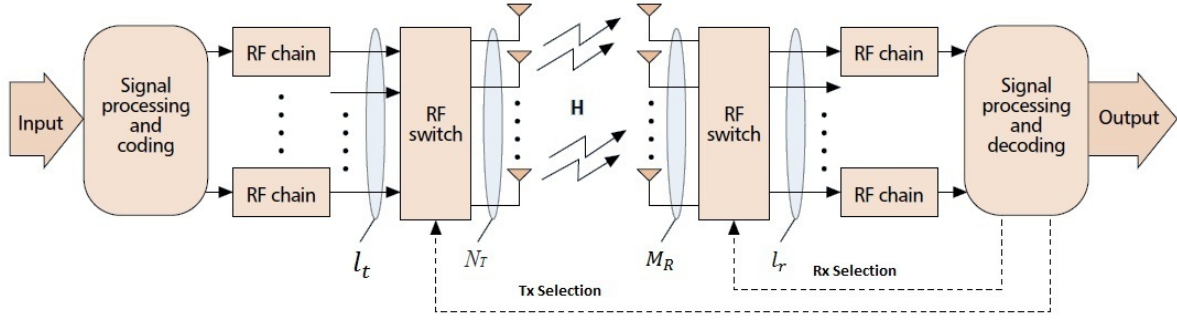
Figure 1.1: Block diagram of a MIMO transmission scheme with transmit and receive antenna selection.

1.2 Antenna Selection

In a Multiple-Input Multiple-Output (MIMO) transmission system, adding complete Radio Frequency (RF) chains typically result in increased complexity, size and cost. These negative effects can be drastically reduced by using antenna selection. This is because antenna elements and digital signal processing is considerably cheaper than introducing complete RF chains. In addition, many of the benefits of MIMO schemes can still be obtained [1] [2]. Besides, perfect CSI is not required at the transmitter as the antenna selection information can be computed at the receiver and reported to the transmitter by means of a low-rate feedback channel.

In Figure 1.1, we show a typical MIMO wireless system with antenna selection capabilities at both the transmit and the receive sides. The system is equipped with N_T transmit and M_R receive antennas, whereas a lower number of RF chains has been considered ($l_t < N_T$ and $l_r < M_R$ at the transmitter and receiver, respectively). In accordance with the selection criterion, the best sub-set of l_t transmit and l_r receive antennas is selected. In order to convey the antenna selection command to the transmitter, a feedback channel is needed but this can be achieved with a low-rate feedback as only $\binom{N_T}{l_t}$ bits are required.

Originally, antenna selection algorithms were born with the purpose of improving link *reliability* [3] by exploiting spatial diversity. More precisely, a reduced complexity system with antenna selection can achieve the same diversity order as the system with all antennas in use. However, as MIMO schemes gained popularity, antenna selection algorithms began to be adopted in *spatial multiplexing* schemes aimed at increasing the system capacity. A brief review of the state of the art is presented below, where different methodologies are classified according to the context: spatial diversity or spatial multiplexing.

1.2.1 Antenna Selection for Spatial Diversity

Antenna selection was introduced by Jakes as a simple and low-cost solution capable of exploiting receive diversity in a Single-Input Multiple-Output (SIMO) scheme [4]. In a wireless environment, by separating the receive antennas far enough [1] the correlation between the channel fades is low. Then, by selecting the best receive antenna in terms of channel gains, a diversity order equal to the number of

---

[1]In older literature it is stated that for mobile terminals surrounded by other objects, quarter-wavelength spacing is sufficient, whereas for high base station a separation of 10-20 wavelengths is required [5]. In recent literature [6] it has been demonstrated experimentally that even short distances of 0.1 λ can provide high data throughput. Large antenna providers like Kathrein have considerably shortened their antenna sizes in the last years.

receive antennas is obtained. Winters considered a similar procedure in a Multiple-Input Single-Output (MISO) system to exploit diversity at the transmit side with the help of a feedback channel [7]. In that work, the antenna selection algorithm was very simple: when the received Signal-to-Noise Ratio (SNR) was below a specific threshold a command is sent to the transmitter to indicate that the transmit antenna must be switched.

For the SIMO case, more sophisticated receive antenna selection algorithms based on hybrid selection/maximal-ratio combining techniques were derived in [8] [9] [10]. The basic idea of those algorithms was to select the best (in terms of SNR) l_r out of M_R receive antennas and combine the received signals by means of a Maximum Ratio Combining (MRC) procedure. By doing so, apart from exploiting the diversity gain, array gain can also be achieved. The extension to MIMO systems were presented by Molisch *et al.* [11] [12] in a scenario where antenna selection was only performed at the transmitter in combination with a Maximum Ratio Transmission (MRT) strategy. It was shown that by selecting the best sub-set of transmit antennas, the degradation in system performance is only minor in comparison with the saving in terms of hardware cost. The obtained results can be easily generalized to those cases performing antenna selection at the receive side of the MIMO link due to the reciprocity of the SNR maximization problem. An interesting result was obtained in [13] for those systems performing MRC at the receiver side and an antenna selection mechanism (with a single active antenna) at the transmitter. It was shown that the achieved diversity order is equal to $M_R B$, with B denoting the position taken by the channel gain of the selected antenna when arranging the channel gains of the different transmitters in an increasing order.

The combination of antenna selection with Orthogonal Space-Time Block Coding (OSTBC) was studied by Gore and Paulraj in [3]. It was proven that the diversity order obtained through antenna selection is identical to that of a situation with all the antennas in use. Regarding the degradation in terms of SNR when antenna selection is carried out at the receiver, it was shown in [14] that it can be upper bounded by $10\log10(M_R/l_r)$dB. In a similar context, both transmit and receive antenna selection mechanisms in combination with Quasi-Orthogonal Space-Time Block Coding (Q-OSTBC) schemes were analyzed in [15] [16]. For the case that antenna selection is combined with Space-Time Trellis Codes (STTC), different results were found: by increasing the total number of receive antennas M_R, the coding gain can be improved but the diversity order remains fixed [17].

1.2.2 Antenna Selection for Spatial Multiplexing

In spatially correlated MIMO fading channels, capacity gains can be lower than expected since spatial multiplexing gains mainly come from resolving parallel paths in rich scattering MIMO environments. With this problem in mind, Gore *et al.* proposed one of the first papers where antenna selection was adopted in a MIMO context [18]. There, the authors showed that system capacity cannot be improved by using a number of transmit antennas greater than the rank of the channel matrix. By considering that, an algorithm was proposed where only antennas satisfying the full rank condition were selected. As a result, system capacity gains were obtained with respect to the full antenna system, since transmit power was efficiently distributed. In order to reduce the complexity of the proposed algorithm (exhaustive search), various sub-optimal algorithms based on the water filling principle [19] were proposed in [20]. Upper bounds of the achievable capacity with antenna selection were derived in [11]. In particular, it was shown that capacity results close to those of the full antenna system can be achieved by selecting the best $l_r \geq N_T$ out of M_R receive antennas. In [21], a sub-optimal approach was proposed for both transmit and receive antenna selection. By starting with the full channel matrix,

those rows (columns) corresponding to the receivers (transmitters) minimizing the capacity loss are iteratively dropped. As shown in [22] [23], almost the same capacity as with an optimal selection scheme can be achieved with an incremental version of the mentioned selection algorithm, i.e., by using a bottom-up selection procedure. In [22] it was also proven that the diversity order achieved with receive antenna selection is the same as that with the full antenna scheme, where the diversity order was defined as the slope of the outage rate. Although a sub-optimal approach with decoupled transmit and receive selection was adopted in [24], similar conclusions in terms of the diversity-multiplexing trade-off curve [25] were drawn. That is, the same trade-off curve as with all antennas in use can be obtained with transmit and receive antenna selection. Heath *et al.*, on the other hand, pointed out that antenna selection approaches based on maximizing the mutual information do not necessarily minimize the error rate when practical receivers are in use [26]. As an alternative, minimum error rate algorithms were derived and analyzed in systems with Zero Forcing (ZF) and Minimum Mean Square Error (MMSE) linear receivers. As for the Zero Forcing (ZF) approach, selection algorithms were also derived in [27] for the case that only channel statistics (covariance matrix) are known at the transmitter. A geometrical approach was presented in [28] in order to reduce the computational complexity.

1.3 Implementation Aspects

In this overview, we concentrate on the more practical aspects that are related to the actual implementation of antenna selection.

1.3.1 Channel Characteristics and Impact on Selection

Most of the theoretical analyses of antenna selection assume a highly simplified channel model in which the entries of the channel matrix $\mathbf{H}$ are independent, identically distributed complex Gaussian entries. Such a channel model can occur, for example, if the antenna arrays at transmitter and receiver are uniform linear arrays, the antenna elements have isotropic patterns, and the multi path components of the channel arrive from all directions. High theoretical capacities are possible for this channel model because its inherent heavy multi path allows for the transmission of multiple, independent data streams that can be spatially separated at the receiver. While such channels provide a good theoretical benchmark, they rarely occur in practice. The following effects have to be taken into account for realistic system assessments.

Signal Correlation

If the antenna elements at the transmitter and receiver are closely spaced, and/or the angular spread of the multi path components is small, then the entries of $\mathbf{H}$ are strongly correlated. This effect is often modeled by means of the so-called Kronecker model [29]. We stress that this model is still a simplification as it does not reflect the dependence of the receive correlation matrix on the transmit directions, and vice versa. A more detailed model was recently proposed by [30]. The Kronecker model is often used for system simulations.

Mutual Coupling

Mutual coupling can impact the performance of antenna selection systems [31]. The nature of this impact depends on the type of antenna matching (termination). Many antenna selection systems either use open-circuit terminations or 50Ω matching.

Unequal Means

If antennas with different patterns and/or polarization are used, the mean received power differs at the different antenna ports. Naturally, ports with higher power tend to be selected more often in an antenna selection scheme [32].

1.3.2 Antenna Selection Training

The issue of training for antenna selection has received relatively little attention in the literature. In order to select the best subset, all the $N_T M_R$ links corresponding to all possible transmitter and receive antenna pairs need to be 'sounded', even though only l_t and l_r elements at the transmitter and receiver, respectively, will eventually be used for data transmission. In general, such sounding can be achieved with a switched approach. For simplicity, let us assume that $R_t = N_T/l_t$ and $P_r = M_R/l_r$ are integers. Then we can divide the available transmit (receive) antenna elements into $R_t(R_r)$ disjoint sets. The "switched" antenna sounding now repeats $R_t \cdot R_r$ times a "standard" training sequence that is suitable for an $l_t \times l_r$ MIMO system. During each repetition of the training sequence, the transmit (receive) RF chains are connected to different sets of antenna elements. Thus, at the end of the $R_t \cdot R_r$ repetitions, the complete channel has been sounded.

In case of transmit antenna selection in frequency division duplex systems in which the forward and reverse links are not identical, the receiver feeds back the optimal subset to the transmitter. Moreover, in reciprocal time division duplex systems, the transmitter can do this even on its own. The switched training procedure increases the overhead of a system that employs antenna selection. Moreover, the training needs to be solved quickly (within the channel's coherence interval) in order for it to be useful. In wireless LANs for indoor applications, the channels vary very slowly. This is exploited in the design of a low overhead MAC-based antenna selection training protocol in the IEEE 802.11n draft specification [33]. Instead of extending the physical (PHY) layer preamble to include the extra training fields (repetitions) for the additional antenna elements, antenna selection training is achieved by transmitting and receiving packets by different antenna subsets. As training information (a single standard training sequence for an $l_t \times l_r$ MIMO system) is embedded in the MAC header field, the packets can carry data payloads, which keeps the training overhead to a minimum. The time available for switching between the antenna subsets is now the guard time between packets, which is of the order of microseconds. This enables the use of slower, Micro-Electro-Mechanical Systems (MEMS)-based switches [34] [35], which have extremely low insertion loss. These type of switches also differ in chip area, operating voltage, carrier frequency and bandwidth, tuning times, etc.

In fast-varying channels, selection can be performed on the basis of channel statistics (e.g., fading correlations), whose variation is orders of magnitude slower than that of fast fading itself. It was shown in [36] that such an antenna selection approach is effective in highly correlated channels.

1.3.3 RF Mismatch

One implementation problem that has largely been ignored in the selection literature is RF imbalance. RF imbalance occurs because the RF parameters for different connections of antenna elements and RF chains at the transmitter and the receiver are different [37]. Unless compensated for, different connections will result in different baseband channel estimates, even though the underlying physical MIMO channel matrix, **H**, is the same. An over-the-air calibration process, which involves communication between the transmitter and the receiver, is therefore required. Training sequences are used to 'calibrate' each possible connection of antenna elements with an RF chain. This results in connection-specific calibration coefficients that can be used to compensate for the RF imbalance when receiving data. In the absence of cross-talk among the RF chains complete compensation is achieved by simply multiplying the base-band signals at the transmitter and receiver with the corresponding calibration coefficients. As each possible connection needs to be calibrated, the training overhead is greater. However, this needs to be performed very infrequently (usually only upon association to the network).

1.3.4 Suboptimal Selection

In addition to RF imbalance, several non-idealities in both hardware and software (signal processing) exist in a practical implementation. It is important to understand how robust antenna selection is to them as they can potentially diminish its advantages. For example, the introduction of a selection switch leads to an insertion loss. In RF preprocessing designs, the phase-shift elements can suffer from phase and calibration errors. Last, but not least, imperfect channel estimates and feedback that occur due to noise during channel estimation and in feedback channels, respectively, can lead to the selection of only sub-optimal subsets and degrade performance.

1.3.5 Bulk Versus Tone Selection in OFDM

For operation in frequency-selective channels, MIMO is often combined with Orthogonal Frequency Division Multiplexing (OFDM).Orthogonal Frequency Division Multiplexing (OFDM) transmits the information on many (overlapping but orthogonal) subcarriers so that each subcarrier (tone) sees a flat-fading channel. Now the channel matrix **H** depends on the tone. In an MIMO-OFDM system with antenna selection, the optimum antenna subsets can vary from tone to tone. Thus, two types of antenna selection are possible: (i) bulk selection, where the selected antenna subset is used for all OFDM sub-channels, and (ii) per-tone selection, where a different subset can be used for each tone. Naturally, the second solution requires a much higher complexity: the signals from all antenna elements have to be converted to/from baseband, and the selection is implemented in baseband. Per-tone selection thus does not save hardware (when compared to full-complexity systems), but only simplifies the signal processing and reduces the feedback, as transmit selection can be viewed as (coarse) precoding.

1.3.6 Hardware Aspects

Finally, we consider the effects of the hardware on the performance. In all the previous sections, we assumed ideal RF switches with the following properties:

- They do not suffer any attenuation or cause additional noise in the receiver.

- They are capable of switching instantaneously.

- They have the same transfer function irrespective of the output and input port.

In practice, these conditions cannot be completely fulfilled.

- The attenuation of typical switches varies between a few tenths of a decibel and several decibels, depending on the size of the switch, the required throughput power (which makes T_X switches more difficult to build than R_X switches), and the switching speed. In the T_X switch, the attenuation must be compensated by using a power amplifier with higher output power. At the receiver, the attenuation of the switch plays a minor role if the switch is placed after the Low Noise receiver Amplifier (LNA). However, that implies that M_R instead of l_r receive amplifiers are required, eliminating a considerable part of the hardware savings of antenna selection systems.

- Switching times are usually only a minor issue. The switch has to be able to switch between the training sequence and the actual transmission of the data, without decreasing the spectral efficiency significantly. In other words, as long as the switching time is significantly smaller than the duration of the training sequence, it does not have a detrimental effect.

- The transfer function has to be the same from each input-port to each output-port, because otherwise the transfer function of the switch distorts the equivalent baseband channel transfer function that forms the basis of all the algorithms. It cannot be considered part of the training because it is not assured that the switch uses the same input-output path during the training as it does during the actual data transmission. An upper bound for the admissible switching errors is the error due to imperfect channel estimation.

1.4 Outline and Research Contributions

The main contribution of this thesis is the study of the performance of antenna selection techniques applied to compact antenna structures from a geometry and optimization of antenna structure perspective in single user MIMO systems. The details of the research contributions for each chapter are presented.

Chapter 2

In this work, receive antenna subset selection schemes are applied to a WiMAX compliant MIMO-OFDM transmission system. Simulation results in terms of average throughput and Bit Error Ratio (BER) on an adaptive modulation and coding link are shown. The main results of this chapter have been published in one conference paper:

- Habib, A., Mehlführer, C., Rupp, M., "Performance Comparison of Antenna Selection Algorithms in WiMAX with Link Adaptation", in *Proceedings of Cognitive Radio Oriented Wireless Networks and Communications, Hannover, June 2009, pp. 1 - 5.*

Chapter 3

The main results of this chapter address the study of combined effects of array orientation/rotation and antenna cross polarization discrimination on the performance of dual-polarized systems with receive antenna selection. We start our analysis with a 1 out of M_R selection and extend it to l_r out of M_R

receive antenna selection, for which we derive numerical expressions for the effective channel gains. These expressions are valid for small values of l_r and M_R, and approximately valid for higher values of l_r and M_R. We compare co-located antenna array structures with their spatial counterpart while deploying receive antenna selection. To this purpose, the performance in terms of MIMO maximum mutual information is presented. A simple norm based on instantaneous channels selects the best antennas. We derive explicit numerical expressions for the effective channel gains. Further a comparison in terms of power imbalance between antenna elements is presented. We also consider multiple-input multiple-output systems where antenna elements are closely placed side by side, and examine the performance of a typical antenna selection strategy in such systems under various scenarios of antenna spacing and mutual coupling with varying antenna elements. We compare a linear array with an NSpoke co-located antenna structure which comprises of antennas separated by an angular displacement rather than spatial. We further improve the performance of such systems by a new selection approach which terminates the nonselected antenna elements with a short circuit. The main results of this chapter have been published in two conference papers and one journal paper:

- Habib, A., Mehlführer, C., Rupp, M., "Receive antenna selection for polarized antennas", in *Proceedings of 18th International Conference on Systems, Signals and Image Processing (IWSSIP), Sarajevo, June 2011, pp. 1-6.*

- Habib, A., Mehlführer, C., Rupp, M., "Performance of compact antenna arrays with receive selection", in *Proceedings of Wireless Advanced (WiAd), London, June 2011, pp. 207-212.*

- Habib, A., Rupp, M., "Antenna Selection in Polarized MIMO Transmissions with Mutual Coupling", in *Journal of Integrated Computer Aided Engineering, 2012.*

Chapter 4

In this chapter we provide another degree of freedom to dual-polarized MIMO transmissions and analyze the performance of antenna selection for triple-polarized MIMO systems with maximum ratio combining receivers. We theoretically analyze the impact of cross-polar discrimination on the achieved antenna selection gain for both dual and triple-polarized MIMO for non line of sight channels. We proceed to derive the outage probabilities and observe that these systems achieve significant performance gains for compact configurations with only a nominal increase in complexity.

The main results of this chapter have been presented in one conference paper:

- Habib, A., "Multiple polarized MIMO with antenna selection", in *Proceedings of 18th IEEE Symposium on Communications and Vehicular Technology in the Benelux (SCVT), Ghent, November 2011, pp. 1-8.*

Chapter 5

In this chapter consider the use of multiple antenna signaling technologies, specifically Space Time Block Coding (STBC) and spatial multiplexing (SM) schemes, in MIMO communication systems employing dual polarized antennas at both ends. In our work, we consider these effects and model a 3×3 system with triple-polarized antennas for both STBC and SM cases. We also present simulation results for both multi-antenna signaling techniques together with hybrid approaches under various Cross Polarization Discrimination (XPD) and correlation scenarios.

The main results of this chapter have been published in one conference paper:

- Habib, A., "Performance of Spatial Multiplexing and Transmit Diversity in Multi-Polarized MIMO Transmissions with Receive Antenna Selection", in *Proceedings of 2nd International Conference on Aerospace Science and Engineering (ICASE), Islamabad, December 2011.*

Chapter 6

We present a low complexity approach to receive antenna selection for capacity maximization, based on the theory of convex optimization. By relaxing the antenna selection variables from discrete to continuous, we arrive at a convex optimization problem. We consecutively optimize not only the selection of the best antennas but also the angular orientation of individual antenna elements in the array for a so-called true polarization diversity system. We also model such polarized antenna systems and then apply convex optimization theory for selecting the best possible antennas in terms of capacity maximization. Channel parameters like transmit and receive correlations, as well as XPD are taken into consideration while modeling polarized systems. We compare our results with Spatially Separated (SP) MIMO with and without selection by performing extensive Monte-Carlo simulations. The main results of this chapter have been presented in two conference papers:

- Habib, A., Krasniqi, B., Rupp, M., "Antenna selection in polarization diverse MIMO transmissions with convex optimization", in *Proceedings of 18th IEEE Symposium on Communications and Vehicular Technology in the Benelux (SCVT), Ghent, November 2011, pp. 1 - 5.*

- Habib, A., Krasniqi, B., Rupp, M., "Convex Optimization for Receive Antenna Selection In Multi-Polarized MIMO Transmissions", in *Proceedings of 19th International Conference on Systems, Signals and Image Processing, (IWSSIP), Vienna, April 2012, pp. 269 - 275.*

<div align="right">

2

</div>

Antenna Selection in Multi-carrier Systems

2.1 Introduction

Multiple antenna systems enable, in addition to time, frequency and code domain, another degree of freedom: the spatial domain. Advanced algorithms are required to exploit all domains in different scenarios, giving a vast variety of trade-offs. Nonetheless, the spatial domain serves as an additional degree of freedom but comes at the cost of expensive analogue and digital hardware. This in turn gives rise to increased power, space and cost requirements. These are important issues, especially in the design of mobile terminals. Antenna (subset) selection techniques at receiver- and/or transmitter-side can help to relax the complexity burden of a higher-order Multiple-Input Single-Output (MIMO) system, while preserving some of its benefits in a MIMO system of lower order. In Frequency Division Duplex (FDD) systems, a limited feedback is required from the receiver to the transmitter in order to perform selection of transmit antenna subsets. In Time Division Duplex (TDD) mode the transmitter might be able to gather the required channel knowledge via its uplink.

In this chapter, we apply receive antenna selection in WiMAX (Worldwide Interoperability for Microwave Access). WiMAX is a wireless communications standard designed to provide 30 to 40 Mbit/s data rates. It is a part of a fourth generation, or 4G, of wireless-communication technology. For such systems two types of antenna arrangements are considered. These are a 2×2 and a 2×4 system, with selection of one and two antennas at the receive side, respectively. Also, selection of one receive antenna in the 2×4 system is performed. In all cases, Alamouti coding is used at the transmitter.

In a practical system, indices of selected subset are calculated at the receiver. These indices are sent to the receive switch, that connects the available RF sections to the selected antennas. All the processing and selection is performed within the receiver architecture. For transmit antenna selection, indices are also calculated at the receiver but have to be fed back to the transmit switch. This feedback has to pass through a channel and therefore it is prone to errors. As only the indices of the selected antennas are to be fed back, few bits are required. In addition to the feedback data for antenna selection, WiMAX also uses a feedback mechanism to select one out of seven possible Adaptive Modulation and Coding (AMC) schemes to adjust to the instantaneous channel quality. In this contribution,

comparisons in terms of throughput and uncoded Bit Error Ratio (BER) for various antenna selection algorithms are presented. Results assuming perfect channel knowledge at the receiver are shown.

2.2   System Model

We consider a MIMO system equipped with N_T transmit and M_R receive antennas as described in Figure 1.1. We assume here that the transmitter employs N_T RF chains whereas the receiver uses $l_r (\leq M_R)$ RF chains. The channel is assumed quasi-static fading. As we are simulating a multi-carrier Orthogonal Frequency Division Multiplexed (OFDM) system, we transmit data through N number of sub-carriers in the channel. The input-output relationship of a MIMO system using all antenna elements and applied to a single sub-carrier, is described by

$$\mathbf{y} = \sqrt{\frac{\gamma}{N_T}} \mathbf{H}_{M_R N_T} \mathbf{x} + \mathbf{v} \tag{2.1}$$

where $\mathbf{y}$ is a received signal vector with dimensions M_R, vector $\mathbf{x}$ is a transmitted signal vector with N_T dimension, vector $\mathbf{v}$ is additive white Gaussian noise with energy $1/2$ per complex dimension, γ is the average Signal-to-Noise Ratio (SNR) at each receive antenna, and $\mathbf{H}_{M_R,N_T}$ is the complete MIMO channel matrix between the N_Tth transmit and the M_Rth receive antenna for a single subcarrier,

$$\mathbf{H}_{M_R,N_T} = \begin{pmatrix} h_{1,1} & h_{1,2} & \cdots & h_{1,N_T} \\ h_{2,1} & h_{1,2} & \cdots & h_{2,N_T} \\ \vdots & \vdots & \ddots & \vdots \\ h_{M_R,1} & h_{M_R,2} & \cdots & h_{M_R,N_T} \end{pmatrix}, \tag{2.2}$$

where the size of $\mathbf{H}_{M_R,N_T}$ is $M_R \times N_T$. In all the simulations performed, the time-dependent statistical properties are defined according to a block fading definition [38], with Pedestrian B power delay profile. This power profile has six well separated taps and was selected for simulations due to its significant frequency selective nature [39]. Receive antenna selection is performed for every frame, i.e., one block of data. The sub-channel matrix after applying antenna selection is shown below.

$$\mathbf{H}_{l_r,N_T}^{(r)} = \begin{pmatrix} h_{r(1),1} & h_{r(1),2} & \cdots & h_{r(1),N_T} \\ h_{r(2),1} & h_{r(2),2} & \cdots & h_{r(2),N_T} \\ \vdots & \vdots & \ddots & \vdots \\ h_{r(l_r),1} & h_{r(l_r),2} & \cdots & h_{r(l_r),N_T} \end{pmatrix}, \tag{2.3}$$

where $r(\cdot)$ represents the selected index set of the rows. This set is evaluated in the next sections. The matrix $\mathbf{H}_{l_r,N_T}$ is the channel representation after the receive antenna subset selection.

2.3   Antenna Selection Algorithms

Various antenna subset selection algorithms have been reported in literature in the past. Among those, a few are presented here and applied to the WiMAX system for comparison purpose. For all selection algorithms, the complexity of signal processing required at the receiver increases with the number of

antenna elements. The number of possible subset antenna combinations B_R required can be calculated from the following.

$$B_R = \left(\begin{array}{c} M_R \\ l_r \end{array} \right) = \frac{M_R!}{l_r!(M_R - l_r)!}. \tag{2.4}$$

All the methods mentioned in the next sections, perform calculations assuming full and perfect channel knowledge at the receiver. In actual systems the channel matrix can be estimated from the training sequence contained in every transmitted frame. After acquisition of the channel matrix, rows of this matrix are selected depending on the selection algorithm. An inherent disadvantage of antenna (subset) selection is that the Channel State Information (CSI) cannot be obtained at the same time. Search over all possible subset combinations is required to acquire the full channel knowledge, and to select the antenna combination which has the highest benefit for the communication link. Furthermore, this search increases the risk that the selection is performed based on outdated channel knowledge, particularly when the channel changes very rapidly. This stimulates the need of fast antenna selection algorithms as mentioned in [22] [23].

The system block diagram with antenna selection is shown in Figure 1.1. The RF chain depicted in Figure 1.1 at the transmitter, converts the digital baseband symbol streams to analog radio-frequency. Thus, each RF-chain must have at least one of several components like a mixer, power amplifier, filter, impedance converters etc. Some of the required analog components do not have to be replicated necessarily for each RF-path since their functionality can be reused (e.g., local oscillators). The structure of the receiver RF-path is similar to the reverse structure of the transmitter.

In this chapter functional aspects of the channel, the Alamouti coding and decoding schemes as well as antenna selection algorithms are taken into consideration. All the remaining parts in the signal chain (switch, converters, RF) are treated as ideal operating components. This results in many assumptions. We have assumed here that no distortion is introduced by the analog up- and down-conversion units and no crosstalk is present between the RF chains. We have also assumed here that perfect synchronization is present between the transmitter and the receiver at all times. Also, as perfect CSI is present at the receiver, no channel estimation errors are made. The receive switch, performing the actual antenna selection, is, assumed to be lossless and consisting of identical, linear transfer characteristics associated with the respective input-output pairs.

2.3.1 Norm Based Method

The norm based method is the most simple antenna selection algorithm. The method is inspired by the fact that selection based on maximum norm maximizes the signal to noise ratio and minimizes the instantaneous probability of error at the receiver [3]. Norm-based selection may be used because of its low computational complexity. This method calculates the Frobenius norm of all the rows of the channel matrix $\mathbf{H}_{M_R,N_T}$ and selects only that subset which has maximum norm. The resulting sub-channel matrix would contain l_r out of M_R rows of the corresponding channel matrix $\mathbf{H}_{M_R,N_T}$. The norm method is given as follows

$$F_{\text{norm}}^{n_r} = \sum_{n_t=1}^{N_T} ||\mathbf{H}_{n_r,n_t}||_F, \tag{2.5}$$

where $n_r = 1, 2, 3, ..., M_R$ and $\mathbf{H}_{n_r,n_t}$ is the n_rth row of the channel matrix $\mathbf{H}_{M_R,N_T}$. The antenna subset r_{norm} is calculated below as

$$r_{\text{norm}} = \arg\max_{r\in R} \sum_{n_r=r(1)}^{r(l_r)} F_{\text{norm}}^{n_r} \tag{2.6}$$

$r_{\text{norm}} \in R$. The entity $r(1)$ represents the first element of the set r. If a selection of one out of four is performed, $r(1)$ would be one element from $R\{r(1)\} = \{1,2,3,4\}$. If a selection of two out of four is performed, $[r(1), r(2)]$ would be two elements of the set $R\{[r(1), r(2)]\} = \{[1,2],[1,3],[1,4],[2,3],[2,4],[3,4]\}$. The selection of r_{norm} rows is obtained by searching for the sub-channel matrix which has maximum norm of all the combinations of $\mathbf{H}_{M_R,N_T}$.

2.3.2 Mutual Information Optimization Method

A method based on instantaneous mutual information is presented here. This method selects the receive antennas which give the maximum mutual information among all possible subsets. It is worth mentioning here that the transmitter has no knowledge of the channel so it distributes the power equally among all antennas and all sub-carriers. Only the receiver has the perfect channel knowledge. The mutual information of the channel is formulated as follows [40]

$$C^{(r)} = \log_2\det\left(\mathbf{I}_{l_r} + \frac{\gamma}{N_T}\mathbf{H}_{l_r,N_T}^{(r)}(\mathbf{H}_{l_r,N_T}^{(r)})^{\text{H}}\right), \tag{2.7}$$

where H represents the Hermitian transpose. The antenna subset r_{mcap} is calculated below as

$$r_{\text{mcap}} = \underset{r\in R}{\arg\max} C^{(r)}. \tag{2.8}$$

The selection of r_{mcap} rows is calculated by searching for the sub-channel matrix which has maximum mutual information of all the sub matrices of $\mathbf{H}_{M_R,N_T}$.

2.3.3 Eigenvalue Based Methods

Two methods are explained here [40] which depend on the smallest eigenvalues of the channel matrix. These methods can be used for the frequency selective channel using OFDM based symbol transmission. Therefore, this method is worth mentioning and implementing because it has been proven that the smallest eigenvalue of $(\mathbf{H}_{M_R,N_T}^{(r)})^{\text{H}}\mathbf{H}_{M_R,N_T}^{(r)}$ has the highest impact on the performance of linear receivers (Zero Forcing equalizer) [26] for flat fading channels. This is extended to frequency selective channels as given in [40].

Maximum Minimum Eigenvalue Method (MMEM)

The algorithm based on the maximum of minimum eigenvalues is presented below

$$r_{\text{mmem}} = \arg\max_{r\in R} \min_{n=1,...N} \min_i \lambda_i^{(r,n)}, \tag{2.9}$$

where λ_i is the ith eigenvalue of the matrix $(\mathbf{H}_{l_r,N_T}^{(r)})^{\text{H}}\mathbf{H}_{l_r,N_T}^{(r)}$ for nth sub-carrier. The selection of r_{mmem} rows is performed by searching for the sub-channel matrix which has minimum eigenvalue of all the subsets of $\mathbf{H}_{M_R,N_T}$ for each subcarrier.

Maximum Ratio Eigenvalue Method (MREM)

The method described here is motivated by the proposals given in [41] [42]. The algorithm selects the channel with the maximum ratio between the minimum and the maximum eigenvalue. This ratio basically is an indicator of the degree of spread of all the eigenvalues of the $\mathbf{H}_{M_R,N_T}$. Lower spread means higher ratio and therefore a better conditioned channel and vice versa. The method is expressed below [40] as

$$r_{\mathrm{mrem}} = \arg\max_{r \in \mathrm{R}} \frac{\min_{n=1,\ldots\mathrm{N}} \min_i \lambda_i^{(r,n)}}{\max_{n=1,\ldots\mathrm{N}} \max_i \lambda_i^{(r,n)}}, \tag{2.10}$$

where λ_i is the ith eigenvalue of the matrix $(\mathbf{H}_{l_r,N_T}^{(r)})^{\mathrm{H}}\mathbf{H}_{l_r,N_T}^{(r)}$ for nth sub-carrier. The selection of r_{mrem} rows is performed by searching for the sub-channel matrix with maximum ratio of minimum and maximum eigenvalues of all the subsets of $\mathbf{H}_{M_R,N_T}$ for each subcarrier.

2.3.4 Perfect Antenna Selection

All the methods presented above, are compared with a perfect selection algorithm based on maximizing the throughput. For each sub-channel matrix, the throughput is simulated and the subset with the highest throughput is selected. The selection is shown below.

$$r_{\mathrm{MTP}} = \arg\max_{r \in \mathrm{R}} (\mathrm{TP})^{(r)}. \tag{2.11}$$

The r_{MTP} rows are selected by searching for the sub-channel matrix which has maximum throughput of all the sub matrices of $\mathbf{H}_{M_R,N_T}$. The methods described in the previous sections are only based on instantaneous channel knowledge, so they can be implemented independently of the equalizer. The Maximum Ratio Eigenvalue Method (MREM) is more complex than the Maximum Minimum Eigenvalue Method (MMEM), as two eigenvalues have to be calculated instead of one per subcarrier. Depending on the channel matrix, it is possible that the eigenvalues are too small and are below the noise floor. Under these conditions, MMEM and MREM may give poor throughput performance. The perfect channel selection is only for comparison purpose as practically it is very difficult to implement such methods.

2.4 Simulation Results

A standard compliant WiMAX simulator [43] was used for all the simulations. In our simulation we use $N = 256$ sub-carriers, M_R is 2 and 4 for a 2×2 and 2×4 system, respectively, while N_T is fixed to 2; l_r is either 1 for a 2×2 or 1 or 2 for a 2×4 system. Comparisons of subset selection methods in terms of average throughput and uncoded BER are performed. In all our simulations we use a quasi-static MIMO channel model and assume that the channel remains static during a frame of transmitted data. From the simulation parameters mentioned, it can be seen that a scenario of rich scattering environment is considered which is a typical case in wireless systems.

An average of at least a 3dB difference can be seen between a 2×2 system and all the selected systems in Figure 2.1(a). Similar to the 2×2 case, an average of at least 3dB difference can be seen between a 2×4 system and all the selected systems in Figure 2.1(b). At SNR values from 12dB to 25dB, the average throughput of all the schemes increases.
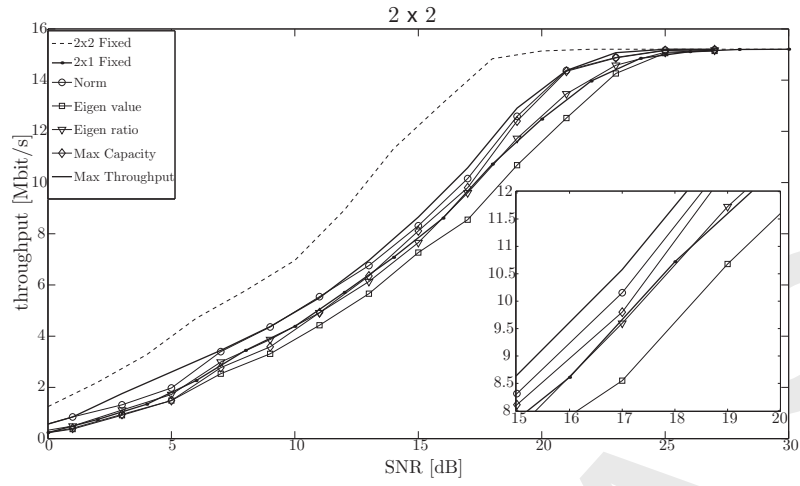
(a) 1 out of 2 selection at Rx.
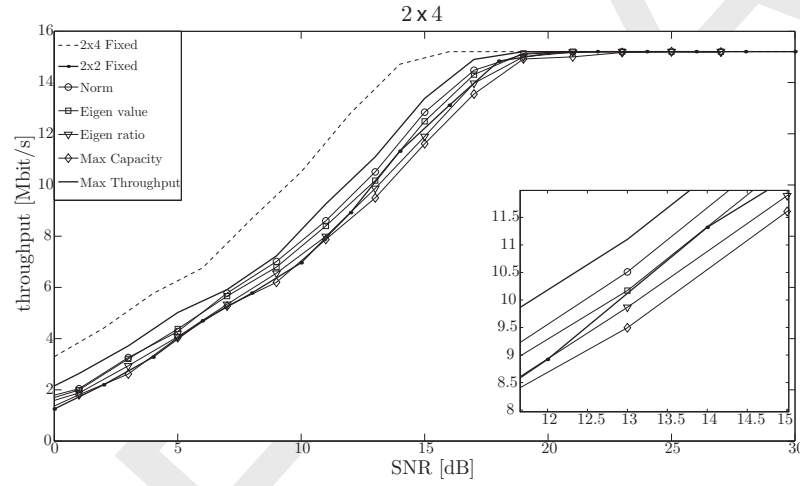
(b) 2 out of 4 selection at Rx.
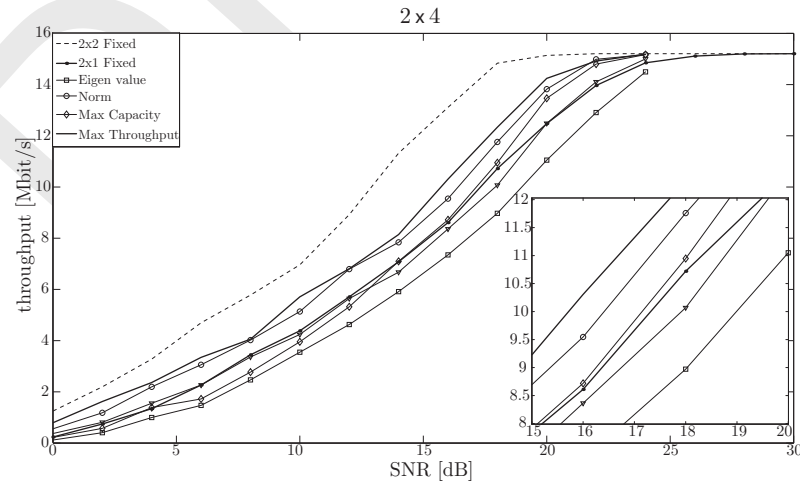
(c) 1 out of 4 selection at Rx.

Figure 2.1: Throughput comparison of antenna selection algorithms with two transmit antennas and two or four antennas at receive side, respectively.
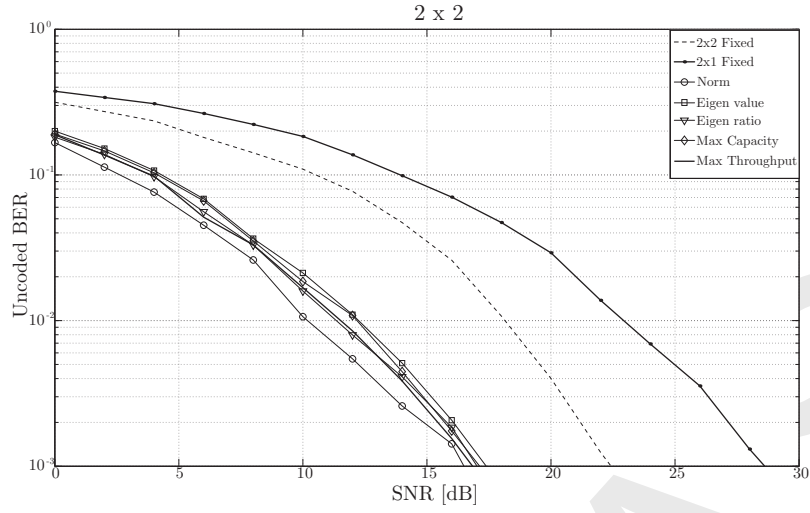
(a) 1 out of 2 selection at Rx.
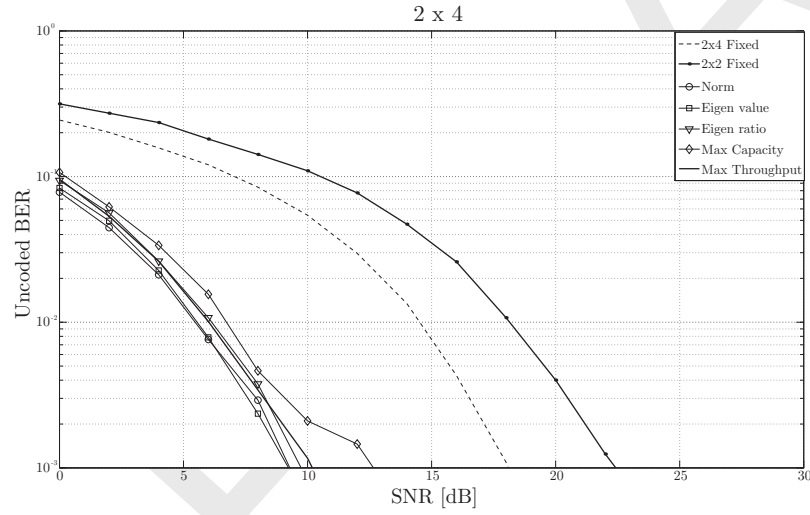
(b) 2 out of 4 selection at Rx.
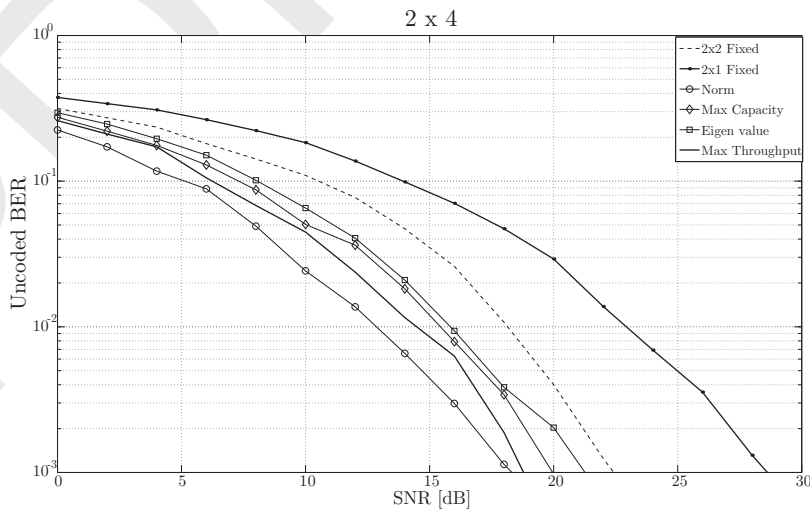
(c) 1 out of 4 selection at Rx.

Figure 2.2: Uncoded bit error ratio comparison of antenna selection algorithms with two transmit antennas and two or four antennas at receive side, respectively.

The method based on maximum mutual information behaves well for flat fading channel models. Therefore, this method is normally taken as an upper bound for comparison with other sub-optimal methods in flat fading channels. But for the case of frequency selective channels this method does not give the best throughput and minimum BER. The reason is that for different sub-carriers different antenna subsets may be optimal. Another reason for the sub-optimal behavior of this method is that sub-optimal receivers and channel coding is used in simulations. In practical systems, also channel coding with sub-optimal receivers are used for low complexity system design. Antenna selection through mutual information optimization may give significant benefits in moderate frequency selective channels.

The complexity of MREM is slightly higher than MMEM, as it requires the calculation of both maximum and minimum eigenvalues and their ratio per frequency tone n and subset combination r. An average difference of 1dB is noticed in a 2×2 system. For a 2×4 system the gain is even less pronounced. This difference is maximum at throughput values of approximately 12Mbit/s. The reason in the difference is obvious. MREM provides channels of better condition numbers. Moreover, the both the eigenvalue methods are very sensitive to channel estimation errors.

The behavior of the norm based method is good for SNRs ranging from 16 to 22dB. It has an advantage of 2dB at throughput of 12Mbit/s from the eigen value based methods for a 2×2 system. From Figures 2.1(a), 2.1(b) and 2.1(c) it is clear that the simple norm based method gives the best throughput performance. In Figure 2.1(c) this gain is even more pronounced.

In all the throughput comparisons, a reference throughput curve indicating a 2×1 system without antenna selection is also included. From the results it can be seen that more or less all the methods except the MMEM, behave better than a simple 2×1 system without antenna selection. Similarly for reference, a 2×2 system without antenna selection is included in Figure 2.1(b). The same behavior can be seen in the 2×4 system as well. In Figure 2.1(c) the gains are more pronounced compared to the previous figures.

The BER curves are calculated as follows. For each channel realization and antenna subset combination the BER values for each Adaptive Modulation and Coding (AMC) scheme are calculated. The best antenna subset is selected according to methods described earlier. The BER performance behaves somewhat similar to throughput performance. The norm based methods in Figures 2.2(a), 2.2(b) and 2.2(c) achieves the minimum BER compared to all the other methods. The only inconsistent behavior while comparing Figure 2.1 and Figure 2.2 is the performance of the selection based method on maximum throughput. The norm based method behaves better in terms of BER performance compared to maximum throughput based selection. As mentioned earlier the throughput curves in Figure 2.1 are for coded bits, so they give the best result. But in Figure 2.2 the BER curves are for uncoded bits. The MREM is not included in Figure 2.1(c) and Figure 2.2(c) for the sake of clarity.

2.5   Conclusions

In this chapter we introduced the application of receive antenna selection on multicarrier systems. We assumed perfect channel knowledge at the receiver for the calculation of best antenna subsets for various selection algorithms. We ignored any channel estimation mechanisms at the receiver side [44]. The results can be more realistic if we include various channel estimation techniques for multicarrier systems [45] [46]. The zero delay in the feedback was considered. In realistic systems the effect of non-zero delay has to be included which would further effect the calculation of antenna subsets for various channel conditions [47]. Antenna selection can also be performed at the transmitter for various

power allocation and rate adaptation techniques [48]. We ignored all these effects to only get the results for selection algorithms rather than the effects of the system.

After introducing the applications of antenna selection in OFDM based MIMO systems we move forward to the application to 2D compact antenna structures in the next chapter.

Antenna Selection in 2-D Polarized MIMO

3.1 Introduction

In the analysis of Multiple-Input Single-Output (MIMO) systems, an array of vertical antennas is normally considered when the receiver has no space limitations. In compact portable devices, such as mobile handsets and laptops, if a spatial array of vertical antennas is realized, high correlation between the closely spaced antenna elements severely effects the performance. Applying dual polarized antennas at the receiver or at the transmitter proves effective in alleviating performance loss due to low correlation between the antenna elements. Also there can be a leakage of power from one antenna to another. This effect is known as antenna Cross Polarization Discrimination (XPD), and is eminent in both co-located dual-polarized antenna arrays and spatially separated antenna arrays. The effect of correlation is more dominant in closely spaced antenna arrays and less dominant in systems with dual-polarized antennas. XPD is due to non-ideal antenna polarization patterns. Because of this leakage, a simple rotation in the antenna array causes a mismatch in the incoming incident Electro-Magnetic (EM) wave. The amount of this leakage has an impact on the overall performance of the system [49]. Multiple Dual Polarized (DP) antennas are strong candidates to be put into practice in 3GPP Long Term Evolution (LTE) [50] systems. Antenna arrays combined with receive antenna selection techniques can improve the quality of wireless communication systems through reduction of fading impact. If a dual-polarized receive antenna is employed, a further benefit is the mitigation of polarization mismatch caused by the random orientation of portable devices. In this chapter multiple co-located (fed from the same point) receive antennas are considered. We apply Receive Antenna Selection (RAS), starting with 1 out of 2 selection and then extend this to 1 out of M_R receive antennas. Finally, the results are generalized for the l_r out of M_R selection case to study the limits on performance. The combined effect of array rotation, power imbalance, and l_r out of M_R receive antenna selection is studied. Analysis and simulation is performed for flat Rayleigh fading channels. Accurate expressions and approximate bounds for the effective channel gains are provided for a generic l_r out of M_R selection. A simple Maximum Ratio Combiner (MRC) is applied at the receiver for signal detection. Robustness analysis is presented for a generic l_r out of M_R receive antenna selection by

finding the CDF of the effective channel gains through simulations. From limiting values of effective channel gains, a minimum antenna set (l_r, M_R) is found. We then proceed further to include the effects of mutual coupling and analyze the performance of multi-polarized antennas for MIMO transmissions with receive antenna selection. A literature overview from existing work is presented in the following for dual polarized systems.

3.1.1　Dual Polarized Antenna Modeling

The utilization of multiple polarizations of the electromagnetic wave to extract diversity has been well known and understood for a long time [51]. The capacity of the dual polarized MIMO channel is evaluated and compared to the capacity of a single polarized MIMO system. On the same principles we calculate the mutual information in our work as we assume equal power from the transmitting antennas. In [52] [53], the potential advantages of employing dual-polarized arrays in multi-antenna wireless systems for various channels is studied. In [54] [55], a model is proposed to determine the XPD as a function of the channel condition under different antenna configurations. In this chapter it is shown that the antenna XPD is not only sensitive to different channel conditions but also to different receiver orientations.

3.1.2　Dual Polarized MIMO with Rotation

In [56] the impact of the polarization on the performance of the MIMO channel with cross-polarized antennas has been investigated based on an outdoor macro-cell measurement at 2.53 GHz. A simple model which can capture the major characteristics of the cross polarized channel has been proposed. It has been shown that the polarization diversity outperforms the spatial diversity in a Line Of Sight (LOS) scenario, but shows relatively small gain in a rich scattering scenario.

3.1.3　Antenna Selection for Dual Polarized MIMO

In [57], the performance of antenna selection on dual polarized MIMO channels with linear Minimum Mean Square Error (MMSE) receiver processing is analyzed. A study on the impact of XPD on the achieved selection gain is carried out. BER results obtained indicate that antenna selection with dual-polarized antennas can achieve significant performance gains for compact configurations. In [58], dual polarized MIMO exploiting the Spatial Channel Model (SCM) [39] is investigated in terms of performance for a certain environment. Applying this channel model, the channel capacity is estimated as a function of the XPD and the spatial fading correlation.

3.2　System Model with Rotation and XPD

The rotation of an antenna array can be modeled by multiplying the channel matrix with a rotation matrix [56]. If we define the amount of energy leakage between the two polarizations of an antenna as α, the antenna XPD is specified by [49], $\text{XPD} = \frac{1-\alpha}{\alpha}$ where $0 \leq \alpha \leq 1$. Therefore when

$$\lim_{\alpha \to 0} \text{XPD} = \infty; \qquad \lim_{\alpha \to 1} \text{XPD} = 0.$$

All antenna elements considered in this chapter are assumed as simple monopoles. The transmitter contains a single vertically polarized antenna and the receiver consists of M_R antenna elements in an

N-Spoke configuration [59], as shown in Figure 3.1. The feeding points of all antenna elements are co-located. In [59], a similar antenna configuration is used to compare polarization diversity to spatial diversity. We further assume that the antenna elements are isotropically radiating in all directions with unity gain and there is no angular correlation between them. Note that in a practical system, a certain amount of correlation exists between the antenna elements, as calculated in [59–61]. In order to be able to derive analytical expressions for the channel gains, however, we will neglect the angular correlation here.

3.2.1 General MRC Receiver

The model for a generic $1 \times M_R$ Single-Input Multiple-Output (SIMO) system with MRC is explained in the following. Subsequently a model for RAS with MRC will be shown. The channel matrix is written as

$$\mathbf{h} = [h_1, h_2, \cdots, h_{M_R}]^{\mathrm{T}},$$

and the received signal vector by

$$\mathbf{y} = \mathbf{h} \cdot x + \mathbf{v}, \tag{3.1}$$

where $x \in \mathcal{C}$ and $\mathbf{v} \in \mathcal{C}^{M_R}$ with $\mathbf{v}$ being a noise vector with i.i.d. and circularly symmetric complex-valued Gaussian entries with variance $1/2\ \sigma_v^2$ for each real dimension. The detected symbol at the MRC output is shown as

$$\hat{x} = \mathbf{h}^{\mathrm{H}} \cdot \mathbf{h} \cdot x + \mathbf{h}^{\mathrm{H}} \cdot \mathbf{v}, \tag{3.2}$$

where $(\cdot)^{\mathrm{H}}$ denotes the Hermitian. The received signal for receive antenna selection is then given by

$$\mathbf{y}^{(\mathcal{S}_{l_r})} = \mathbf{h}^{(\mathcal{S}_{l_r})} \cdot x + \mathbf{v}^{(\mathcal{S}_{l_r})}, \tag{3.3}$$

where the MRC only combines the received signals from the selected antennas identified by the set of indices of an ordered set $\mathcal{S}_{l_r} = \{n_1, n_2, \cdots, n_{l_r}\}$ where $n_i \in [1, 2, \cdots, M_R]$ and $n_1 < n_2 < ... < n_{l_r}$. The detected symbol after receive antenna selection is then

$$\hat{x}^{(\mathcal{S}_{l_r})} = \mathbf{h}^{(\mathcal{S}_{l_r})\mathrm{H}} \cdot \mathbf{h}^{(\mathcal{S}_{l_r})} \cdot x + \mathbf{h}^{(\mathcal{S}_{l_r})\mathrm{H}} \cdot \mathbf{v}^{(\mathcal{S}_{l_r})}, \tag{3.4}$$

The gain of full complexity receiver is given by

$$G_{M_R/M_R} = E\left[\mathbf{h}^{\mathrm{H}} \cdot \mathbf{h}\right], \tag{3.5}$$

while the gain of receiver with antenna selection is given by

$$G_{l_r/M_R} = E\left[\mathbf{h}^{(\mathcal{S}_{l_r})\mathrm{H}} \cdot \mathbf{h}^{(\mathcal{S}_{l_r})}\right]. \tag{3.6}$$

A generic model of the system is shown in Figure 3.1 with all the essential components. We assume here for simplicity that the channel is known at the receiver and there is a perfect synchronization between the transmitter and the receiver. Also we do not dwell into the realizations of the switch and the RF chain. We assume an ideal switch without any insertion losses. We further assume that the channel does not change during the switching period.
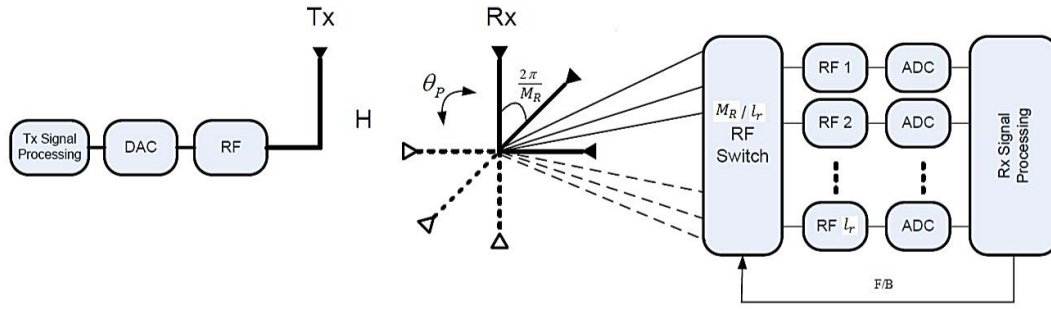
Figure 3.1: N-Spoke antenna configuration (1 Tx and M_R Rx) with receive antenna selection.

3.2.2 SIMO $1 \times M_R$ with Polarization

The receiver is assumed to be randomly oriented in space. Due to this a polarization mismatch loss can occur as discussed in [62]. The orientation can be represented in a three dimensional co-ordinate system, but here, for simplicity we only consider one direction so that the orientation/rotation is represented by a single angle θ_p with respect to the vertical antenna element of the array. The effect of antenna orientation is well discussed in [63] [64]. The averaging is hence performed for all the rotation angles. We start with the analysis of a single receive antenna case. The channel matrix is multiplied with an XPD matrix and then with a rotation matrix as shown in [56]. A simple model which can identify the basic characteristics of the polarized MIMO channel is proposed in this chapter [56]. This model can describe the cross-polarized channel in realistic scenario better. The power is divided into each orthogonal component of antenna element as shown in Figure 3.2. Next we show simulations for
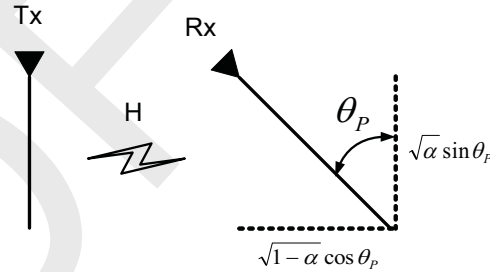
Figure 3.2: Orthogonal polarization components of Single-Input Single-Output (SISO) receive antenna.

$1 \times M_R$ SIMO with MRC at the receiver. The channel matrix for $1 \times M_R$ SIMO is

$$\mathbf{h}_{M_R} = \begin{bmatrix} h_1 \left(\sqrt{1-\alpha} \cos(\theta_p + k_1 \frac{2\pi}{M_R}) + \sqrt{\alpha} \sin(\theta_p + k_1 \frac{2\pi}{M_R}) \right) \\ h_2 \left(\sqrt{1-\alpha} \cos(\theta_p + k_2 \frac{2\pi}{M_R}) + \sqrt{\alpha} \sin(\theta_p + k_2 \frac{2\pi}{M_R}) \right) \\ \vdots \\ h_{M_R} \left(\sqrt{1-\alpha} \cos(\theta_p + k_{M_R} \frac{2\pi}{M_R}) + \sqrt{\alpha} \sin(\theta_p + k_{M_R} \frac{2\pi}{M_R}) \right) \end{bmatrix}, \tag{3.7}$$

where $k_{M_R} = n; n = 0, 1, \cdots, M_R - 1$ are the scaling factors depending on the orientation of a single antenna, and $0 \leq \alpha \leq 1$. As we have realized an MRC receiver, we sum the squares of the channel

coefficients for each row of the channel matrix in Equation (3.7) and take the average over all realizations. The effective channel gain is then shown by Equation (3.10). In Figure 3.3, a 1×3 SIMO antenna configuration is shown as an example.
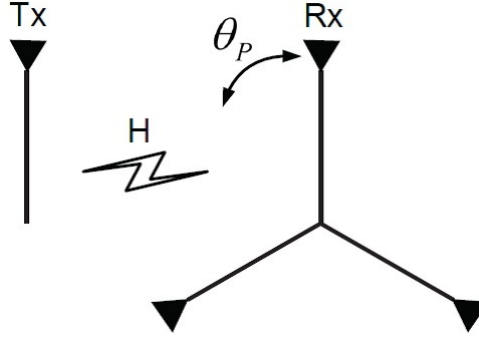
Figure 3.3: 1×3 SIMO antenna configuration.

3.2.3 RAS $1/M_R$ and l_r/M_R with Polarization

Next we simulate the effect of XPD and rotation on the channel gains of $1/M_R$ RAS. The notation l_r/M_R is used to denote receive antenna selection, selecting l_r out of M_R receive antennas. We start by selecting $l_r = 1$ out of M_R from the channel matrix given by Equation (3.7), with the largest norm, $\bar{n} \in [1, 2, \cdots, M_R]$ being the index of the selected antenna element. The corresponding channel coefficient h_{1/M_R} becomes a scalar.

$$h_{1/M_R} = \left[h_{\overline{n}} \left(\sqrt{1-\alpha} \cos(\phi_{\overline{n}}) + \sqrt{\alpha} \sin(\phi_{\overline{n}}) \right) \right], \tag{3.8}$$

where $\phi_{\overline{n}} = \theta_p + k_{\overline{n}} \frac{2\pi}{M_R}$. The effective channel gain is expressed in Equation (3.11) and approximate value in Equation (3.12). A similar matrix $\mathbf{h}_{l_r/M_R} = [h_1, h_2, \cdots, h_{l_r}]^T$ can be constructed, containing only the channel coefficients of the l_r selected antenna elements, indices of which would be from an ordered set given by $(\mathcal{S}_{l_r}) = \{n; \|h_n\|_F > \|h_{l_r+1}\|_F\} = [n_1, n_2, \cdots, n_{l_r}]$. The new channel matrix with l_r/M_R selection is then

$$\mathbf{h}_{l_r/M_R} = \begin{bmatrix} h_{n_1} \left(\sqrt{1-\alpha} \cos(\phi_{n_1}) + \sqrt{\alpha} \sin(\phi_{n_1}) \right) \\ h_{n_2} \left(\sqrt{1-\alpha} \cos(\phi_{n_2}) + \sqrt{\alpha} \sin(\phi_{n_2}) \right) \\ \vdots \\ h_{n_{l_r}} \left(\sqrt{1-\alpha} \cos(\phi_{n_{l_r}}) + \sqrt{\alpha} \sin(\phi_{n_{l_r}}) \right) \end{bmatrix}, \tag{3.9}$$

where $\phi_{n_m} = \theta_p + k_{n_m} \frac{2\pi}{M_R}$.

3.3 Analytical Calculations for Average Values of Channel Gains and Generalization

To determine the average values analytically over all $\alpha's$ and over all $\theta_p's$ we do the following for $1/2$ RAS. As $E \left\| h_1^2 \right\| = E \left\| h_2^2 \right\| = 1$ for Rayleigh fading channels, we deduce the following inequality from

$$G_{M_R/M_R}(\theta_p) = \sum_{n=1}^{M_R} E\left[|h_n|^2 \left(\sqrt{1-\alpha}\cos\left(\theta_p + \frac{(n-1)2\pi}{M_R}\right) + \sqrt{\alpha}\sin\left(\theta_p + \frac{(n-1)2\pi}{M_R}\right)\right)^2\right]. \tag{3.10}$$

$$G_{1/M_R}(\theta_p) = E\left[\max\left\{|h_1|^2\left(\sqrt{1-\alpha}\cos(\phi_1) + \sqrt{\alpha}\sin(\phi_1)\right)^2, \cdots, |h_{M_R}|^2\left(\sqrt{1-\alpha}\cos(\phi_{M_R}) + \sqrt{\alpha}\sin(\phi_{M_R})\right)^2\right\}\right]. \tag{3.11}$$

$$G_{1/M_R}(\theta_p) \approx \max\left\{E\left[|h_1|^2\right]\left(\sqrt{1-\alpha}\cos(\phi_1) + \sqrt{\alpha}\sin(\phi_1)\right)^2, \cdots, E\left[|h_{M_R}|^2\right]\left(\sqrt{1-\alpha}\cos(\phi_{M_R}) + \sqrt{\alpha}\sin(\phi_{M_R})\right)^2\right\}. \tag{3.12}$$

where $\phi_n = \theta_p + k_n\frac{2\pi}{M_R}$.

$$\left(\sqrt{1-\alpha}\cos\theta_p + \sqrt{\alpha}\sin\theta_p\right)^2 > \left(\sqrt{1-\alpha}\cos\left(\theta_p + \frac{2\pi}{3}\right) + \sqrt{\alpha}\sin\left(\theta_p + \frac{2\pi}{3}\right)\right)^2 > \left(\sqrt{1-\alpha}\cos\left(\theta_p + \frac{4\pi}{3}\right) + \sqrt{\alpha}\sin\left(\theta_p + \frac{4\pi}{3}\right)\right)^2. \tag{3.13}$$

$$G_{M_R/M_R} = \frac{1}{2\pi}\int_0^{2\pi}\left[\sum_{n=1}^{M_R} E\left\{|h_n|^2\left(\sqrt{1-\alpha}\cos\left(\theta_p + \frac{(n-1)2\pi}{M_R}\right) + \sqrt{\alpha}\sin\left(\theta_p + \frac{(n-1)2\pi}{M_R}\right)\right)^2\right\}\right]d\theta_p. \tag{3.14}$$

$$G_{2/M_R,\alpha=0} = \frac{2M_R}{\pi}\int_0^{\frac{\pi}{2M_R}}\cos^2(\theta_p)\,d\theta_p + \frac{M_R-1}{\pi}\int_0^{\overline{M_R-1}}\cos^2(\theta_p)\,d\theta_p. \tag{3.15}$$

an approximation of Equation (3.11) given in Equation (3.12):

$$\left(\sqrt{1-\alpha}\cos\theta_p + \sqrt{\alpha}\sin\theta_p\right)^2 > \left(\sqrt{1-\alpha}\sin\theta_p + \sqrt{\alpha}\cos\theta_p\right)^2.$$

Solving the inequality for $\alpha = 0$ we find that $\cos^2\theta_p > \sin^2\theta_p$, which results in the interval $0 < \theta_p < \frac{\pi}{4}$ and

$$G_{1/2,\alpha=0} = \frac{4}{\pi}\int_0^{\frac{\pi}{4}}\left(\cos^2\theta_p\right)d\theta_p = 0.8183.$$

Similarly from Equation (3.12) for 1/3 RAS, we obtain the inequality Equation (3.13). Now solving the inequality in Equation (3.13) for $\alpha = 0$ we find that $\cos^2\theta_p > \cos^2\left(\theta_p + \frac{2\pi}{3}\right) > \cos^2\left(\theta_p + \frac{4\pi}{3}\right)$ which results in the interval $0 < \theta_p < \frac{\pi}{6}$ and

$$G_{1/3,\alpha=0} = \frac{6}{\pi}\int_0^{\frac{\pi}{6}}\cos^2\theta_p d\theta_p = 0.9135.$$

Equation (3.12) can be solved for other values of α, but the calculations are not shown here for space limitations.

3.3.1   SIMO $1 \times M_R$

For SIMO we have the relation depicted in Equation (3.14). This gives the average effective channel gains to be

$$G_{M_R/M_R,\alpha=0} = \frac{1}{2}M_R. \tag{3.16}$$

We observe that the relation is very simple and only a linear function of M_R.

3.3.2   RAS $1/M_R$

The intervals calculated in the previous section, show that they are multiples of $\frac{\pi}{2M_R}$. Hence we obtain the following relations.

$$G_{1/M_R,\alpha=0} = \frac{2M_R}{\pi}\int_0^{\frac{\pi}{2M_R}}\cos^2\theta_p d\theta_p = \frac{1}{2} + \frac{M_R}{\pi}\sin\frac{\pi}{2M_R}\cos\frac{\pi}{2M_R}. \tag{3.17}$$

We recognize that the relation is a function of simple trigonometric identities.

3.3.3   RAS l_r/M_R

Now we derive the expression for an l_r/M_R selection. We derive the result for 2/3 and 2/4 RAS and then generalize it. The first inequality shown below yields the largest interval corresponding to the largest channel gain.

$$\cos^2 \theta_p > \cos^2 \left(\theta_p + \frac{2\pi}{3} \right) > \cos^2 \left(\theta_p + \frac{4\pi}{3} \right),$$

$0 < \theta_p < \frac{\pi}{6}$, and the second largest inequality below gives the second largest interval

$$\cos^2 \left(\theta_p + \frac{2\pi}{3} \right) > \cos^2 \left(\theta_p + \frac{4\pi}{3} \right),$$

$0 < \theta_p < \frac{\pi}{2}$. Calculating the gains from these intervals and summing them gives

$$G_{2/3,\alpha=0} = \frac{6}{\pi} \int_0^{\frac{\pi}{6}} \cos^2 \theta_p d\theta_p + \frac{2}{\pi} \int_0^{\frac{\pi}{2}} \cos^2 \theta_p d\theta_p. \tag{3.18}$$

With the same procedure above we calculate the channel gains for 2/4 selection

$$G_{2/4,\alpha=0} = \frac{8}{\pi} \int_0^{\frac{\pi}{8}} \cos^2 \theta_p d\theta_p + \frac{3}{\pi} \int_0^{\frac{\pi}{3}} \cos^2 \theta_p d\theta_p. \tag{3.19}$$

After generalization we reach to Equation (3.15). For values of $l_r > 2$, it is very tedious to solve the inequalities. These inequalities can be solved numerically through MATLAB or MAPLE software tools or an approximate solution can be presented, as shown here with the advantage to obtain some explicit formulations. For approximation we just added the first l_r terms of G_{1/M_R} from Equation (3.17), but with $\frac{\pi}{n}$ instead of $\frac{\pi}{2n}$ intervals, as listed below.

$$G_{3/M_R,\alpha=0} \approx \left[\sum_{n=M_R-3}^{M_R-1} \frac{n}{\pi} \int_0^{\frac{\pi}{n}} \cos^2 (\theta_p) \, d\theta_p \right]. \tag{3.20}$$

$$G_{4/M_R,\alpha=0} \approx \left[\sum_{n=M_R-4}^{M_R-1} \frac{n}{\pi} \int_0^{\frac{\pi}{n}} \cos^2 (\theta_p) \, d\theta_p \right]. \tag{3.21}$$

$$G_{5/M_R,\alpha=0} \approx \left[\sum_{n=M_R-5}^{M_R-1} \frac{n}{\pi} \int_0^{\frac{\pi}{n}} \cos^2 (\theta_p) \, d\theta_p \right]. \tag{3.22}$$

$$G_{l_r/M_R,\alpha=0} \approx \left[\sum_{n=M_R-L_r}^{M_R-1} \frac{n}{\pi} \int_0^{\frac{\pi}{n}} \cos^2 (\theta_p) \, d\theta_p \right]. \tag{3.23}$$

Monte-Carlo simulations are performed to generate channel coefficients according to Equation (3.7) for SIMO and Equation (3.8) for selection systems for $\alpha = 0$ and averaged over rotation angles. Results from these expressions and comparison with simulation are shown in Figure 3.4. Theoretical results are shown in dotted and simulations in solid lines. It can be observed that the curves for $1/M_R$ and M_R/M_R receive antenna selection serve as lower and upper bound respectively, for the channel gains of l_r/M_R RAS.
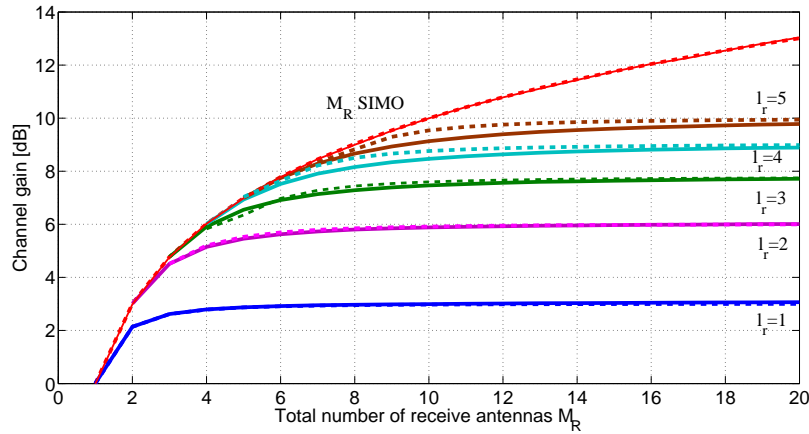
Figure 3.4: Channel gains for $1 \times M_R$ SIMO and l_r/M_R RAS wrt. SISO.

3.3.4   Limiting Values for l_r/M_R RAS

Next we derive the limiting values of l_r/M_R RAS analytically.

$$\lim_{M_R \to \infty} G_{l_r/M_R} = \lim_{M_R \to \infty} \left[\sum_{n=M_R-l_r}^{M_R-1} \frac{n}{\pi} \int_0^{\frac{\pi}{n}} \cos^2\left(\theta_p\right) d\theta_p \right] \tag{3.24}$$

$$= l_r \left(1 + \lim_{M_R \to \infty} \frac{M_R}{2\pi} \sin \frac{2\pi}{M_R} \right), \tag{3.25}$$

$$= l_r \left(1 + \lim_{x \to 0} \frac{1}{x} \sin(x) \right), \tag{3.26}$$

$$= 2l_r, \tag{3.27}$$

for $l_r = 1, 2, 3, 4, \dots M_R$. Various values of l_r and corresponding actual selection gains in the limit, are shown in the Table 3.1. The analytical expressions for values $l_r > 2$ as seen from the curves in Figure 3.4, serve as an upper bound. The difference between the effective channel gains decreases as l_r is increased for a given M_R. This happens because of the dependence of mean channel gains on the average angular separation $\frac{2\pi}{M_R}$ between l_r selected antennas. As the number of selected antennas l_r is increased the average angular spacing between the selected antennas is decreased, so does the difference. From Figure 3.4 we observe that the channel gains almost attain their maximum values

Table 3.1: Minimum receive antenna set for l_r/M_R to achieve the maximum % of gain.

l_r	Max.Gain	Req.M_R	Ach.Gain	Ach.Gain %
1	3.01	2	2.85	95
2	6.02	4	5.72	95
3	7.78	6	7.39	95
4	9.03	8	8.57	95
5	10	10	9.5	95

after a certain number of antenna elements M_R. The total number of used antennas can be reduced without compromising much performance. From the graph, for each l_r/M_R curve, we can calculate the

minimum M_R which gives almost 100% of the maximum value of the channel gains. The results of calculating the minimum set is shown in Table 3.1. The first column shows the value of the number of selected antennas l_r. In the second column the maximum value of the channel gains are given from Equation (3.24). The third column shows the values of M_R required to achieve a certain percentage of the maximum channel gain. The achieved gains and corresponding used percentages, are shown in the next columns. If we take 95% of the maximum value as an example, the loss in the gains is not much but we can save a number of antenna elements. From the table it is conlcuded that l_r should be at least half of the total number of receive antennas to achieve almost the maximum performance.
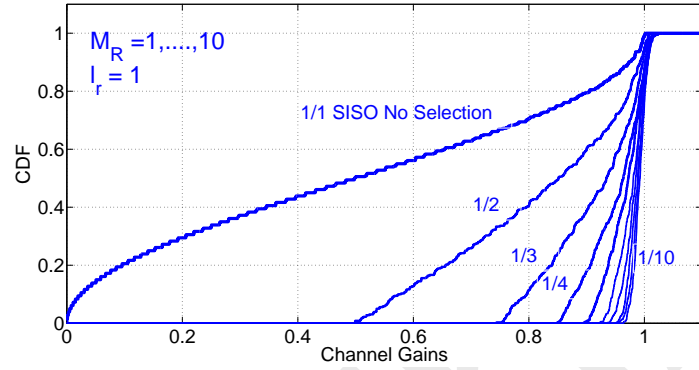
(a) CDF of channel gains for l_r/M_R where $M_R = 1, ...10, l_r = 1$.
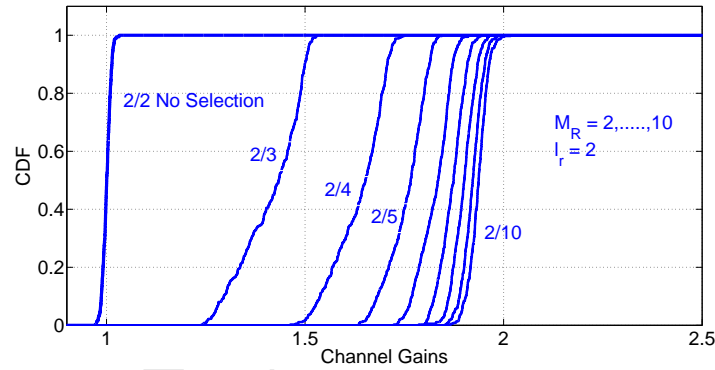
(b) CDF of channel gains for l_r/M_R where $M_R = 2, ...10, l_r = 2$.
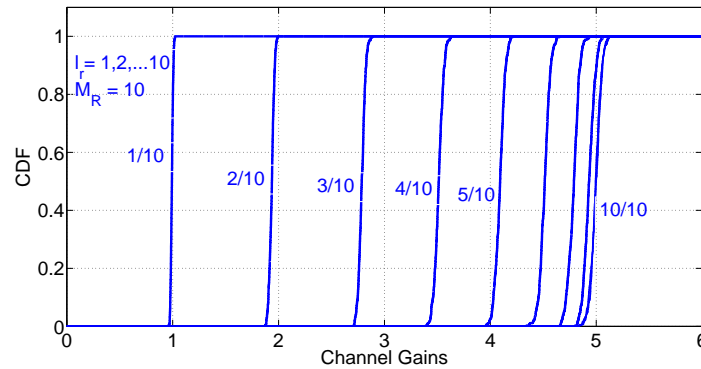
(c) CDF of channel gains for l_r/M_R where $M_R = 10, l_r = 1, ...10$.

Figure 3.5: CDF of channel gains with receive antenna selection.

3.4   Robustness Analysis

The CDF plots shown here provide the measure of robustness against antenna rotation and orientation. It also reveals the measure of variance of channel gains. In Figure 3.5(a) we show CDF plots for $1/M_R$ RAS. From the plots we observe that as M_R increases, the slopes of the curves increase, and the corresponding range of the gains decrease and hence robustness against channel variations increases. As seen from the graphs, variance depends on the available diversity branches M_R. Also it can be observed that the mean of the channel gain is dependent on the number selected antenna l_r. The ratio $\frac{l_r}{M_R}$ shows as the inverse of the slope. Therefore as M_R increases, the slope increases and hence the decrease in variance. In Figure 3.5(b) we show the CDF plot for $2/M_R$ RAS. A behavior similar to $1/M_R$ RAS, can be found in this plot ,i.e., the slope increases as M_R increases. In Figure 3.5(c) we show the comparison of CDF plots for various values of $l_r/10$ receive antenna selection.

3.5   Comparison of Compact Antenna Arrays

To overcome the space limitations in MIMO, there are other ways of providing diversity, such as polarization [49], [51], angle and pattern diversity [65]. Signals from a pair of antennas with orthogonal polarization are combined together to provide polarization diversity. Extensions to three orthogonally polarized antenna elements further augment the degrees of freedom for incoming signals and hence the diversity [66]. Co-located antennas with different radiation patterns can be combined together to provide pattern diversity. Pattern diversity makes use of directional antennas which are physically separated by a very short distance. Similarly co-located radiating elements with different angular spacing can be used to realize angular diversity. One of the main drawbacks of MIMO systems with arrays of parallel dipoles is their sensitivity to a polarization mismatch [53], due to random orientations of the device. To reduce this effect, the benefits of polarization and/or pattern diversity can be exploited [65]. Various channel models have been used in literature for evaluating multiple antenna systems but for the sake of intuition and to include the effects of antenna geometry, we use the double-directional analytical channel model as investigated in [67]. The advantage of using such model is that it incorporates the following:

- Random mobile terminal rotation effects

- Antenna polarization

- Spatial, pattern and polarization diversity of array.

Other than the above characteristics; the representation is intuitive as shown to be the product of antenna and channel effects. However, in this chapter we modify the model from its original to include correlation properties between the antenna elements. The values of correlation have been taken from [61]. In this chapter, models for accurate estimation of correlation for hybrid spatial-angular MIMO systems are given. The model presented in [61] is valid for Rayleigh fading channels and isotropic scatterings. We choose a simple model from that work to obtain the correlation values and include them into our channel model for further analysis. The utilization of multiple polarizations of the electromagnetic wave to extract diversity is well known and understood for a long time. The capacity of the dual polarized MIMO channel is evaluated and compared to the capacity of a single polarized array.
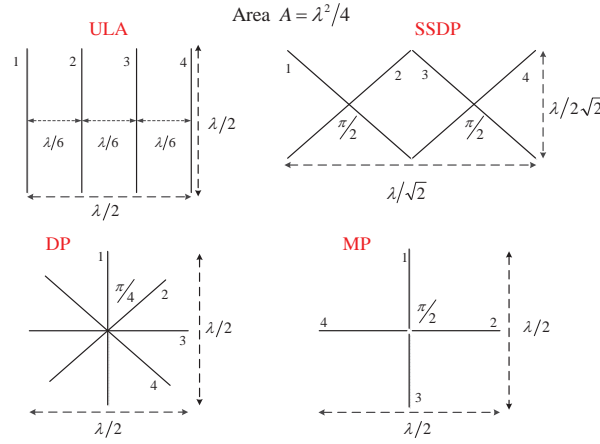
Figure 3.6: Antenna configurations with four elements.

A channel model for M_R receive antennas and a single transmit antenna is given by

$$\mathbf{H} = (\mathbf{P}_{M_R \times 2}\mathbf{G}_{2 \times 2}\mathbf{X}_{2 \times 1}) \odot \left(\mathbf{R}_{M_R \times M_R}^{1/2}\mathbf{U}_{M_R \times 1}\right), \tag{3.28}$$

where

$$\mathbf{P}_{M_R \times 2} = \begin{bmatrix} \cos(\theta_p + \varphi_1) & \sin(\theta_p + \varphi_1) \\ \cos(\theta_p + \varphi_2) & \sin(\theta_p + \varphi_2) \\ \vdots & \vdots \\ \cos(\theta_p + \varphi_{M_R}) & \sin(\theta_p + \varphi_{M_R}) \end{bmatrix},$$

represents the orientation/rotation of the array and the dual polarized nature of each receive antenna element. The $\odot$ operator defines a scalar multiplication [49]. Here, θ_p is the orientation or rotation of the array in space and φ_n is the orientation of individual antenna elements respect to each other and defined in the next section.

$$\mathbf{G}_{2 \times 2} = \begin{bmatrix} G_C(\phi) & G_X(\phi) \\ -G_X(\phi) & G_C(\phi) \end{bmatrix},$$

is the gain matrix at azimuth angle ϕ, $G_C(\phi)$ is the co-polar gain pattern and $G_X(\phi)$ is the cross polar component. This matrix depicts the pattern diversity effect.

$$\mathbf{X}_{2 \times 1} = \begin{bmatrix} \sqrt{1-\alpha} & \sqrt{\alpha} \end{bmatrix}^{\mathrm{T}},$$

represents the XPD matrix defined in [49], [53], [52] where $0 \le \alpha \le 1$ is the amount of power transfered from one antenna element to another. The antenna XPD is specified earlier. We assume here an equal antenna XPD loss between each pair of antenna elements. However, the study of a variable XPD loss could also be an interesting work for the future. Here, $\mathbf{U}_{M_R \times 1}$ is the matrix containing i.i.d. complex Gaussian fading coefficients and $\mathbf{R}_{M_R \times M_R}$ is the normalized correlation matrix. This matrix is calculated according to the results taken from [61]. The matrix representing the pattern diversity is ignored here for simplification as we consider an omni-directional azimuth gain pattern for both orthogonal components. Therefore here, we only consider the effects of polarization diversity. Hence the model given in Equation (3.28) can be simplified to

$$\mathbf{H} = (\mathbf{P}_{M_R \times 2}\mathbf{X}_{2 \times 1}) \odot \left(\mathbf{R}_{M_R \times M_R}^{1/2}\mathbf{U}_{M_R \times 1}\right). \tag{3.29}$$

The basic transmission system with receive antenna selection is given in Figure 3.1. The maximum mutual information is given by

$$C = \log_2 \det\left(\mathbf{I} + \frac{\gamma}{N_T}\mathbf{H}\mathbf{H}^{\mathrm{H}}\right), \tag{3.30}$$

where N_T is the number of transmit antennas and γ is the mean signal to noise ratio. The performance with receive antenna selection is calculated by selecting those rows of channel matrix $\mathbf{H}$ which have the maximum Frobenius norm and then calculating the maximum mutual information. Thus previous equation with receive antenna selection becomes

$$C_\Lambda = \log_2 \det\left(\mathbf{I}_\Lambda + \frac{\gamma}{N_T}\mathbf{H}_\Lambda\mathbf{H}_\Lambda^{\mathrm{H}}\right), \tag{3.31}$$

where Λ denotes the receive antenna subset.

3.6 Correlation in Antenna Arrays

(a) Spatial correlation function.   (b) Angular correlation function.
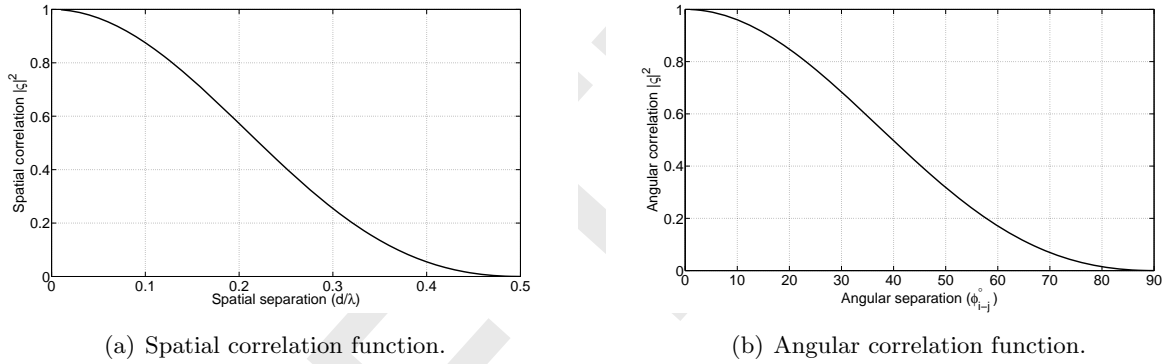
Figure 3.7: Correlation functions in Antenna Arrays.

The spatial correlation between two consecutive identical antennas can be found in [61], given as

$$\varsigma_r = \sin(z_s)/z_s, \tag{3.32}$$

and its power is presented in Figure 3.7(a), where $z_s = 2\pi d_r/\lambda$ and d_r is the inter-element distance. The correlation function between antenna elements separated by an angular displacement is established by an equivalence between angular and spatial separation. This is called true polarization diversity [59] and shown below as

$$\varsigma_a = \sin(z_a)/z_a, \tag{3.33}$$

where $z_a = 2\pi\theta_r$. For a small number of receiving antennas and under Rayleigh fading scenarios the angular separation θ_r can be made equivalent to a spatial separation by

$$\theta_r = \varphi_{i-j}/180°, \tag{3.34}$$

where $\varphi_{i-j} = \varphi_i - \varphi_j$ is the angular difference between two dipoles, and φ_i and φ_j are the orientation angles of dipoles i and j with respect to vertical axis. The power of angular correlation function is shown in Figure 3.7(b).

3.7 Geometrical Considerations of Antenna Array Configurations

The model presented in the previous section was applied to the four configurations as shown in Figure 3.6. Each configuration contains four antenna elements arranged in a different way. The total area or aspect ratio was kept constant so as to have a fair comparison in terms of performance. Selection of antenna subsets is performed on the basis of the maximum Frobenius norm of rows of channel matrices. For the sake of simplicity we ignore the effects of mutual coupling [68] between the ports of antenna elements. The first array is the most common setting with spatially separated dipole arrays spaced equally apart with inter-element distance of $\lambda/6$, also called Uniform Linear Array. The second configuration contains a pair of cross dipoles. The centers of the dipoles are separated by a distance of $\lambda/(2\sqrt{2})$. This configuration is named as Spatially Separated Dual Polarized (SSDP) arrays. In the third configuration we have an arrangement of dipoles whose centers or feed points are co-located with no inter-element distance. All the dipoles are separated with an angular displacement as defined in the previous section. The configuration is called N-Spoke Dipole Array (DP) here. The last configuration contains an array of monopoles whose edges are co-located. We have assumed here that the ground planes for each monopole are somehow separated from each other, named N-Spoke Monopole Array (MP) here. The correlations are defined again according to the angular displacement rather than spatial. Dipoles and monopoles mentioned in the last three configurations produce various patterns due to slant angles hence introducing both pattern and polarization diversity, but here for the sake of simplicity we assume only polarization diversity. In all of this chapter we consider a single vertical antenna at the transmit side. Extension to multiple transmit antennas with various transmission strategies can also be exploited. As an explanation of the construction of the correlation matrix $\mathbf{R}_{M_R \times M_R}$ we take the example of a spatially separated cross dipole array. The angular separation between each pair of dipoles is $\varphi = 90°$. $\varphi_{1-2} = \varphi_1 - \varphi_2 = \varphi_{3-4} = \varphi_3 - \varphi_4 = 90°$. And $d_1 = \varphi_{1-2}/180° = d_2 = \varphi_{3-4}/180° = 1/2$. The angular correlation coefficients $\varsigma = \sin(z_a)/z_a = 0$. As the pairs are separated by a spatial distance of $\lambda/(2\sqrt{2})$, the spatial correlation coefficient is given by $\varsigma = \sin(\pi/\sqrt{2})/(\pi/\sqrt{2}) = 0.3582$. The total normalized correlation matrix is given by the Kronecker product of two correlation matrices $\mathbf{R}_{\text{SSDP}} = \mathbf{R}_{\text{sp}}^{1/2} \otimes \mathbf{R}_{\text{cp}}^{1/2} / \left\| \mathbf{R}_{\text{sp}}^{1/2} \otimes \mathbf{R}_{\text{cp}}^{1/2} \right\|$ with

$$\mathbf{R}_{\text{sp}} = \begin{bmatrix} 1 & 0.3582 \\ 0.3582 & 1 \end{bmatrix}, \tag{3.35}$$

and

$$\mathbf{R}_{\text{cp}} = \begin{bmatrix} 1 & 0 \\ 0 & 1 \end{bmatrix}, \tag{3.36}$$

where $\mathbf{R}_{\text{cp}}$ and $\mathbf{R}_{\text{sp}}$ are the correlation matrices for cross dipoles and spatially separated dipoles, respectively. The complete matrix is given below.

$$\mathbf{R}_{\text{SSDP}} = \begin{bmatrix} 0.844 & 0 & 0.156 & 0 \\ 0 & 0.844 & 0 & 0.156 \\ 0.156 & 0 & 0.844 & 0 \\ 0 & 0.156 & 0 & 0.844 \end{bmatrix}, \tag{3.37}$$

3.8 Theoretical Analysis and Simulation Results

In order to find the algebraic expressions we analyze effective channel gains on the example of monopoles. The same procedure can be adopted for other configurations. The theoretical work presented here is along the sames lines as in [69]. In [69] only one structure of an antenna array was analyzed. The model for a generic $1 \times M_R$ SIMO system with MRC was explained in Section 3.2.1. We follow the same procedure along with the Equations (3.1)-(3.6) and apply them for all types of antenna arrays. As an example the channel matrix for 1×4 SIMO, following the model defined in Equation (3.29) is given by

$$\mathbf{h}_{4\times 1} = \begin{bmatrix} h_1\left(\sqrt{1-\alpha}\cos(\phi_1) + \sqrt{\alpha}\sin(\phi_1)\right) \\ h_2\left(\sqrt{1-\alpha}\cos(\phi_2) + \sqrt{\alpha}\sin(\phi_2)\right) \\ h_3\left(\sqrt{1-\alpha}\cos(\phi_3) + \sqrt{\alpha}\sin(\phi_3)\right) \\ h_4\left(\sqrt{1-\alpha}\cos(\phi_4) + \sqrt{\alpha}\sin(\phi_4)\right) \end{bmatrix}, \tag{3.38}$$

where $\phi_n = \theta + \varphi_{i-j}$ and φ_{i-j} is defined in Equation (3.34) earlier. The channel coefficients h_1, h_2, h_3, h_4 contain the effects of correlation, calculated from Equation (3.32) and Equation (3.33) for various antenna configurations. As we have realized an MRC receiver, we sum the squares of the channel coefficients for each row of the channel matrix in Equation (3.38) and take the average over all realizations. The effective channel gain is then shown by Equation (3.41). We analyze $1/4$ and $l_r/4$ RAS with polarization next. We start by selecting $l_r = 1$ out of 4 from the channel matrix given by Equation (3.38), with the largest norm, $\bar{n} \in [1, 2, 3, 4]$ being the index of the selected antenna element. The corresponding channel coefficient $h_{1/4}$ becomes a scalar.

$$h_{1/4} = \left[h_{\bar{n}}\left(\sqrt{1-\alpha}\cos\left(\phi_{\bar{n}}\right) + \sqrt{\alpha}\sin\left(\phi_{\bar{n}}\right)\right) \right], \tag{3.39}$$

The effective channel gain is expressed in Equation (3.42) and an approximate value in Equation (3.43). A similar matrix $\mathbf{h}_{l_r/4} = [h_1, h_2, h_3, h_4]^T$ can be constructed, containing only the channel coefficients of the l_r selected antenna elements, indices of which would be from an ordered set given by $(\mathcal{S}_{l_r}) = \{n; \|h_n\|_F > \|h_{l_r+1}\|_F\} = [n_1, n_2, \cdots, n_{l_r}]$. The new channel matrix with $l_r/4$ selection is then given by

$$\mathbf{h}_{l_r/4} = \begin{bmatrix} h_{n_1}\left(\sqrt{1-\alpha}\cos(\phi_1) + \sqrt{\alpha}\sin(\phi_1)\right) \\ h_{n_2}\left(\sqrt{1-\alpha}\cos(\phi_2) + \sqrt{\alpha}\sin(\phi_2)\right) \\ h_{n_3}\left(\sqrt{1-\alpha}\cos(\phi_3) + \sqrt{\alpha}\sin(\phi_3)\right) \\ h_{n_4}\left(\sqrt{1-\alpha}\cos(\phi_3) + \sqrt{\alpha}\sin(\phi_4)\right) \end{bmatrix}, \tag{3.40}$$

For a monopole configuration, the correlation matrix $\mathbf{R} = \mathbf{I}$, because all $\varsigma_a = 0$ from Equation (3.33). The channel gains are dependent, both on rotation and XPD. Here, for the sake of simplicity we do average only over rotation while keeping $\alpha = 0$. The same analysis can be performed for other values of α and then averaged. Now for $1/4$ RAS we do the following. As $E\left\|h_1^2\right\| = E\left\|h_2^2\right\| = E\left\|h_3^2\right\| = E\left\|h_4^2\right\| = 1$ for Rayleigh fading channels, we deduce the following inequality from an approximation of Equation (3.43). We solve it for $\alpha = 0$ and obtain $\cos^2\theta_p > \cos^2\left(\theta_p + \frac{\pi}{2}\right) > \cos^2\left(\theta_p + \frac{2\pi}{2}\right) > \cos^2\left(\theta_p + \frac{3\pi}{2}\right)$. This results in the interval $0 < \theta_p < \frac{\pi}{4}$ so

$$G_{1/4,\alpha=0} = \frac{4}{\pi}\int_0^{\frac{\pi}{4}} \left(\cos^2\theta_p\right) d\theta_p = 0.8183.$$

Similarly solving for $2/4$ RAS we have $\cos^2\left(\theta_p + \frac{\pi}{2}\right) > \cos^2\left(\theta_p + \frac{2\pi}{2}\right) > \cos^2\left(\theta_p + \frac{3\pi}{2}\right)$. We obtain the interval as $\frac{\pi}{4} < \theta_p < \frac{\pi}{2}$. We have

$$G_{M_R/M_R}(\theta_p) = \sum_{n=1}^{M_R} E\left[|h_n|^2 \left(\sqrt{1-\alpha}\cos\left(\theta_p + \frac{(n-1)2\pi}{M_R}\right) + \sqrt{\alpha}\sin\left(\theta_p + \frac{(n-1)2\pi}{M_R}\right)\right)^2\right]. \tag{3.41}$$

$$G_{1/M_R}(\theta_p) = E\left[\max\left\{|h_1|^2\left(\sqrt{1-\alpha}\cos\left(\phi_1\right) + \sqrt{\alpha}\sin\left(\phi_1\right)\right)^2, \cdots, |h_{M_R}|^2\left(\sqrt{1-\alpha}\cos\left(\phi_{M_R}\right) + \sqrt{\alpha}\sin\left(\phi_{M_R}\right)\right)^2\right\}\right]. \tag{3.42}$$

$$G_{1/M_R}(\theta_p) \approx \max\left\{E\left[|h_1|^2\right]\left(\sqrt{1-\alpha}\cos\left(\phi_1\right) + \sqrt{\alpha}\sin\left(\phi_1\right)\right)^2, \cdots, E\left[|h_{M_R}|^2\right]\left(\sqrt{1-\alpha}\cos\left(\phi_{M_R}\right) + \sqrt{\alpha}\sin\left(\phi_{M_R}\right)\right)^2\right\}. \tag{3.43}$$

$$G_{3/4,\alpha=0} = \frac{4}{\pi}\int_0^{\frac{\pi}{4}}\left(\cos^2\theta_p\right)d\theta_p + \frac{4}{\pi}\int_{\frac{\pi}{4}}^{\frac{\pi}{2}}\cos^2\left(\theta_p + \frac{\pi}{2}\right)d\theta_p + \frac{4}{\pi}\int_{\frac{\pi}{4}}^{\frac{\pi}{2}}\cos^2\left(\theta_p + \frac{3\pi}{2}\right)d\theta_p = 1.83. \tag{3.44}$$

$$G_{M_R/M_R} = \frac{2}{\pi}\int_0^{\frac{\pi}{2}}\left[\sum_{n=1}^{M_R} E\left\{|h_n|^2\left(\sqrt{1-\alpha}\cos\left(\theta_p + \frac{(n-1)2\pi}{M_R}\right) + \sqrt{\alpha}\sin\left(\theta_p + \frac{(n-1)2\pi}{M_R}\right)\right)^2\right\}\right]d\theta_p. \tag{3.45}$$

$$G_{2/4,\alpha=0} = \frac{4}{\pi}\int_0^{\frac{\pi}{4}}\left(\cos^2\theta_p\right)d\theta_p + \frac{4}{\pi}\int_{\frac{\pi}{4}}^{\frac{\pi}{2}}\cos^2\left(\theta_p + \frac{\pi}{2}\right)d\theta_p = 1.628.$$

Calculating in the similar fashion we have for 3/4 RAS shown in Equation (3.44). For full complexity SIMO we have the relation depicted in Equation (3.45). The theoretical results for the case of monopole configuration are compared with the simulation in Figure 3.8(a). Analysis with the same method for other configurations can be easily performed but not shown here due to space limitations.

Simulation results are shown in terms of mutual information, both with and without receive antenna selection. Here, l_r is the number of antennas to be selected and l_r is the total number of antennas available. Also, l_r/M_R denotes the selection of l_r antenna elements out of M_R elements. The results are shown for various performance parameters. The two most important parameters are the XPD and the rotation. In the figures shown next we display the results from simulations considering these parameters. In Figure 3.8(b) we show the comparison between the configurations of Figure 3.6. We show the performance for a full complexity system as well as for receive antenna selection. From the figure we observe that the configuration with monopole structure has the maximum mutual information when used in conjunction with selection. Construction of such array is practically very difficult but due to very less angular correlation, it performs better compared to other structures. For a full complexity system, the Spatially Separated Dual Polarized (SSDP) configuration performs better. Although for a Uniform Linear Array (ULA) the mutual information increases while increasing l_r but the performance degrades for values of 3/3 and 4/4 full complexity system. This is due to inter-element distance becoming less than $\lambda/2$. In the Figure 3.9(a) we compare 2/4 selection for various antenna configurations. Non-Antenna Selection (NAS) in the simulation represents a full complexity system with no antenna selection. From the figure we observe that the mutual information of a Uniform Linear Array (ULA) is strongly deteriorated by a decrease in the XPD. The performance of both monopole and dipole structure is similar. The mutual information decreases for decreasing XPD but again increases for lower values of XPD. Thus all the structures other than ULA, are robust to power imbalance between dual polarized antenna elements. In Figure 3.9(b) we compare a 2/4 selection for various antenna configurations by varying the orientation angle of the structures. We observe from the figure that again the ULA is effected by the orientation angle and other structures are almost insensitive to the change in orientation. From the previous two figures we also observe that mutual information depends both on array orientation as well as XPD. In Figures 3.10(a), 3.10(b), 3.10(c), 3.10(d) we show the mutual information with selection for various configurations and its dependence on
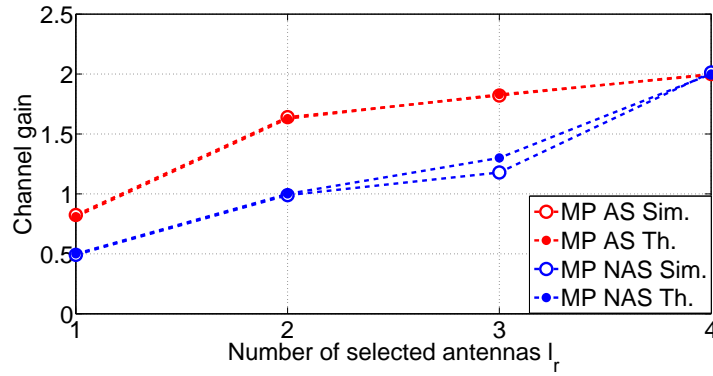
(a) Comparison of monopole array with $l_r/4$ selection and M_R/M_R full complexity array at 30 dB SNR.
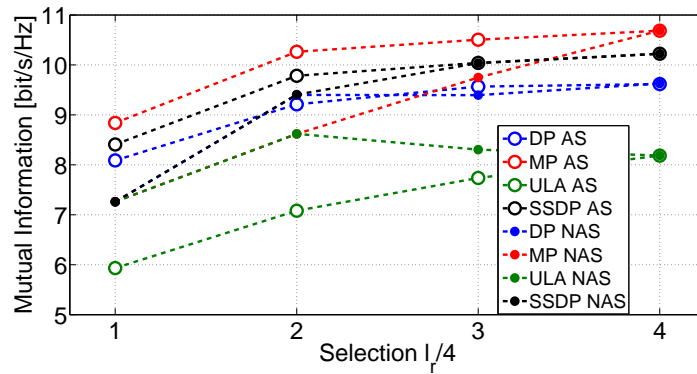
(b) Comparison of antenna configurations with $l_r/4$ receive antenna selection at 30 dB SNR and averaged over 90° rotation.

Figure 3.8: Performance comparison of antenna configurations.

both XPD and orientation. The variation of mutual information in dipole configuration is very small when compared to the monopole structure, but its behavior is different. The dipole configuration has four minimum and maximum contour lines. The monopoles have three maximum and two minimum contours. The variation along rotation and XPD for SSDP configuration is opposite to monopole configurations with two maximum and three minimum contour lines. The ULA configuration is badly effected by higher values of both rotation and XPD. The performance degrades quickly after the values of $\alpha = 0.6$ and $\psi = 60^o$. From Figure 3.8(b) we see that the arrangement with monopoles shows the best performance with antenna selection. This is because the selection process always selects either Antenna 1 or 3 in case of 1/4 selection, which are highly un-correlated. Its performance is better in average as compared to dipole configuration because for dipole, always Antenna 1 is selected, which is always vertical oriented. The performance of the SSDP configuration is better than dipoles because on average, either Antennas 1 or 3 is selected which are both inclined by 45° and also spatially separated. The ULA performs the worst as all the antenna are selected on average. The same intuitive reasoning can be applied for the 2/4 and 3/4 selection. The performance is different for full complexity systems on the average. As an example if we take a three antenna full complexity system, SSDP reveals the best performance because it is constructed from two orthogonal antennas with an additional spatially separated and 45°inclined antenna. The mutual information for monopoles is slightly better than
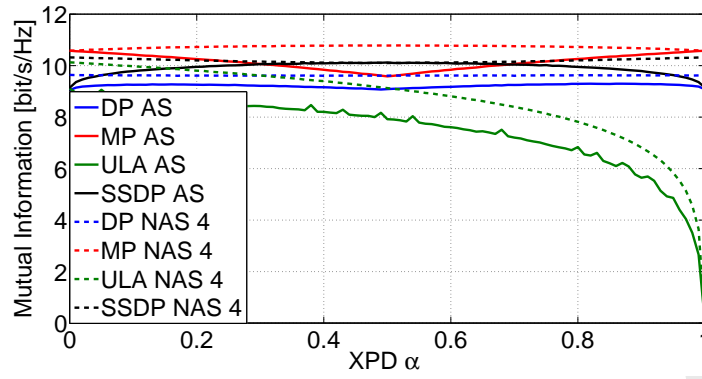
(a) Comparison of antenna configurations with 2/4 selection with varying XPD
at 30 dB SNR and $\Psi = 0$.
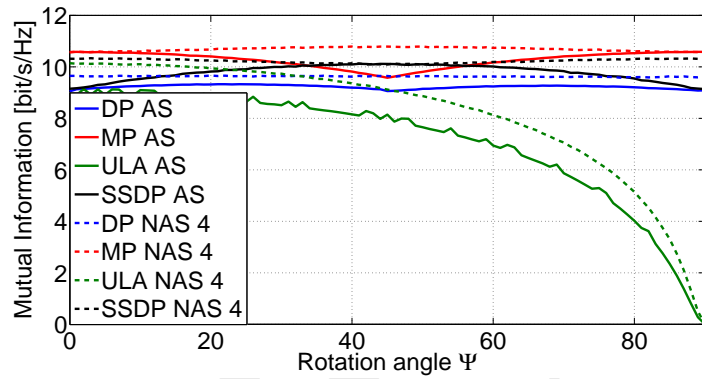
(b) Comparison of antenna configurations with 2/4 selection with varying
rotation at 30 dB SNR and $\alpha = 0$.

Figure 3.9: Performance comparison of antenna configurations with XPD and rotation.

that of a dipole arrangement because all the three antennas are separated $90°$ apart compared to $60°$ separation for a dipole configuration. The ULA performance is degraded due to decreasing spatial distance and hence an increase in correlation.

3.9   Polarized MIMO Transmissions with Mutual Coupling

In this section we compare two different antenna array configurations, the linear array and N-Spoke by including the effects of mutual coupling at the receive side. The antenna configurations are depicted in Figure 3.6. Methods to calculate mutual coupling effects in linear antenna array configurations and N-Spoke configurations are shown. We also show the effect of inter-element separation on mutual coupling in side-by-side antenna arrays. Similarly we show the effect of angular separation on the overall mutual coupling in N-Spoke configurations. We calculate the capacity bounds for systems with simple receive antenna selection methods. We discuss the simulation results and a comparison with the theoretical bounds is given. The effect of varying XPD and orientation of antenna arrays on the performance is given.
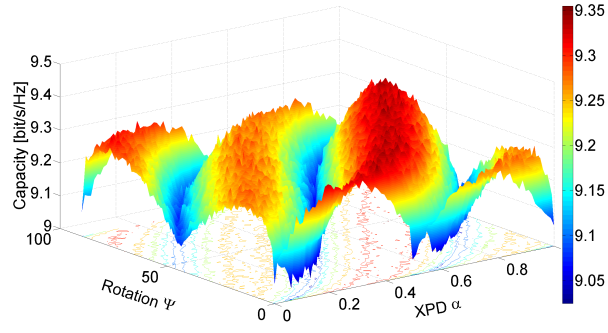
(a) Dipole antenna (DP) with 2/4 selection with varying rotation and XPD at 30 dB SNR.
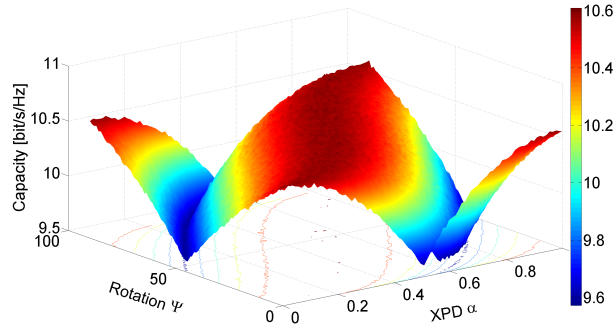
(b) Monopole antenna (MP) with 2/4 selection with varying rotation and XPD at 30 dB SNR.
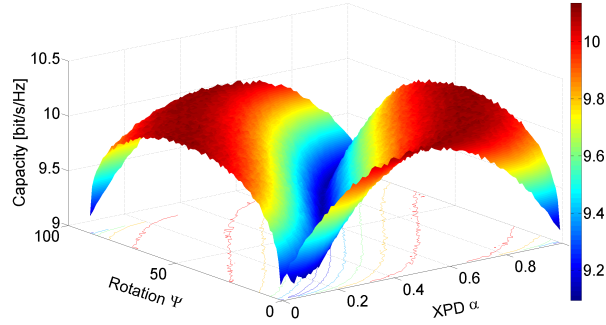
(c) Spatially Separated Dual Polarized antenna (SSDP) with 2/4 selection with varying rotation and XPD at 30 dB SNR.
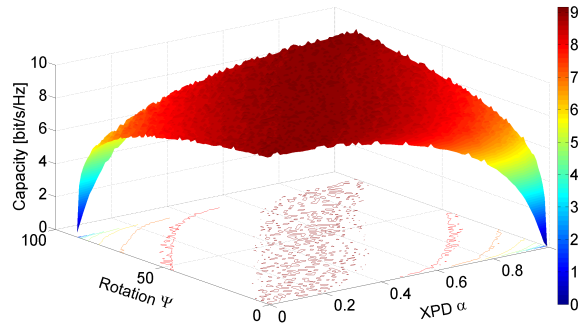
(d) Uniform Linear Array antenna (ULA) with 2/4 selection with varying rotation and XPD at 30 dB SNR.

Figure 3.10: Performance comparison of antenna configurations with combined XPD and rotation.

3.9.1   MIMO Channel Model with Mutual Coupling

A channel model for M_R receive antennas and a single transmit antenna is given by

$$\mathbf{H} = \left(\mathbf{P}_{M_R \times 2} \mathbf{G}_{2 \times 2} \mathbf{X}_{2 \times 1} \right) \odot \left(\mathbf{C}_{M_R \times M_R} \mathbf{R}^{1/2}_{M_R \times M_R} \mathbf{U}_{M_R \times 1} \right), \tag{3.46}$$

where

$$\mathbf{P}_{M_R \times 2} = \begin{bmatrix} \cos(\theta_p + \varphi_1) & \sin(\theta_p + \varphi_1) \\ \cos(\theta_p + \varphi_2) & \sin(\theta_p + \varphi_2) \\ \vdots & \vdots \\ \cos(\theta_p + \varphi_{M_R}) & \sin(\theta_p + \varphi_{M_R}) \end{bmatrix}, \tag{3.47}$$

represents the orientation/rotation of the array and the dual polarized nature of each receiving antenna element. The $\odot$ operator defines an element-wise scalar multiplication [49]. Here, θ_p is the orientation or rotation of the array in space and φ_n is the orientation of individual antenna elements with respect to the vertical oriented antenna element taken as reference.

$$\mathbf{G}_{2 \times 2} = \begin{bmatrix} G_C(\phi) & G_X(\phi) \\ -G_X(\phi) & G_C(\phi) \end{bmatrix}, \tag{3.48}$$

is the gain matrix at azimuth angle ϕ, $G_C(\phi)$ denotes the co-polar gain pattern and $G_X(\phi)$ is the cross polar component. This matrix depicts the pattern diversity effect.

$$\mathbf{X}_{2 \times 1} = \begin{bmatrix} \sqrt{1-\alpha} & \sqrt{\alpha} \end{bmatrix}^{\mathrm{T}}, \tag{3.49}$$

represents the XPD matrix defined in [49, 52, 53] where $0 \leq \alpha \leq 1$ is the fraction of power transferred from one antenna element to another. The antenna XPD is specified earlier. The matrix $\mathbf{U}_{M_R \times 1}$ contains i.i.d complex Gaussian fading coefficients and $\mathbf{R}_{M_R \times M_R}$ is the normalized correlation matrix. This matrix is calculated according to the results taken from [61]. The coupling matrix $\mathbf{C}_{M_R \times M_R}$ represents the mutual coupling between closely spaced antenna elements. The details of the construction of this matrix will be elaborated in Section 3.9.3. The difference in Equation (3.28) and Equation (3.46) is only this coupling matrix. Matrix $\mathbf{G}_{2 \times 2}$, representing the pattern diversity, is ignored here for simplification as we consider an omni-directional azimuth gain pattern for both orthogonal components, thus $\mathbf{G}_{2 \times 2} = \mathbf{I}$. The model given in Equation (3.46) can thus be simplified to

$$\mathbf{H} = \left(\mathbf{P}_{M_R \times 2} \mathbf{X}_{2 \times 1} \right) \odot \left(\mathbf{C}_{M_R \times M_R} \mathbf{R}^{1/2}_{M_R \times M_R} \mathbf{U}_{M_R \times 1} \right). \tag{3.50}$$

Although the channel model defined above consists of a single transmit antenna and multiple receive antennas, the inclusion of dual-polarized antennas makes it a MIMO channel with diversity two on the transmit side, rather than a SIMO channel. We thus refer to it as MIMO throughout the chapter. To separate the mutual coupling and correlation effect we rewrite Equation (3.50)

$$\begin{aligned} \mathbf{H} &= \left(\mathbf{P}_{M_R \times 2} \mathbf{X}_{2 \times 1} \right) \odot \mathbf{C} \mathbf{R}^{1/2} \mathbf{U} \\ &= \left(\mathbf{P}_{M_R \times 2} \mathbf{X}_{2 \times 1} \right) \odot \mathbf{C} \mathbf{H}_{\mathrm{nc}}, \end{aligned} \tag{3.51}$$

Here, we have defined $\mathbf{H}_{\mathrm{nc}} = \mathbf{R}^{1/2} \mathbf{U}$, where the subscript nc denotes non-mutual coupling. The elements of the matrix $\mathbf{R}$ are taken from Equation (3.52) defined later. We have also removed the dimensions of the matrices $\mathbf{H}_{\mathrm{nc}}$ and $\mathbf{C}$ for easier notation. The model presented in the previous section
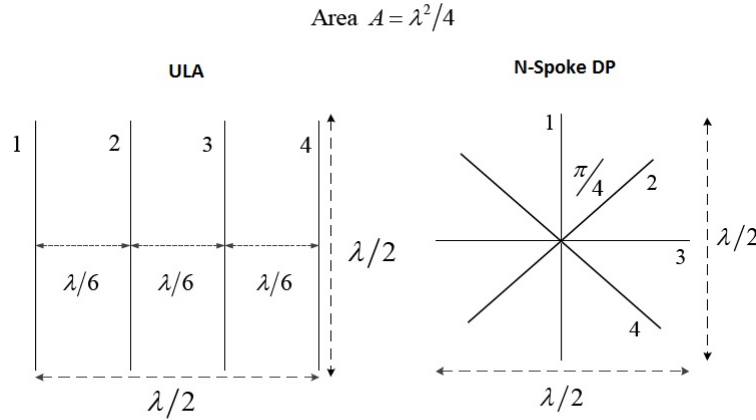
Figure 3.11: Antenna configurations with four elements.

was applied to the two configurations shown in Figure 3.11. The aspect ratio was kept the same for both structures as to have a fair comparison in terms of performance. The first array is the most common setting with spatially separated dipoles spaced equally apart. In the second configuration we have an arrangement of dipoles whose centers or feed points are co-located with no inter-element distance. All the dipoles are separated with an angular displacement. We define L_t and L_r as the aperture lengths for transmitter and the receiver side. In particular, we are more interested in the case where the aperture size is fixed to $\lambda/2$, which corresponds to the space limitation of the User Equipment (UE). We denote l as the dipole length, r as the dipole radius, and d_r as the side-by-side distance between the adjacent dipoles at the receiver side. Thus, we have $d_r = L_r/(M_R - 1)$. For angular systems we have a fixed aperture size of $\lambda/2$ with an angular separation of $\theta_r = 180/M_R$. The inter-element distance d_r largely depends on the radius r of the dipole. This limits the total number of antennas that can be stacked in given aperture size. From [70] and [71] the practical measure for r is given to be 0.025λ. Thus, a maximum of nine antenna elements can be stacked in such configurations. For fair comparison we use nine antenna elements for the N-Spoke configuration as well. The radiation patterns of all the elements in a side-by-side configuration is constant. In the N-Spoke structure the dipoles produce different patterns due to slant angles hence introducing both pattern and polarization diversity, but here for the sake of simplicity we assume only polarization diversity.

3.9.2   Combined Correlation Model

We us he combined spatial-polarization correlation function as given in [72] is a separable function of space d_r and angle θ_r variables, shown below

$$\varsigma(d_r, \theta_r) = \operatorname{sinc}(kd_r)\cos\theta_r. \tag{3.52}$$

If we have a side-by-side configuration, $\varsigma_r = \operatorname{sinc}(kd_r)$ and $\varsigma_a = \cos\theta_r$ for the angular separated configuration. We use these simple models in order to describe correlation values. Depending upon the type of structure used, i.e., spatial or angular, we compute the values from Equation (3.52) and use these values to construct the correlation matrix $\mathbf{R}$ in Equation (3.51).
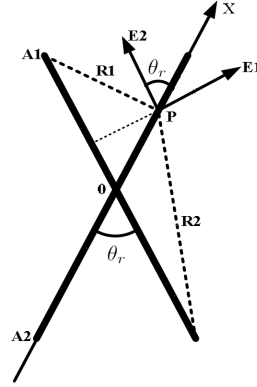
Figure 3.12: Angular antenna array.

3.9.3   Mutual Coupling for Angularly Spaced Antenna

Let us now return to the mutual coupling matrix $\mathbf{C}$ from Equation (3.51). The mutual coupling effects for a pair of co-located dipole antennas as displayed in Figure 3.12 separated by an angle θ_r are presented in [73]. We extend this model of two antennas to M_R antenna elements. For spatial systems we formulate the mutual coupling effects as described in the existing models [74–77] and the references within. The mutual coupling in an array of co-linear side-by-side wire dipoles can be modeled using the theory described in [78,79]. Assuming the array is formed by M_R wire dipoles, the coupling matrix can be calculated using the following relationship involving the mutual coupling matrix [75] as,

$$\mathbf{C} = (Z_A + Z_T)(\mathbf{Z}_r + Z_T \mathbf{I}_{M_R})^{-1}, \tag{3.53}$$

where Z_A is the antenna impedance in isolation, for example, when the wire dipole is $\lambda/2$, its value is $Z_A = 73 + j42.5\Omega$ [74]. The impedance Z_T at each receiver element is chosen as the complex conjugate of Z_A to obtain the impedance match and maximum power transfer. The mutual impedance matrix $\mathbf{Z}_r$ is given by

$$\mathbf{Z}_r = \begin{bmatrix} Z_A + Z_T & Z_{12} & \cdots & Z_{1M_R} \\ Z_{21} & Z_A + Z_T & \cdots & Z_{2M_R} \\ \vdots & \vdots & \ddots & \vdots \\ Z_{M_R 1} & Z_{M_R 2} & \cdots & Z_A + Z_T \end{bmatrix}. \tag{3.54}$$

Note that this expression provides the circuit representation for mutual coupling in array antennas. It is valid for single mode antennas. The wire dipoles assumed here fall into this category. For a side-by-side array configuration of wire dipoles having length l equal to 0.5λ, the expressions for Z_{mn} can be adapted from [77] and [78]. The mutual impedance matrix $\mathbf{Z}_r$ is a function of the dipole length l, the antenna spacing d_r, angular spacing θ_r, and the antenna placement configurations. To calculate the mutual coupling between antenna structures, separated by an angular displacement we refer to work in [70,73]. A layout of two antennas in cross-polarized configuration is shown in Figure 3.12. We now calculate the mutual coupling of two antenna elements separated by any cross-angle, and then generalize them to the N-Spoke configuration with M_R antennas. In Figure 3.12 the elements $A1$ and $A2$ represent two fine half-wavelength dipole antennas each with length of $2l$ where $l = \lambda/4$ as explained in [73]. We also assume here that both of these antenna elements are in the same plane. The common

point of these two antennas is located at the origin of the coordinate system. The angular displacement is given by θ_r. From Figure 3.12 we observe two mutually orthogonal electric field components E1 and E2 at the point P of antenna $A2$, which are generated by the current flowing into $A1$. These electric field components, from the geometry, can be expressed as [73]:

$$\mathsf{E1} = j30I_m \left[\frac{x\cos\theta_r - l}{x\sin\theta_r} \frac{e^{-jkR1}}{R1} + \frac{x\cos\theta_r + l}{x\sin\theta_r} \frac{e^{-jkR2}}{R2} - 2\cot\theta_r\cos kl\frac{e^{-jkx}}{x} \right], \tag{3.55}$$

$$\mathsf{E2} = j30I_m \left[\frac{e^{-jkR1}}{R1} + \frac{e^{-jkR2}}{R2} - 2\cos kl\frac{e^{-jkx}}{x} \right], \tag{3.56}$$

where $R1$ is the distance between the upper end point of $A1$ and the P-point, given by $R1 = \sqrt{(x\sin\theta_r)^2 + (l - x\cos\theta_r)^2}$, and $R2 = \sqrt{(x\sin\theta_r)^2 + (l + x\cos\theta_r)^2}$ is the distance between the lower end point of $A1$ and the P-point. Here, x is the distance between the center of $A2$ and the P-point, I_m the maximum current value at $A2$, $k = 2\frac{\pi}{\lambda}$, and λ is the carrier wavelength. The electric field vector $\mathbb{E}$ at the P-point along with X-axis is given by

$$\mathbb{E} = \mathsf{E1}\sin\theta_r + \mathsf{E2}\cos\theta_r. \tag{3.57}$$

The current distribution at dipole $A2$ is given by

$$I_2 = I_m \sin\left[k(l - x)\right]. \tag{3.58}$$

According to the definition given in [70], the mutual impedance between $A1$ and $A2$ can be calculated as

$$Z_{12} = \frac{1}{\sin^2(kl)} \int_{-l}^{l} \frac{\mathbb{E}}{I_m} \sin\left[k(l - x)\right] dx. \tag{3.59}$$

Since $A1$ and $A2$ are two fine half-wavelength dipole antennas, that is, $l = \frac{\lambda}{4}$, we have

$$Z_{12} = \int_{-l}^{l} \frac{\mathbb{E}}{I_m} \sin\left[k(l - x)\right] dx. \tag{3.60}$$

The above equation is the desired expression of the mutual impedance. For the self impedances of A1 and A2, the expression in [71] is used. The effect of angular displacement θ_r on the mutual coupling for a co-located polarized pair of antennas is shown in Figure 3.13(a). We observe that $\Re\{Z_{mn}\}$ for angularly separated systems decreases monotonically with increasing angle, varying from almost 76Ω to -76Ω from maximum to minimum, while the imaginary part remains basically zero. The effect of spatial displacement d_r on the mutual coupling for a pair of spatially separated antennas is displayed in Figure 3.13(b). For spatially separated systems, $\Re\{Z_{mn}\}$ has a different behavior than the angularly separated system and achieves its minimum at approximately $d_r = 0.65\lambda$. The $\Im\{Z_{mn}\}$ has a minimum at $d_r = 0.4\lambda$.

3.10   Receive Antenna Selection with Mutual Coupling

The basic transmission system with receive antenna selection is depicted in Figure 3.1. The performance of this MIMO system is calculated on the basis of maximum mutual information. Assuming the Channel
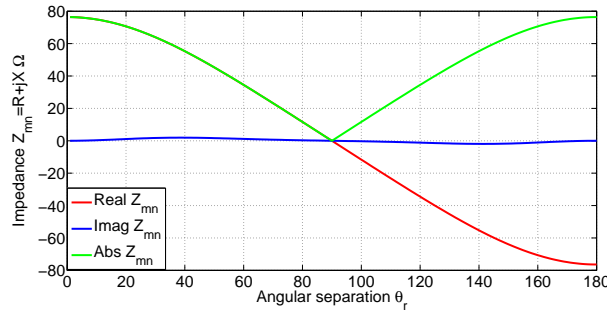
(a) Variation of mutual impedance Z_{mn} from Equation (3.60) with variable angular separation θ_r in an N-Spoke configuration.
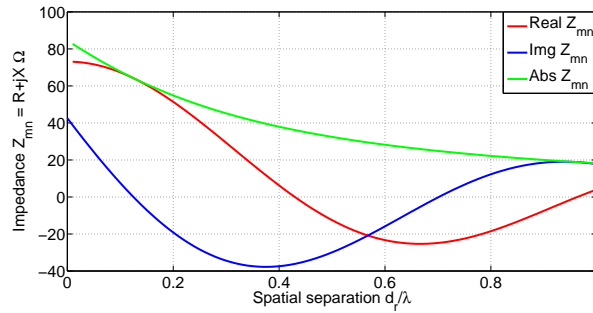
(b) Variation of mutual impedance Z_{mn} from Equation (3.60) with variable spatial separation d_r/λ in a ULA configuration.

Figure 3.13: Mutual impedance in antenna configurations.

State Information (CSI) is known to the receiver but unknown to the transmitter, and that the transmit power P is evenly distributed among the antennas, the mutual information [80] for a given channel realization is given by

$$C(\mathbf{H}) = \log_2 \det\left(\mathbf{I}_{M_R} + \frac{\gamma}{N_T}\mathbf{H}\mathbf{H}^\dagger\right), \tag{3.61}$$

where N_T is the number of transmit antennas, γ is the average SNR at each receiver branch and $\frac{P}{\sigma_n^2}$. The mutual information is in the units of (bit/s/Hz). The performance with receive antenna selection is calculated by selecting those l_r out of M_R receive antennas that maximize the Frobenius norm for a given channel realization. In other words we select those rows of the channel matrix $\mathbf{H}$ which have the maximum norm and then calculate their mutual information. Thus, the previous equation with receive antenna selection becomes

$$C(\tilde{\mathbf{H}}) = \log_2 \det\left(\mathbf{I}_{l_r} + \frac{\gamma}{N_T}\tilde{\mathbf{H}}\tilde{\mathbf{H}}^\dagger\right), \tag{3.62}$$

where $\tilde{\mathbf{H}}$ represents the selected sub matrix. In [31, 81–83], receive antenna selection is analyzed for linear arrays with mutual coupling. As antenna selection algorithms choose the best receive antenna subset according to the channel condition, it is important to understand how the channel matrix of the selected antenna subset is formed. If the channel links are independent or correlated and no mutual coupling effects are present, $\mathbf{C}$ is an identity matrix and $\mathbf{H} = \mathbf{H}_{nc}$. In this case, the channel matrix of the selected antenna subset, $\tilde{\mathbf{H}}$, is formed by deleting the rows associated with the unselected receive antennas from $\mathbf{H}$. This problem becomes significant in the presence of mutual coupling. Now the

channel matrix of the selected antenna subset can be written as follows,

$$\tilde{\mathbf{H}} = \left(\tilde{\mathbf{P}}_{M_R \times 2} \tilde{\mathbf{X}}_{2 \times 1} \right) \odot \tilde{\mathbf{C}} \tilde{\mathbf{H}}_{\mathrm{nc}}, \tag{3.63}$$

where $\tilde{\mathbf{H}}_{\mathrm{nc}}$ now of lower dimension, can be formed in the same way as in the previous case. To obtain $\tilde{\mathbf{C}}$, we need to form $\tilde{\mathbf{Z}}_r$ and $\tilde{\mathbf{C}}$. The mutual coupling matrix of the selected antenna subset, $\tilde{\mathbf{C}}$, should only consider the mutual coupling effects among the selected antennas, and is thus formed by deleting the rows and the columns associated with the unselected antennas from $\mathbf{Z}_r$. Similarly, the load impedance matrix $\mathbf{Z}_T \mathbf{I}_{l_r}$ can be formed by deleting the diagonal elements associated with the unselected antennas from $\mathbf{I}_{M_R}$. Now the matrix given in Equation (3.53) becomes,

$$\tilde{\mathbf{C}} = (\mathbf{Z}_A + \mathbf{Z}_T)(\tilde{\mathbf{Z}}_r + \mathbf{Z}_T \mathbf{I}_{l_r})^{-1}, \tag{3.64}$$

where $\mathbf{I}_{l_r}$ is an identity matrix of dimension $l_r \times l_r$. Although we are not using the antenna ports, when performing subset selection, their physical presence still introduces some coupling effect. Here we assume a simple method that ignores the coupling effects of non-selected antennas.

New Selection Algorithm

The selection method presented in the previous section was based on a simple norm based method and it was assumed that the non-selected antenna elements were terminated with $\mathbf{Z}_T$, and even more that they are physically not present when not selected. However, even if these are terminated they are still coupling with their neighbors, an effect that needs to be considered as well. In the new selection algorithm, also based on a simple norm method, we short circuit $\mathbf{Z}_T = 0$, the non-selected antenna elements. The new mutual coupling matrix from Equation (3.53) now looks like,

$$\tilde{\mathbf{C}} = (\mathbf{Z}_A + \mathbf{Z}_T)(\mathbf{Z}_r + \mathbf{Z}_T \mathbf{Q})^{-1}, \tag{3.65}$$

where $\mathbf{Q}$ is a $M_R \times M_R$ diagonal matrix which is formed with $q_{i,i} = 0$ for non-selected antenna combinations and $q_{m,n} = 0$ for $m \neq n$. The matrix $\mathbf{Q}$ contains l_r elements equal to one and the rest $M_R^2 - l_r$ elements equal to zero. This matrix is important in calculating the capacity bounds presented in the next section. For explanation of the structure of various matrices we give an example of an $M_R = 4$, N-Spoke antenna system. The mutual impedance matrix is given by Equation (3.67). With a simple norm based selection we take the example of 3/4 selection. Now one of the subsets (selecting antennas 1 to 3) $\tilde{\mathbf{Z}}_r$ with dimensions of 3×3 would look like Equation (3.68). The matrix $(\tilde{\mathbf{Z}}_r + \mathbf{Z}_T \mathbf{I}_{l_r})$ from Equation (3.64) is given by Equation (3.69). For the new selection algorithm we have the following matrix for $\mathbf{Q}$,

$$\mathbf{Q} = \begin{bmatrix} 1 & 0 & 0 & 0 \\ 0 & 1 & 0 & 0 \\ 0 & 0 & 1 & 0 \\ 0 & 0 & 0 & 0 \end{bmatrix}. \tag{3.66}$$

With this taken into consideration, the matrix $\mathbf{Z}_r + \mathbf{Z}_T \mathbf{Q}$ in Equation (3.65) takes on the values shown in Equation (3.70). The main difference in both methods is that we do not delete the non-selected rows and columns from the matrix $\mathbf{Z}_r$ in the new selection method, rendering the matrix $\tilde{\mathbf{C}}$ to remain in the dimension, i.e., $M_R \times M_R$. In Equation (3.70) we terminated the non-selected antenna ports with a short circuit.

$$\mathbf{Z}_r = \begin{bmatrix} 146 & 50.44 + 1.82i & 0 & -50.44 - 1.82i \\ 50.44 - 1.82i & 146 & 50.44 + 1.82i & 0 \\ 0 & 50.44 - 1.82i & 146 & 50.44 + 1.82i \\ -50.44 + 1.82i & 0 & 50.44 - 1.82i & 146 \end{bmatrix}. \tag{3.67}$$

$$\tilde{\mathbf{Z}}_r = \begin{bmatrix} 146 & 50.44 + 1.82i & 0 \\ 50.44 - 1.82i & 146 & 50.44 + 1.82i \\ 0 & 50.44 - 1.82i & 146 \end{bmatrix}. \tag{3.68}$$

$$\tilde{\mathbf{Z}}_r + \mathbf{Z}_T \mathbf{I}_{l_r} = \begin{bmatrix} 219.37 - 42.54i & 50.44 + 1.82i & 0 \\ 50.44 - 1.82i & 219.37 - 42.54i & 50.44 + 1.82i \\ 0 & 50.44 - 1.82i & 219.37 - 42.54i \end{bmatrix}. \tag{3.69}$$

$$\mathbf{Z}_r + \mathbf{Z}_T \mathbf{Q} = \begin{bmatrix} 219.37 - 42.54i & 50.44 + 1.82i & 0 & -50.44 - 1.82i \\ 50.44 - 1.82i & 219.37 - 42.54i & 50.44 + 1.82i & 0 \\ 0 & 50.44 - 1.82i & 219.37 - 42.54i & 50.44 + 1.82i \\ -50.44 + 1.82i & 0 & 50.44 - 1.82i & 146 \end{bmatrix}. \tag{3.70}$$

3.11   Analysis of Capacity with Selection

We work along similar lines as in [72] and [84] to establish the capacity lower and upper bounds with receive antenna selection for the simple norm based method. A different bound is required for modified receive antenna selection as the structure of impedance matrix is different. We assume l_r receive antennas are selected and the resulting matrices $\tilde{\mathbf{C}}$ and $\tilde{\mathbf{H}}_{\mathrm{nc}}$ are full rank matrices. Now using the singular value decomposition (SVD), we have

$$\tilde{\mathbf{C}} = \mathbf{V}_r \mathbf{\Lambda}_r \mathbf{P}_r, \tag{3.71}$$

where $\mathbf{V}_r$ and $\mathbf{P}_r$ are unitary matrices and $\mathbf{\Lambda}_r$ is the diagonal matrix containing the singular values of $\tilde{\mathbf{C}}$. The channel matrix with selection becomes $\tilde{\mathbf{H}} = \mathbf{V}_r \mathbf{\Lambda}_r \mathbf{P}_r \tilde{\mathbf{H}}_{nc}$. We define here $\hat{\mathbf{H}}_{\mathrm{nc}} = \mathbf{P}_r \tilde{\mathbf{H}}_{nc}$. Since $\mathbf{P}_r$ is a unitary matrix, $\hat{\mathbf{H}}_{nc}\hat{\mathbf{H}}_{nc}^{\dagger}$ has the same eigenvalues as $\tilde{\mathbf{H}}_{nc}\tilde{\mathbf{H}}_{nc}^{\dagger}$. The mutual information with receive antenna selection can be written as

$$C\left(\tilde{\mathbf{H}}\right) = \log_2 \det\left(\mathbf{I}_{l_r} + \frac{\gamma}{N_T} \tilde{\mathbf{H}}\tilde{\mathbf{H}}^{\dagger}\right) \tag{3.72}$$

$$= \log_2 \det\left(\mathbf{I}_{l_r} + \frac{\gamma}{N_T} \mathbf{V}_r \mathbf{\Lambda}_r \hat{\mathbf{H}}_{nc}\hat{\mathbf{H}}_{nc}^{\dagger}\mathbf{\Lambda}_r^{\dagger}\mathbf{V}_r^{\dagger}\right) \tag{3.73}$$

$$\overset{(a)}{=} \log_2 \det\left(\mathbf{I}_{l_r} + \frac{\gamma}{N_T} \mathbf{\Lambda}_r \hat{\mathbf{H}}_{nc}\hat{\mathbf{H}}_{nc}^{\dagger}\mathbf{\Lambda}_r^{\dagger}\right) \tag{3.74}$$

$$\overset{(b)}{=} \log_2 \det\left(\mathbf{I}_{l_r} + \frac{\gamma}{N_T} \mathbf{\Lambda}_r^{\dagger}\mathbf{\Lambda}_r \hat{\mathbf{H}}_{nc}\hat{\mathbf{H}}_{nc}^{\dagger}\right) \tag{3.75}$$

$$= \log_2 \det\left(\mathbf{I}_{l_r} + \mathbf{\Theta}\mathbf{\Omega}_1\right), \tag{3.76}$$

since (a) $\det(\mathbf{I} + \mathbf{U}\mathbf{A}\mathbf{U}^{\dagger}) = \det(\mathbf{I} + \mathbf{A})$ and (b) $\det(\mathbf{I} + \mathbf{A}\mathbf{B}) = \det(\mathbf{I} + \mathbf{B}\mathbf{A})$ for any unitary matrix $\mathbf{U}$ and any square matrix $\mathbf{A}$ and $\mathbf{B}$. Here we also define $\mathbf{\Omega}_1 = \frac{\gamma}{N_t} \hat{\mathbf{H}}_{nc}\hat{\mathbf{H}}_{nc}^{\dagger}$ and $\mathbf{\Theta} = \mathbf{\Lambda}_r^{\dagger}\mathbf{\Lambda}_r$, and let $\left\{\lambda_{\mathbf{\Omega}_1}^{(\mathrm{i})}\right\}$ and $\left\{\lambda_{\mathbf{\Theta}}^{(\mathrm{i})}\right\}$ denote the sorted eigenvalues of $\mathbf{\Omega}_1$ and $\mathbf{\Theta}$ in descending order.

3.11.1 Upper Bound

Define $\boldsymbol{\Xi}$ as a $l_r \times l_r$ diagonal matrix $\boldsymbol{\Xi} = \mathrm{diag}\left[\lambda_{\boldsymbol{\Omega}_1}^{(1)}, \cdots, \lambda_{\boldsymbol{\Omega}_1}^{(\mathrm{N_T})}, 1, \cdots, 1\right]$. Using Equation (3.76), we can show that

$$C\left(\tilde{\mathbf{H}}\right) \leq \log_2\det\left(\mathbf{I}_{l_r} + \boldsymbol{\Theta\Xi}\right). \tag{3.77}$$

Similarly we note that equality is obtained for $l_r = 1$. At higher SNR values, the upper bound can be written as

$$C_{\mathrm{Upper}} = \sum_{i=1}^{N_T} \log_2\lambda_{\boldsymbol{\Omega}_1}^{(i)} + \sum_{i=1}^{l_r} \log_2\lambda_{\boldsymbol{\Theta}}^{(i)}. \tag{3.78}$$

In our case as $N_T = 2$, so that the above equation becomes,

$$C_{\mathrm{Upper}} = \sum_{i=1}^{2} \log_2\lambda_{\boldsymbol{\Omega}_1}^{(i)} + \sum_{i=1}^{l_r} \log_2\lambda_{\boldsymbol{\Theta}}^{(i)}. \tag{3.79}$$

3.11.2 Lower Bound

The instantaneous capacity in Equation (3.74) can be rewritten as

$$C\left(\tilde{\mathbf{H}}\right) = \log_2\det\left(\mathbf{I}_{N_T} + \frac{\gamma}{N_T}\hat{\mathbf{H}}_{nc}^{\dagger}\boldsymbol{\Theta}\hat{\mathbf{H}}_{nc}\right) \tag{3.80}$$

and further lower bounded by

$$C\left(\tilde{\mathbf{H}}\right) > \log_2\det\left(\frac{\gamma}{N_T}\hat{\mathbf{H}}_{nc}^{\dagger}\boldsymbol{\Theta}\hat{\mathbf{H}}_{nc}\right). \tag{3.81}$$

Define $\boldsymbol{\Omega}_2 = \frac{\gamma}{N_T}\hat{\mathbf{H}}_{nc}^{\dagger}\hat{\mathbf{H}}_{nc}$ and $\boldsymbol{\Omega}_2$ has N_T nonzero eigenvalues which are the same as in $\boldsymbol{\Omega}_1$. Applying inequality (12) of [84] on Equation (3.81) yields

$$C\left(\tilde{\mathbf{H}}\right) > \log_2\prod_{i=1}^{N_T}\lambda_{\boldsymbol{\Omega}_2}^{(i)} + \log_2\prod_{i=l_r-N_T+1}^{l_r}\lambda_{\boldsymbol{\Theta}}^{(i)}. \tag{3.82}$$

We then obtain the lower bound as

$$C_{\mathrm{Lower}} = \sum_{i=1}^{N_T}\log_2\lambda_{\boldsymbol{\Omega}_1}^{(i)} + \sum_{i=1}^{l_r}\log_2\lambda_{\boldsymbol{\Theta}}^{(i)} - \sum_{i=1}^{l_r-N_T}\log_2\lambda_{\boldsymbol{\Theta}}^{(i)}. \tag{3.83}$$

At higher SNR values,

$$C_{\mathrm{Upper}} = C_{\mathrm{Lower}} + \sum_{i=1}^{l_r-N_T}\log_2\lambda_{\boldsymbol{\Theta}}^{(i)}. \tag{3.84}$$

The above equation shows the existence of a gap between upper and lower bounds. This gap is quantified by a value $\sum_{i=1}^{l_r-N_T}\log_2\lambda_{\boldsymbol{\Theta}}^{(i)}$, which becomes zero when $N_T = l_r$. For $N_T = 2$, Equation (3.83) becomes,

$$C_{\text{Lower}} = \sum_{i=1}^{2} \log_2 \lambda_{\mathbf{\Omega}_1}^{(i)} + \sum_{i=1}^{l_r} \log_2 \lambda_{\mathbf{\Theta}}^{(i)} - \sum_{i=1}^{l_r-2} \log_2 \lambda_{\mathbf{\Theta}}^{(i)}. \tag{3.85}$$

$$C_{\text{Lower}} = \sum_{i=1}^{2} \log_2 \lambda_{\mathbf{\Omega}_1}^{(i)} + \sum_{i=1}^{2} \log_2 \lambda_{\mathbf{\Theta}}^{(i)}. \tag{3.86}$$

We note here the upper bound in Equation (3.78) and lower bound in Equation (3.83) can be written as a function of two independent and disjoint contributions: one from $\tilde{\mathbf{H}}_{nc}$ and one from $\tilde{\mathbf{Z}}_r$, because $\tilde{\mathbf{Z}}_r$ does not depend on the channel instantiation. Analytical results and expressions for ULA and N-Spoke configurations with receive antenna selection in terms of channel gains can be found in [69] and [85]. From the structure of $\mathbf{Q}$ in Section 3.10 we observe that the eigenvalues of non-selected antennas, terminated with ($\mathbf{Z}_T = 0$), become more significant for the performance of the system. Considering this fact we define capacity bounds for the new selection algorithms as follows,

$$C_{\text{Upper}}^{SC} = \sum_{i=1}^{2} \log_2 \lambda_{\mathbf{\Omega}_1}^{(i)} + \sum_{i=1}^{M_R-l_r} \log_2 \lambda_{\mathbf{\Theta}}^{(i)} \tag{3.87}$$

$$C_{\text{Lower}}^{SC} = \sum_{i=1}^{2} \log_2 \lambda_{\mathbf{\Omega}_1}^{(i)} + \log_2 \lambda_{\mathbf{\Theta}}^{(M_R-l_r)}, \tag{3.88}$$

where the effect of only $M_R - l_r$ is taken in the equations.

3.12   Simulation Results and Discussion

The simulation results for both configurations mentioned in the previous sections with both types of receive antenna selection methods are shown in Figures 3.14(a) and 3.14(b), respectively. The capacity is calculated by averaging over all channel realizations. For simplicity we compare the performances of both the configurations at $\theta_p = 0°$ and $\alpha = 0$. We have also plotted the 95% confidence intervals to show the validity of our data. From Figure 3.14(a) for N-Spoke configuration we see that the capacity increases slightly till $M_R = 4$, for full complexity systems. For values of $M_R > 4$, the capacity starts decreasing because the effects of mutual coupling and correlation becomes strong due to smaller angular spacings. So just by increasing the number of antennas, do not increase the capacity any further. We also find from Figure 3.14(a) for $l_r/6$ selection that for all values of l_r, the new selection method performs better than simple selection method. In fact for values of $l_r = 4, 5$, the new Antenna Selection (AS) scheme even outperforms the full complexity system. In a similar fashion for $l_r/9$ selection we observe that the new AS performs better than the simple AS method for all values of l_r. It also outperforms the full complexity system for $l_r = 7, 8$. The performance of the ULA antenna structures is different from the N-Spoke counterpart. For values of $M_R > 3$, the capacity saturates to increase any further even by increasing the number of antennas. Even applying the simple norm based selection method does not help in improving the performance. We however find that the new selection method boosts the performance for almost all values of l_r. By comparing Figures 3.14(a) and 3.14(b) we observe that for side by side antenna configuration, the new AS scheme provides more gain relative to the N-Spoke structures even for low values of l_r. We illustrate the CDF of the simulations and the bounds of the capacity for a system with l_r receive antenna selection. The Figure 3.15(a) shows

the comparison at 10 dB SNR and Figure 3.15(b) at 30 dB SNR values. We recognize from the CDF curves of Figure 3.15(a) and Figure 3.15(b) at small values of $l_r = 2$ for any SNR value, the lower bounds are tight. The performance is different for upper bounds. We observe that as we increase to $l_r = 3$ the upper bound becomes more loose. In Figure 3.15(c) we show the comparison of bounds with simulations for the N-Spoke structure with the new selection method. From the figure we find that increasing the value of l_r, both the bounds get tighter. In these figures we have shown results for only N-Spoke configurations. The results for ULA configurations are not shown here because they follow the same trends as for N-Spoke structure. The Figures 3.14(a) and 3.14(b) show the performance through simulation for array orientation values of $\theta_p = 0°$ and XPD values of $\alpha = 0$. Due to this the corresponding orientation matrix from Equation (3.47) and XPD matrices from Equation (3.49) have values,
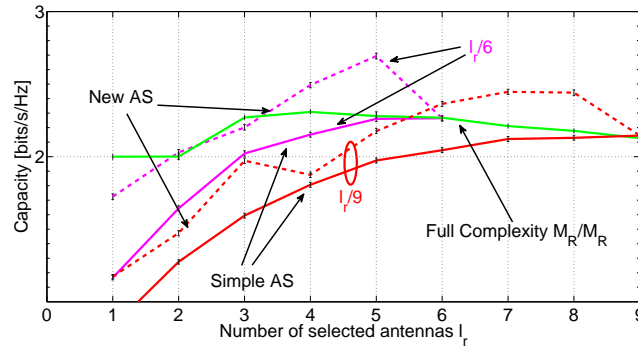
(a) Capacity of N-Spoke MIMO system with receive antenna selection $l_r/6$, $l_r/9$, $\theta_p = 0°$ and XPD $\alpha = 0$ at 10 dB SNR.
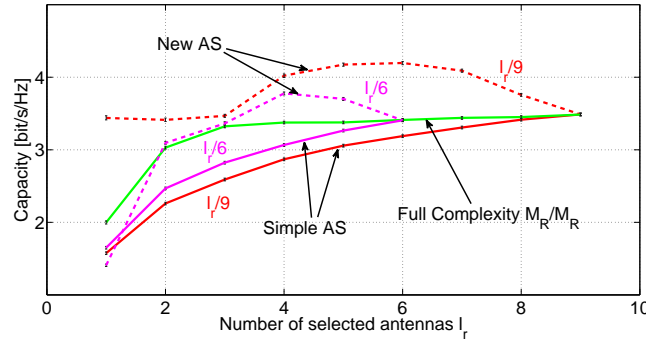
(b) Capacity of ULA MIMO system with receive antenna selection $l_r/6$, $l_r/9$, $\theta_p = 0°$ and XPD $\alpha = 0$ at 10 dB SNR.

Figure 3.14: Capacity Performance in antenna configurations.

$$\mathbf{P}_{M_R \times 2}^{ULA} = \begin{bmatrix} 1 & 0 \\ 1 & 0 \\ \vdots & \vdots \\ 1 & 0 \end{bmatrix}, \tag{3.89}$$

for ULA configuration as φ_{n_r} is 0 for all antennas.
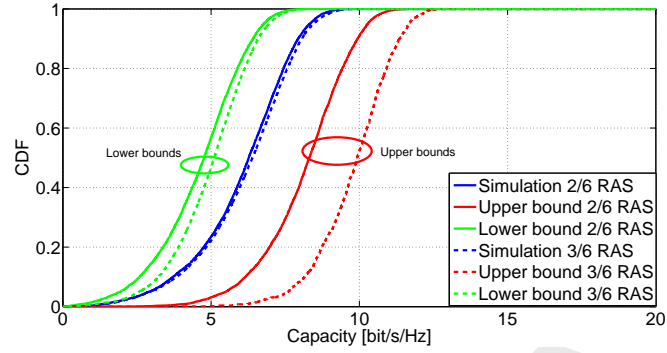
(a) CDF of capacity of N-Spoke with simple selection and its upper bound Equation (3.79) and lower bound Equation (3.86) for $M_R = 6$, $l_r = 2, 3$, $\theta_p = 0°$ and XPD $\alpha = 0$ at 10 dB SNR.
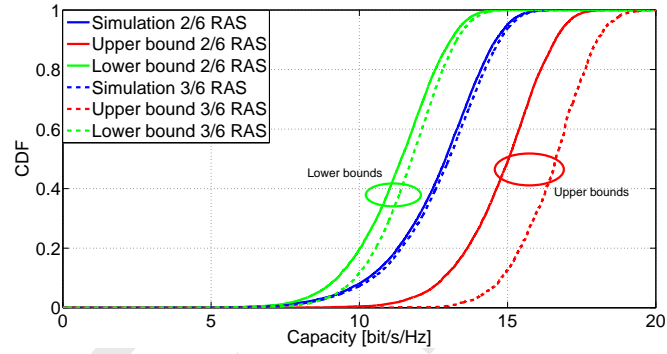
(b) CDF of capacity of N-Spoke with simple selection and its upper bound Equation (3.79) and lower bound Equation (3.86) for $M_R = 6$, $l_r = 2, 3$, $\theta_p = 0°$ and XPD $\alpha = 0$ at 30 dB SNR.
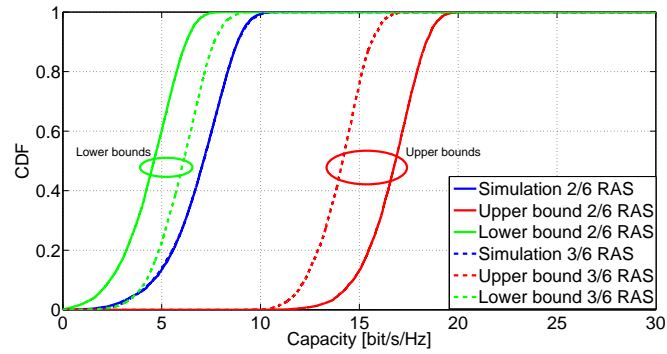
(c) CDF of capacity of N-Spoke with new selection method and its upper bound Equation (3.87) and lower bound Equation (3.88) for $M_R = 6$, $l_r = 2, 3$, $\theta_p = 0°$ and XPD $\alpha = 0$ at 10 dB SNR.

Figure 3.15: CDF of N-Spoke configurations with antenna selection.
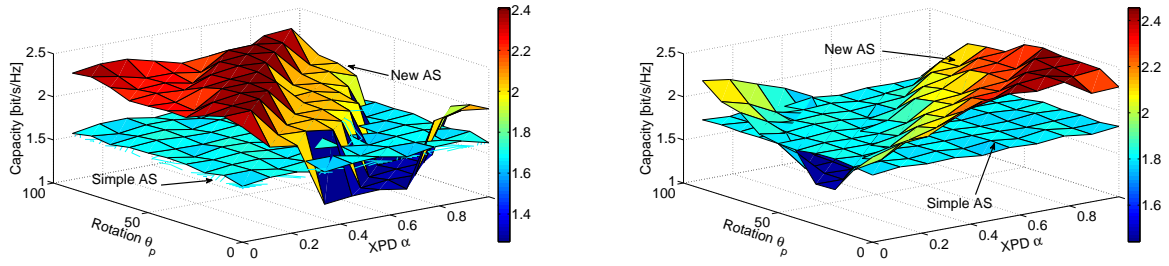
(a) Capacity of N-Spoke MIMO system with 2/6 simple norm and new receive antenna selection for varying array orientation θ_p and XPD α at 10 dB SNR.

(b) Capacity of N-Spoke MIMO system with 4/9 simple norm and new receive antenna selection for varying array orientation θ_p and XPD α at 10 dB SNR.
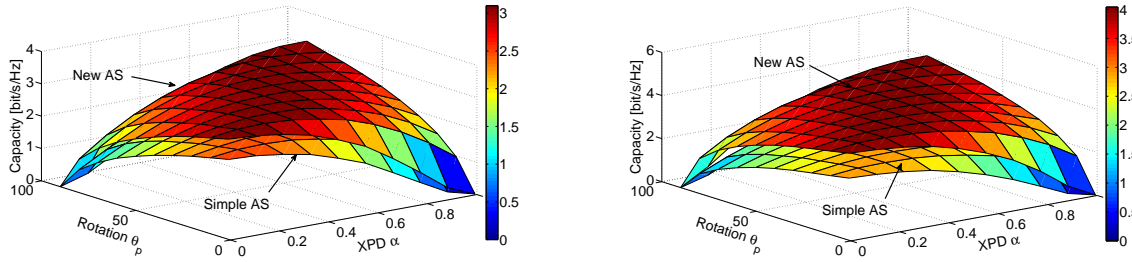
(c) Capacity of ULA MIMO system with 2/6 simple norm and new receive antenna selection for varying array orientation θ_p and XPD α at 10 dB SNR.

(d) Capacity of ULA MIMO system with 4/9 simple norm and new receive antenna selection for varying array orientation θ_p and XPD α at 10 dB SNR.

Figure 3.16: CDF of antenna configurations for varying rotation and XPD with antenna selection.

$$
\mathbf{P}^{NSp}_{M_R \times 2} =
\begin{bmatrix}
\cos(\varphi_1) & \sin(\varphi_1) \\
\cos(\varphi_2) & \sin(\varphi_2) \\
\vdots & \vdots \\
\cos(\varphi_{N_R}) & \sin(\varphi_{N_R})
\end{bmatrix},
\tag{3.90}
$$

$$
\mathbf{X}_{2 \times 1} = \begin{bmatrix} 1 & 0 \end{bmatrix}^{\mathrm{T}},
\tag{3.91}
$$

for both configurations. We also show here an example correlation matrix for a four antenna element N-Spoke structure shown in Figure 3.11, elements of which are calculated from Equation (3.52). As it is purely a structure of elements with no spatial distance between the antenna elements so Equation (3.52) now becomes $\varsigma_a = \cos \theta_r$,

$$
\mathbf{R} =
\begin{bmatrix}
1 & 0.7 & 0 & 0.7 \\
0.7 & 1 & 0.7 & 0 \\
0 & 0.7 & 1 & 0.7 \\
0.7 & 0 & 0.7 & 1
\end{bmatrix},
\tag{3.92}
$$

where $\theta_r = \pi/4, \pi/2, 3\pi/4$. The effect of rotation and varying XPD values are shown in Figures 3.16(a), 3.16(b), 3.16(c) and 3.16(d) for N-Spoke and ULA antenna configurations applying a simple norm based receive antenna selection algorithm. The N-Spoke structure is more robust to the variations in α and θ_p for the average capacity values compared to the ULA configuration. The average capacity values in a ULA configuration almost go to zero for either $\alpha = 0$ or $\theta_p = 90^0$. Effectively it

means that the performance of ULA configurations is severely degraded with changing orientation and antenna power imbalance as compared to an N-Spoke structure. We also observe in Figures 3.16(a) and 3.16(b) that the variation of capacity is less for a simple AS scheme for various values of α and θ_p. For a 2/6 system the capacity remains almost at 1.5bit/s/Hz and 1.7bit/s/Hz for 4/9 system. The new AS scheme is robust to orientation effects at low values of XPD for a 2/6 system and also has a higher capacity gain. The 4/9 system is more robust to XPD effects and lower values of orientation.

3.13 Conclusions

We examine and investigate the effects of various parameters of antenna arrays and then analyze the performance with receive antenna selection. We compare an N-Spoke antenna structure with a fixed compact area to a ULA structure. We find a method to accurately calculate the mutual coupling effects in the N-Spoke configuration and combine the effects of channel correlations. A conventional channel norm based strategy is applied to select the best channels and subsequently we propose a novel selection algorithm to further enhance the performance. To analytically verify our simulations we presented tight lower bounds and loose upper bounds for capacity calculations. We concluded that although a complete channel model for characterizing antenna arrays consists of many parameters but the most important and critical is the mutual coupling effect present in the system. From the coupling analysis we also found that N-Spoke configurations in spite of having severe mutual coupling effects compared to side by side structures, they have compact structures due to which it is a promising structure for future wireless standards when used jointly with smart antenna selection schemes.

The electromagnetic field transmitted from the antenna can be defined by using the complex-valued Poynting vector $\mathbb{E} \times \mathbb{H}^*$, where $\mathbb{E}$ and $\mathbb{H}$ denote electric and magnetic field components, respectively [70]. In close vicinity of the antenna the Poynting vector is complex consisting of major reactive and minor radiating fields whereas radiating fields dominate in far-field region of $D = 2l^2/\lambda$, where l is the largest dimension of antenna, D is the distance between transmitter and receiver and λ the wavelength of the field. In that region electromagnetic fields decay as $1/D$, and they can be defined by using two orthogonal vector components in spherical coordinates. The spherical electromagnetic wave can be approximated as a plane wave in the far-field region when received by a receiver antenna. Our work did not consider poynting vector and its effect on multipolarized MIMO systems. We also did not consider the effects of radiation pattern of individual antennas. This can also be included to get more realistic results in our channel model. Comparisons in terms of performance measures like BER and throughput can be performed and analytical bounds can be calculated.

After analyzing antenna systems which are planar and 2-D in nature we move forward to 3-D antenna structures in the next chapter.

4

Antenna Selection in 3-D Polarized MIMO

4.1 Introduction

Most of the Multiple-Input Multiple-Output (MIMO) systems require an inter-element spacing of the order of a wavelength to achieve significant gains in Non Line of Sight (NLOS) channels; even larger spacing is required for Line of Sight (LOS) channels [86] [53]. In this regard, dual-polarized antennas have received much attention as a smart option for realizing MIMO architectures in compact devices [52]. Recently, considerations are even carried out using triple-polarized antenna systems to exploit the additional degree of freedom for wireless communications [87] [88]. Antenna selection, when combined with multiple-polarized antennas, may be an answer that could enable compact systems to exploit the benefits of the MIMO architecture with only a minimal increase in complexity. Compact antenna configurations with antenna selection for MIMO communications have been studied in [69] [57] [85]. However, MIMO channels with polarization diversity cannot be modeled like pure spatial channels, because such subchannels of the MIMO channel matrix are not identically distributed [89]. They differ in terms of average received power, Ricean K-factor, Cross Polarization Discrimination (XPD) and correlation properties [55]. As a result, the performance of antenna selection for these channels needs to be calculated. The main objective of this chapter is to analyze the performance of Transmit Receive Antenna Selection (TRAS) and Transmit Antenna Selection (TAS) for MIMO channels in the presence of polarization diversity. We provide a theoretical treatment for the 2×2 dual-polarized and 3×3 triple-polarized Rayleigh MIMO channel [90]. For the mathematical analysis in this chapter, we proceed on similar lines as in [57].

(a) Configuration of dual-polarized system.   (b) Configuration of triple-polarized system.
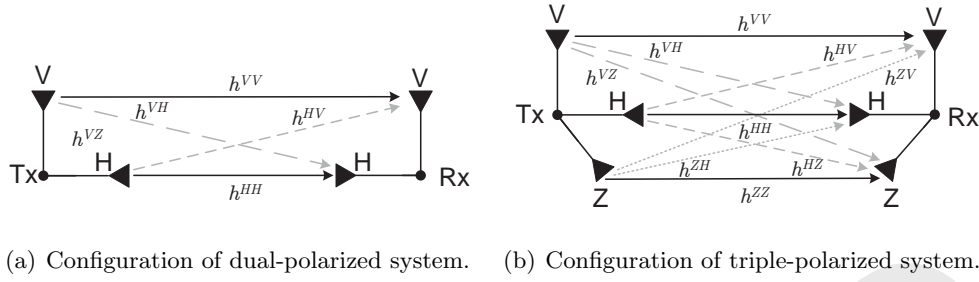
Figure 4.1: Configurations of multi-polarized systems.

4.2   Dual and Triple-Polarized MIMO

Dual and triple-polarized antennas can be envisaged as an array of two and three co-located antennas with orthogonal polarizations, respectively. By using a dual or triple-polarized feed, an antenna can transmit two or three orthogonally polarized waves on the same frequency [87] [88] [67]. Another such set of antennas can then receive the two or three orthogonally polarized waves and separate them by means of an electrically identical dual or triple-polarized feed. Consider a system with N_T transmit and M_R receive antennas. When all the antennas are vertically polarized, the subchannels of the MIMO channel matrix **H** are usually assumed to be identically distributed. However, when antennas with different polarizations are employed at either ends of the link, the properties of the co-polar subchannels differ significantly from those of the cross-polar subchannels. Hence for dual-polarized configurations, the channel matrix can be conveniently written as

$$\mathbf{H}_{DP} = \left[\begin{array}{cc} h^{VV} & h^{VH} \\ h^{HV} & h^{HH} \end{array} \right]. \tag{4.1}$$

The configuration is shown in the Figure 4.1(a). Similarly the channel matrix for triple-polarized configuration can be written as

$$\mathbf{H}_{TP} = \left[\begin{array}{ccc} h^{VV} & h^{VH} & h^{VZ} \\ h^{HV} & h^{HH} & h^{HZ} \\ h^{ZV} & h^{ZH} & h^{ZZ} \end{array} \right]. \tag{4.2}$$

The transmitted radio signal, as it traverses through the wireless medium, experiences multiple reflections and scattering, resulting in a coupling of the orthogonal state of polarization. This phenomenon is referred to as depolarization. XPD for dual-polarized channel is defined as,

$$\begin{aligned} X_V &= E\left\{ \left| h^{VV} \right|^2 \right\} / E\left\{ \left| h^{HV} \right|^2 \right\}, \\ X_H &= E\left\{ \left| h^{HH} \right|^2 \right\} / E\left\{ \left| h^{VH} \right|^2 \right\}, \end{aligned} \tag{4.3}$$

Similarly for triple-polarized channels we have the following XPD definitions as,

$$
\begin{aligned}
X_{VH} &= E\left\{\left|h^{VV}\right|^2\right\} / E\left\{\left|h^{HV}\right|^2\right\}, \\
X_{HV} &= E\left\{\left|h^{HH}\right|^2\right\} / E\left\{\left|h^{VH}\right|^2\right\}, \\
X_{ZV} &= E\left\{\left|h^{ZZ}\right|^2\right\} / E\left\{\left|h^{VZ}\right|^2\right\}, \\
X_{VZ} &= E\left\{\left|h^{VV}\right|^2\right\} / E\left\{\left|h^{ZV}\right|^2\right\}, \\
X_{HZ} &= E\left\{\left|h^{HH}\right|^2\right\} / E\left\{\left|h^{ZH}\right|^2\right\}, \\
X_{ZH} &= E\left\{\left|h^{ZZ}\right|^2\right\} / E\left\{\left|h^{HZ}\right|^2\right\},
\end{aligned}
\tag{4.4}
$$

where $h^{IJ} : I, J \in \{V, H, Z\}$ is an element of the sub-matrix $\mathbf{H}^{IJ}$ and $E\{Z\}$ denotes the expectation of Z. Typically XPD values are high in channels with limited scattering such as LOS channels and much lower in NLOS channels. However high XPD values have been observed even in NLOS channels, in some measurement campaigns [55]. Further, owing to the different propagation characteristics of horizontally polarized waves and vertically polarized waves, $E\left\{\left|h^{VV}\right|^2\right\} > E\left\{\left|h^{HH}\right|^2\right\} = \beta \leq 1$ and $E\left\{\left|h^{VV}\right|^2\right\} > E\left\{\left|h^{ZZ}\right|^2\right\} = \gamma \leq 1$. This happens due to the Brewster angle phenomenon for horizontally polarized transmission [91]. This discrepancy could also arise from the differences in the antenna patterns of the orthogonally polarized elements [92]. These subchannel power losses translate into a performance loss for dual-polarized MIMO systems when compared to spatial MIMO [55]. Under LOS conditions, the co-polar subchannels are Ricean distributed whereas the cross-polar subchannels are Rayleigh distributed. This is expected due to the fact that the cross-polar subchannel gains result from depolarization of the transmitted signal. Correlation between the elements of the MIMO channel is detrimental to its performance. For spatial MIMO, a large inter-element spacing is required to lower the correlation between the subchannels in some environments [55]. However for dual-polarized MIMO, the correlation between the elements from different sub matrices is very low even under LOS channel conditions [55]. Thus, there are significant differences between dual or triple-polarized MIMO channels compared to spatial MIMO channels. Taking into account these subchannel power losses, the average squared Frobenius norm of this channel matrix (Equation (4.1)) can be written as [93],

$$
\bar{W}_{DP} = M_R{}^V N_T{}^V + \beta(M_R{}^H N_T{}^H) + \frac{1}{X_V}(M_R{}^H N_T{}^V) + \frac{\beta}{X_H}(M_R{}^V N_T{}^H) \leq M_R N_T. \tag{4.5}
$$

Similarly the average squared Frobenius norm for a triple polarized channel matrix (Equation (4.2)) can be written as,

$$
\begin{aligned}
\bar{W}_{TP} = {}& M_R{}^V N_T{}^V + \beta(M_R{}^H N_T{}^H) + \gamma(M_R{}^Z N_T{}^Z) + \frac{1}{X_{VH}}(M_R{}^H N_T{}^V) + \frac{1}{X_{VZ}}(M_R{}^Z N_T{}^V) + \\
& \frac{1}{X_{HZ}}(M_R{}^Z N_T{}^H) + \frac{1}{X_{ZH}}(M_R{}^H N_T{}^Z) + \frac{\beta}{X_{HV}}(M_R{}^V N_T{}^H) + \frac{\gamma}{X_{ZV}}(M_R{}^V N_T{}^Z) \leq M_R N_T.
\end{aligned}
\tag{4.6}
$$

The average squared Frobenius norm represents the total energy in the channel. For identically distributed Rayleigh channels we normalize the channel matrix so that its average squared Frobenius norm is equal to $M_R N_T$ [94]. From Equations (4.5) and (4.6) we note that as the XPD increases or as β decreases, $\bar{W}_{DP}$ and $\bar{W}_{TP}$ diminishes. As a result, the array gain achieved by using dual-polarized or triple-polarized antennas is smaller when compared to pure spatially separated antennas. Thus MIMO systems employing polarization diversity suffer Signal-to-Noise Ratio (SNR) and diversity penalties, when compared to their spatial counterparts.

4.3 Effect of XPD on Joint Transmit/Receive Selection Gain

Antenna selection refers to the process of selecting the "optimal" l_t out of the N_T available transmit antennas and/or the "optimal" l_r out of the M_R receive antennas. Symbolically we denote this process as $(l_r/M_R, l_t/N_T)$ selection. We assume here the availability of a perfect low bandwidth feedback channel for implementing selection at the transmitter. We also assume that the delay of this feedback signal is minimal. In this section we study the influence of XPD on selection gain achieved by using antenna selection for both transmit and receive side. To make the analysis as simple as possible, we first consider a $M_R \times N_T = 2 \times 2$ dual-polarized MIMO channel.

All the subchannels are assumed to be independent complex circularly symmetric Gaussian random variables. This is an appropriate assumption for the typical NLOS indoor channel. Further, we make the simplifying assumptions that all the XPD values given in Section 4.2 are equal to X. Also $1 \leq X \leq \infty$ and $\gamma = \beta = 1$. We start our analysis with joint antenna selection at the transmitter and receiver, i.e., $(1/2, 1/2)$, $(1/3, 1/3)$ and $(2/3, 2/3)$ arrangements. We then move to the analysis of transmit antenna selection, i.e., $(2/2, 1/2)$, $(3/3, 1/3)$ and $(3/3, 2/3)$. We perform this because we analyze transmit antenna selection in a different way as would be shown subsequently in a separate section. For $(1/2, 1/2)$ and $(1/3, 1/3)$ selection, the strategy is to select the Single-Input Single-Output (SISO) subchannel which has the maximum instantaneous power. The instantaneous post processing SNR for the selected SISO channel ($\tilde{h}$) is given by $Y E_s/N_o$ where the random variable, $Y = |\tilde{h}|^2$. For a circularly symmetric complex Gaussian random variable Z with zero mean and variance σ^2, the Cumulative Distribution Function (CDF) of $Z = |h|^2$ is given by, $F_Z(z) = (1 - e^{-z/\sigma^2})$. Since all the elements of $\mathbf{H}$ are assumed to be mutually independent, the Cummulative Distribution Function (CDF) of Y can be derived as follows.

4.3.1 Dual Polarized $(1/2, 1/2)$ TRAS

From Equation (4.3) we have $E\left\{\left|h^{HV}\right|^2\right\} = 1/X_V = 1/X$, so

$$F_Y(y)_{(1/2,1/2)} = \Pr(|h^{VV}|^2 < y)^2 \Pr(|h^{HV}|^2 < y)^2 = (1 - e^{-y})^2 (1 - e^{-yX})^2. \tag{4.7}$$

The Probability Density Function (PDF), $f_Y(y) = \frac{dF_Y(y)}{dy}$ is given by

$$f_Y(y)_{(1/2,1/2)} = 2(e^{-y}(1 - e^{-y})(1 - e^{-yX})^2 + Xe^{-yX}(1 - e^{-yX})(1 - e^{-y})^2). \tag{4.8}$$

Using the identity, $\int_0^\infty x e^{ax} dx = 1/a^2$, $G(X) = E\{Y\}$, which indicates the effective SNR gain achieved by using antenna selection, can be computed to be,

$$G_{(1/2,1/2)}(X) = \frac{3(1+X)}{2X} + \frac{2}{1+2X} + \frac{2}{2+X} - \frac{9}{2(1+X)}. \tag{4.9}$$

The average SNR gain is a monotonically decreasing function of X as shown in Figure 4.2. The selection gain is maximum at 3.2 dB when $X = 1$ and asymptotically diminishes to 1.76 dB. Here we can also calculate the probability that one of the cross-polar subchannels is selected, as follows,

$$\begin{aligned}
Pr_{(1/2,1/2)}(X > x) &= \Pr\left\{(\tilde{h} = h^{VH}) \cup (\tilde{h} = h^{HV})\right\} \\
&= 2Pr\left\{h^{VH} > h^{HV}\right\} \Pr\left\{h^{VH} > h^{HH}\right\} \Pr\left\{h^{VH} > h^{VV}\right\} \\
&= 2(1/2)\Pr\left\{h^{VH} > h^{HH}\right\}^2
\end{aligned}$$

$$= \frac{1}{(1+X)^2}. \tag{4.10}$$

We observe from the above equation that as the XPD increases the probability of the cross-polar subchannels being selected, decreases and thus the average SNR gain diminishes. Further, $\lim_{X \to \infty} Pr_{(1/2,1/2)}(X > x) = 0$, which indicates that in the limiting case, the available degrees of diversity reduces to two when compared to four for $X = 1$. Thus a high XPD results in a diversity loss for dual-polarized MIMO channels when compared to spatial channels.

4.3.2   Triple Polarized $(1/3, 1/3)$ TRAS

From Equations (4.4), following the same procedure as in Section 4.3.1 we have $X_{VH} = X_{HV} = X_{VZ} = X_{ZV} = X_{HZ} = X_{ZH} = X$,

$$
\begin{aligned}
F_Y(y)_{(1/3,1/3)} &= \Pr(|h^{VV}|^2 < y)\Pr(|h^{HH}|^2 < y)\Pr(|h^{ZZ}|^2 < y)\Pr(|h^{VH}|^2 < y) \\
&\quad \Pr(|h^{HV}|^2 < y)\Pr(|h^{VZ}|^2 < y)\Pr(|h^{ZV}|^2 < y)\Pr(|h^{HZ}|^2 < y) \\
&\quad \Pr(|h^{ZH}|^2 < y) \\
&= (1 - e^{-y})^3 (1 - e^{-yX})^6.
\end{aligned} \tag{4.11}
$$

The (Probability Density Function (PDF)) then reads

$$
f_Y(y)_{(1/3,1/3)} = 3(e^{-y}(1 - e^{-y})^2(1 - e^{-yX})^6 + 2Xe^{-y}(1 - e^{-y})^3(1 - e^{-yX})^5). \tag{4.12}
$$

$G_{(1/3,1/3)}(X) = E\{Y\}$ is then calculated as in previous section. Also we can calculate the probability that one of the cross-polar subchannels is selected, as follows,

$$
Pr_{(1/3,1/3)}(X > x) = \frac{1}{(1 + 2X)^3}. \tag{4.13}
$$

Also, $\lim_{X \to \infty} Pr_{(1/3,1/3)}(X > x) = 0$, which indicates that in the limiting case, we observe that the available degrees of diversity reduces to three when compared to nine for $X = 1$. Thus a high XPD results in a diversity loss for triple-polarized MIMO channels when compared to spatial channels.

4.3.3   Triple Polarized $(2/3, 2/3)$ TRAS

As we have to select two antennas at each end of the channel, we have to sum the powers of the individual channels or sum of the squares of independent Gaussian random variables. Thus, the resulting CDF becomes a Chi-squared distribution and not simply an exponential. The complete CDF of selecting such channels is then given by

$$
F_Y(y)_{(2/3,2/3)} = (F_Y(y)_1)(F_Y(y)_2)(F_Y(y)_3), \tag{4.14}
$$

where

$$
\begin{aligned}
F_Y(y)_1 &= \Pr(|h^{VV}|^2 + |h^{HH}|^2 < y)\Pr(|h^{VV}|^2 + |h^{ZZ}|^2 < y)\Pr(|h^{HH}|^2 + |h^{ZZ}|^2 < y) \\
&= (1 - e^{-y/2})^3,
\end{aligned} \tag{4.15}
$$

where each term above is a central Chi-Squared distribution with zero means and $\sigma_1^2 = \sigma_2^2 = 1$.

$$
\begin{aligned}
F_Y(y)_2 &= \Pr(|h^{VV}|^2 + |h^{HZ}|^2 < y)\Pr(|h^{VV}|^2 + |h^{ZH}|^2 < y) \\
&\quad \Pr(|h^{ZZ}|^2 + |h^{VH}|^2 < y)\Pr(|h^{ZZ}|^2 + |h^{HV}|^2 < y) \\
&= \left(\frac{1}{X-1}(e^{-yX} - Xe^{-y} + X - 1) \right)^4,
\end{aligned}
\tag{4.16}
$$

where each term above is generalized central Chi-Squared distributed with zero means and $\sigma_1^2 = 1$, $\sigma_2^2 = 1/X$ [95].

$$
\begin{aligned}
F_Y(y)_3 &= \Pr(|h^{VH}|^2 + |h^{HZ}|^2 < y)\Pr(|h^{HV}|^2 + |h^{HZ}|^2 < y) \\
&= (1 - e^{-2yX}(2yX + 1))^2,
\end{aligned}
\tag{4.17}
$$

where each term is generalized Chi-Squared distributed with zero means and $\sigma_1^2 = 1/X$, $\sigma_2^2 = 1/X$ [95]. This turns out to be an Erlang distribution. The results are shown in Figure 4.2.

4.4   Outage Analysis with TRAS

In this section, we derive the mutual information for both the antenna structures. We perform this for systems with antenna selection and without selection. Later, considering the fact that the mutual information, depending on the channel realizations, is a random variable, we define the outage probability and then derive the same for both configurations. For the given systems, without antenna selection the mutual information can be bounded as follows

$$
I \leq \log\left(1 + \frac{\gamma}{N_T} \sum |h^{IJ}|^2\right),
\tag{4.18}
$$

where $\gamma = E_s/N_0$ and E_s is the transmit signal power. We assume here that the power is divided equally among N_T transmit antennas. The information theoretic outage probability defines an event when the channel mutual information cannot satisfy a certain target rate. This target rate may be set by some application such as audio, video, or some multimedia application. Mathematically, the probability of outage can be written as [96]

$$
\Pr(R) = \Pr(I < R)
\tag{4.19}
$$

where R represents the rate requirement set by some particular application. For our scheme, using the mutual information expression in Equation (4.18) and the outage probability definition in Equation (4.19), we derive the outage probability for the investigated scheme as follows. Methods to formulate outage probability for fading channels are given in [97].

$$
\Pr(I < R)_{(1/2,1/2)} = \int_0^\epsilon f_Y(y)_{(1/2,1/2)} dy,
\tag{4.20}
$$

where ϵ for $(1/2, 1/2)$ system is given by $\frac{(2^R - 1)}{\gamma}$. For triple-polarized channels we have the following outage expressions

$$
\Pr(I < R)_{(1/3,1/3)} = \int_0^\epsilon f_Y(y)_{(1/3,1/3)} dy
\tag{4.21}
$$

$$\Pr(I < R)_{(2/3,2/3)} = \int_0^\epsilon f_Y(y)_{(2/3,2/3)} dy, \tag{4.22}$$

where ϵ for $(1/3, 1/3)$ and $(2/3, 2/3)$ system is given by $\frac{(2^R-1)}{\gamma}$ and $\frac{2(2^R-1)}{\gamma}$, respectively. The results are shown in Figure 4.3(a).
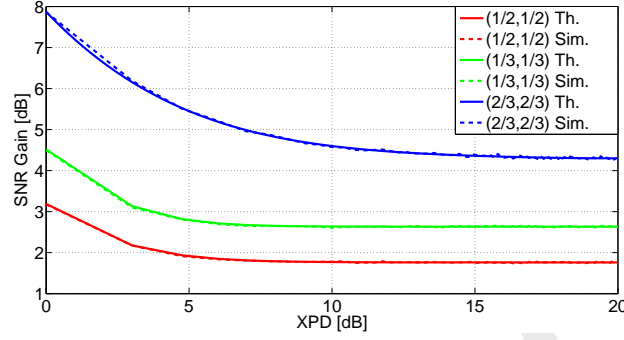
Figure 4.2: Selection gains for polarized systems with transmit/receive antenna selection.
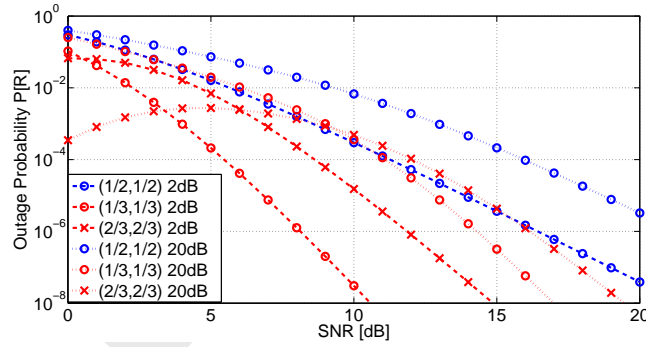
(a) Outage probabilities for joint transmit/receive antenna selection in multi polarized systems at XPD = 2dB and 20dB.
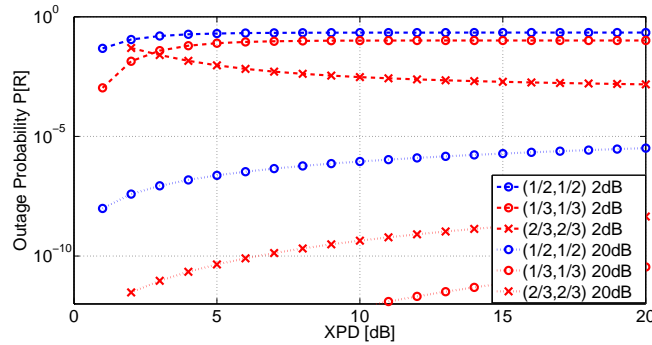
(b) Outage probabilities for joint transmit/receive antenna selection in multi polarized systems at SNR = 2 and 20dB for varying XPD.

Figure 4.3: Outage with joint transmit/receive antenna selection.

From Figure 4.3(a) we see that the performance of a $(1/3, 1/3)$ system is effected severely compared to a $(1/2, 1/2)$ system. This can be explained from Equations (4.10) and (4.13). From the equations

we see that as XPD increases, the available degrees of freedom for a $(1/3, 1/3)$ system decreases from nine to three compared to four to two in a $(1/2, 1/2)$ system. We have also shown here the trend of outage performance with varying XPD at a given SNR for joint transmit/receive antenna selection in Figure 4.3(b). From the figure we observe that the outage performance of a $(2/3, 2/3)$ system improves with increasing XPD values at lower SNRs. All the rest of the systems have a degrading performance for increasing XPD values, both at lower and higher SNRs.

4.5 Effect of XPD on Transmit Selection Gain

Here we try to understand the impact of XPD on the transmit selection gain for $(2/2, l_t/3)$ and $(3/3, l_t/3)$ systems. Such configurations could be used in Wireless Local Area Network (WLAN) or cellular systems where one end of the link is allowed to be more complex than the other. The analysis is general and is applicable to any Orthogonal Space-Time Block Coding (OSTBC) and can be easily adapted for receive antenna selection. The selection strategy outlined below, chooses l_t out of the N_T available transmit antennas to maximize the Frobenius norm of the channel.

$$\tilde{\mathbf{H}} = \operatorname*{argmax}_{S(\overline{\mathbf{H}})} \left\{ \left\| \overline{\mathbf{H}} \right\|_F^2 \right\}, \tag{4.23}$$

where $\tilde{\mathbf{H}}$ is obtained by eliminating $(N_T - l_t)$ columns from $\mathbf{H}$. The term $S(\overline{\mathbf{H}})$ denotes the set of all possible $\tilde{\mathbf{H}}$. Let $Y_k, k = 1, ..., N_T$ denote the squared Frobenius norm of the N_T columns of $\mathbf{H}$. We derive the performance separately for dual-polarized and triple-polarized systems below.

4.5.1 $(2/2, l_t/2)$ TAS

Each column of $\mathbf{H}_{DP}$ has two independent but non-identical zero mean circularly symmetric complex Gaussian random variables with variances 1 and $1/X$, respectively. They have the probability density functions $g_1(y) = e^{-y}$ and $g_2(y) = Xe^{-yX}$, respectively. The random variables $Y_k, k = 1, ..., N_T$ are i.i.d. with unit variance and their probability density function given by

$$f_Y(y)_{(2/2,2/2)} = g_1(y) * g_2(y) = \frac{Xe^{-y}}{X-1}\left(1 - e^{-(X-1)y}\right), \tag{4.24}$$

where, the operator $(*)$ denotes the convolution operation. The cumulative distribution function, can be derived to be

$$F_Y(y)_{(2/2,2/2)} = \int_{-\infty}^{y} f_Y(y)dy = \left(1 - \frac{e^{-y}}{X-1}(X - e^{-(X-1)y})\right). \tag{4.25}$$

Applying the principles of ordered statistics [3], we generate new random variables $Y[k], k = 1, ..., N_T$ from $Y_k, k = 1, ..., N_T$ such that

$$Y_{[N_T]} \ge Y_{[N_T-1]} \ge ... \ge Y_{[k]} \ge ... \ge Y_{[2]} \ge y_{[1]}, \tag{4.26}$$

where $Y_{[k]}$ is the *kth* largest of the N_T random variables distributed according to Equation (4.28). Note that these ordered random variables are no longer statistically independent. The average SNR after selection can then be computed as,

$$E\{\gamma\} = \gamma_0 \left(E\left\{Y_{[N_T]}\right\} + E\left\{Y_{[N_T-1]}\right\} + ... + E\left\{Y_{[N_T-l+1]}\right\} \right), \tag{4.27}$$

$$
\begin{aligned}
E\left\{Y_{[k]}\right\} &= \frac{N_T!}{(k-1)!(N_T-k)!} \int_0^\infty y F_Y(y)^{k-1}(1-F_Y(y))^{N_T-k} f_Y(y) dy \\
&= \frac{N_T!}{(k-1)!(N_T-k)!} \sum_{r=0}^{k-1}(-1)^r \binom{k-1}{r} \int_0^\infty y(1-F_Y(y))^{N_T-k+R} f_Y(y) dy \\
&= \frac{N_T!}{(k-1)!(N_T-k)!} \sum_{r=0}^{k-1}(-1)^r \binom{k-1}{r} J_{N_T-k+r},
\end{aligned}
\tag{4.29}
$$

where $\gamma_0 = \frac{E_S}{l_t N_o}$. The probability density function of of the k-th ordered statistic $Y_{[k]}$ can then be evaluated as [98],

$$
f_k(y) = \frac{N_T!}{(k-1)!(N_T-k)!} F_Y(y)^{k-1}(1-F_Y(y))^{N_T-k} f_Y(y).
\tag{4.28}
$$

The average value of k-th order statistic $T_{[k]}$ can be computed to be as Equation (4.29), where

$$
J_m = \int_0^\infty y(1-F_Y(y))^m f_Y(y) dy.
\tag{4.30}
$$

After calculating the average SNRs for $N_T = 2$ and for $k = 1, 2$ from the expressions above, we arrive at the following results,

$$
E\left\{Y_{[1]}\right\} = 2J_1.
\tag{4.31}
$$

$$
E\left\{Y_{[2]}\right\} = 2(J_0 - J_1).
\tag{4.32}
$$

$$
J_0 = \frac{X}{X-1}\left(1 - \frac{1}{X^2}\right).
\tag{4.33}
$$

$$
J_1 = \left(\frac{X}{X-1}\right)^2\left(\frac{1}{4} - \frac{1}{(X+1)^2}\right) - \frac{X}{(X-1)^2}\left(\frac{1}{(X+1)^2} - \frac{1}{4X^2}\right).
\tag{4.34}
$$

4.5.2 $(3/3, l_t/3)$ TAS

Each column of $\mathbf{H}_{TP}$ has three independent but non-identical zero mean circularly symmetric complex Gaussian random variables with variances 1, $1/X$ and $1/X$, respectively. They have the probability density function given by

$$
\begin{aligned}
f_Y(y) &= g_1(y) * g_2(y) * g_3(y) \\
&= \left(\frac{X}{X-1}\right)^2 e^{-yX}\left(e^{-(X-1)y} - (X-1)y - 1\right).
\end{aligned}
\tag{4.35}
$$

Calculating the value of J_0, J_1, and J_2 we have the following,

$$
J_0 = \frac{2 - 3X + X^3}{X(X-1)^2}.
\tag{4.36}
$$

$$J_1 = \frac{5 + 2X(7 + X(6 + X))}{8X(1 + X)^2}. \tag{4.37}$$

$$J_2 = \frac{104 + X(836 + X(2606 + 9X(431 + 302X + 92X^2 + 8X^3)))}{81X(2 + X)^2(1 + 2X)^3}. \tag{4.38}$$

The average values of ordered SNRs are shown below

$$E\left\{Y_{[1]}\right\} = 3J_2. \tag{4.39}$$

$$E\left\{Y_{[2]}\right\} = 6(J_1 - J_2). \tag{4.40}$$

$$E\left\{Y_{[3]}\right\} = 3(J_0 - 2J_1 + J_2). \tag{4.41}$$

The selection gains in the above Equations (4.39), (4.40) and (4.41) are shown in Figure 4.4.

4.6   Outage Analysis with TAS

In this section we calculate outage probabilities for both dual and triple-polarized MIMO channels with transmit antenna selection. We first calculate the PDFs of the corresponding ordered statistics and then integrate them over the respective range of ϵ. For a $(2/2, 2/2)$ scenario we have from Equation (4.24),

$$
\begin{aligned}
\Pr(I < R)_{(2/2,2/2)} &= \int_0^\epsilon f_Y(y)_{(2/2,2/2)} dy \\
&= \int_0^\epsilon (e^{-y}) * (Xe^{-yX}) dy \\
&= \int_0^\epsilon e^{-y} dy \int_0^\epsilon Xe^{-yX} dy,
\end{aligned}
\tag{4.42}
$$

where $\epsilon = \frac{2(2^R - 1)}{\gamma}$ for dual-polarized systems. The rest of the outages are calculated as follows, together with using ϵ values using Equation (4.28).

$$
\begin{aligned}
\Pr(I < R)_{(2/2,1/2)} &= \int_0^\epsilon f_Y(y)_{(1/2,1/2)} dy \\
&= \int_0^\epsilon 2! F_Y(y)_{(2/2,2/2)} f_Y(y)_{(2/2,2/2)} dy,
\end{aligned}
\tag{4.43}
$$

where $\epsilon = \frac{(2^R - 1)}{\gamma}$ for dual-polarized systems with one antenna selected at the transmit side. Now from Equation (4.35) we have,

$$
\begin{aligned}
\Pr(I < R)_{(3/3,3/3)} &= \int_0^\epsilon f_Y(y)_{(3/3,3/3)} dy \\
&= \int_0^\epsilon g_1(y) * g_2(y) * g_3(y) dy \\
&= \int_0^\epsilon g_1(y) dy \int_0^\epsilon g_2(y) dy \int_0^\epsilon g_3(y) dy \\
&= \int_0^\epsilon g_1(y) dy \int_0^\epsilon 2g_2(y) dy,
\end{aligned}
\tag{4.44}
$$

where $\epsilon = \frac{3(2^R-1)}{\gamma}$ for triple polarized systems and $g_1(y) = (1 - e^{-y})$, $g_2(y) = (1 - e^{-yX})$ and $g_3(y) = (1 - e^{-yX})$. Again from Equation (4.28) we have

$$
\begin{aligned}
\Pr(I < R)_{(3/3,1/3)} &= \int_0^\epsilon f_Y(y)_{(1/3,1/3)} dy \\
&= \int_0^\epsilon 3! F_Y(y)_{(3/3,3/3)} f_Y(y)_{(3/3,3/3)} dy,
\end{aligned}
\tag{4.45}
$$

where $\epsilon = \frac{(2^R-1)}{\gamma}$ for triple polarized systems with one antenna selected at the transmit side. For the configuration $(3/3, 2/3)$ we proceed as follows. We convolve the second (highest) order and the first (2nd highest) order statistics. The highest order statistic is calculated from Equation (4.28) as

$$
f_2(y)_{(3/3,2/3)} = 3! F_Y(y)(1 - F_Y(y)) f_Y(y),
\tag{4.46}
$$

and the 2nd highest order statistics is found to be as

$$
f_1(y)_{(3/3,2/3)} = \frac{3!}{2!}(1 - F_Y(y))^2 f_Y(y).
\tag{4.47}
$$

thus,

$$
\Pr(I < R)_{(3/3,2/3)} = \int_0^\epsilon f_2(y)_{(3/3,2/3)} * f_1(y)_{(3/3,2/3)} dy,
\tag{4.48}
$$

where $\epsilon = \frac{2(2^R-1)}{\gamma}$ for triple-polarized systems with two antennas selected at the transmit side. The analytical results are shown in Figures 4.5(a). Here we have also provided the trends for outage probabilities with respect to varying XPD values for specific SNRs. From Figure 4.5(a) we see that the performance of $(3/3, 3/3)$ and $(2/2, 2/2)$ full complexity systems does not improve much while increasing the SNR. The slopes of the curves are almost the same. Compared to these, the systems with antenna selection perform better when SNR is increased.
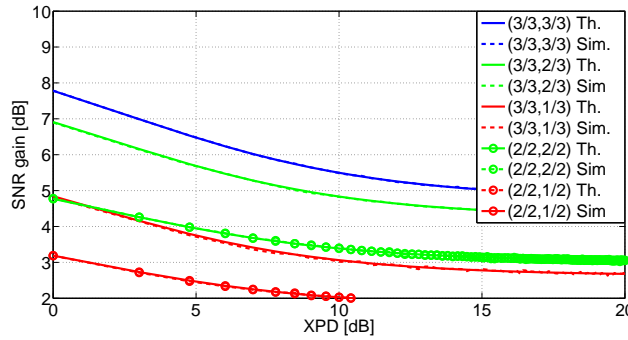
Figure 4.4: Selection gains for polarized systems with transmit antenna selection.

4.7 Simulation Results and Discussion

In Figures 4.2 and 4.4 we compare both the analytical and simulation results for selection gains. The simulations completely verify the analytical results presented in the previous sections. Simulations
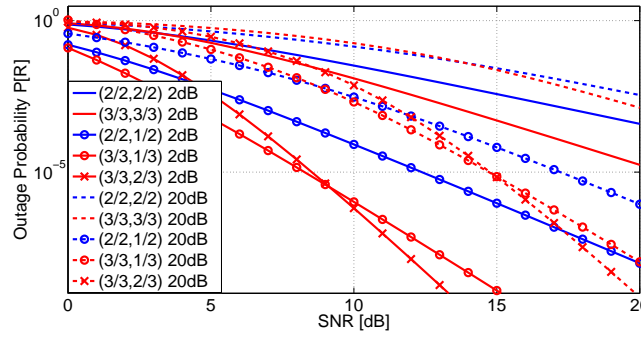
(a) Outage probabilities for transmit antenna selection in multi polarized systems at XPD = 2dB and 20dB.
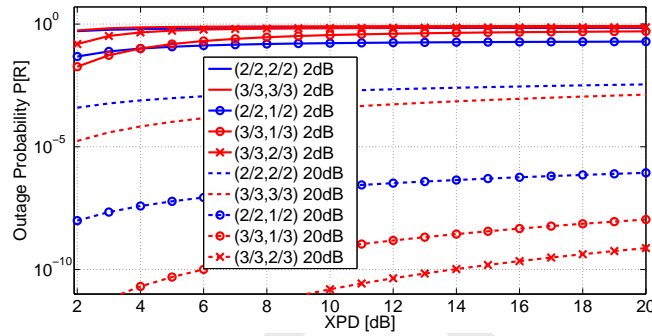
(b) Outage probabilities for transmit antenna selection in multi polarized systems at 2dB and 20dB SNR for varying XPD.

Figure 4.5: Outage with joint transmit antenna selection.

were carried out in the following way. A complex Gaussian matrix with zero mean and unit variance was generated for the given number of antennas. This matrix was multiplied with an XPD matrix to reflect the different variances in the cross-polar components. Selection was performed on the basis of Equation (4.23). For joint transmit/receive antenna selection, first selection is performed on receive side of the link. The non-selected rows are deleted from the complete matrix. Now the columns are selected from the remaining matrix, deleting the non-selected columns. This gives the selected channel. The process is shown below,

$$H_X = [X]_{M_R \times N_T} \odot [H]_{M_R \times N_T}. \tag{4.49}$$

where

$$[X]_{2\times 2} = \left[\begin{array}{cc} 1 & 1/X \\ 1/X & 1 \end{array} \right]. \tag{4.50}$$

and

$$[X]_{3\times 3} = \left[\begin{array}{ccc} 1 & 1/X & 1/X \\ 1/X & 1 & 1/X \\ 1/X & 1/X & 1 \end{array} \right]. \tag{4.51}$$

All the X values are taken as identical. From Figure 4.2 we see that although the $(2/3, 2/3)$ system has the maximum SNR gain, its is effected more by the variations in XPD. The difference in the maximum and the minimum SNR gain for this system is 3.6dB compared to 1.87dB and 1.41dB for $(1/3, 1/3)$ and $(1/2, 1/2)$ systems, respectively. This is because of high probability of any of the selected channels

to be cross-polar. A similar behavior can be observed in Figure 4.4 for transmit antenna selection. Few differences still can be observed. A $(1/2, 1/2)$ is effected more compared to a $(2/2, 1/2)$ system in the range of XPD values from 0 to 14dB. Similarly a $(1/3, 1/3)$ system has more performance loss compared to a $(3/3, 1/3)$ system for a range of XPD values from 0 to 20dB. Comparing a $(2/3, 2/3)$ and a $(3/3, 2/3)$ system, the trend is a little different. For low XPD values, a $(2/3, 2/3)$ system is less effected but this trend changes for larger values of XPD. Thus, the limiting cases can be easily observed from the Figure 4.5(b).

4.8   Conclusions

The analysis in terms of poynting vector as mentioned in the previous chapter can be performed for triple polarized MIMO systems as well. Also the methods applied to obtain channel gains and capacity bounds can be obtained for triple polarized systems for various channels. Some novel space time codes can be devised for enhancing the performance of multipolarized systems.

We simulate and analyze the performance of multi-polarized systems with Spatial Multiplexing (SM) and Transmit Diversity (TD) techniques using receive antenna selection, in the next chapter.

<div style="text-align: right; font-size: 3em;">5</div>

Performance of SM and Diversity in Polarized MIMO with RAS

5.1 Introduction

MIMO transmission techniques, such as Space Time Block Coding (STBC) [99], [100] or Spatial Multiplexing (SM) [101], are known to achieve significant diversity or multiplexing gains. However, in MIMO systems, correlations may occur between channels due to insufficient antenna spacing and the scattering properties of the transmission environment. This may lead to significant degradation in system performance [29]. In order to have an uncorrelated channel between the transmitter and receiver large antenna spacings are required both at the base-station and the subscriber unit. On the other hand, due to this space requirement, deploying multiple antennas may not be feasible in all communication schemes. For this reason, the use of dual-polarized antennas instead of uni-polarized antennas is a cost and space-effective alternative, where two spatially separated uni-polarized antennas are replaced by a single dual-polarized antenna. Communication with dual-polarized antennas require transmitting two independent symbols on the same bandwidth and the same carrier frequency at the same time by using two orthogonal polarizations. However as pointed out in [52] [53], imperfections of transmit and/or receive antennas and XPD are the results of the two depolarization mechanisms: the use of imperfect antenna cross-polar isolation (XPI) and the existence of a Cross-Polar Ratio (XPR) in the propagation channel. These effects degrade the system performance considerably. In [6], a system employing one dual-polarized antenna at the transmitter and one dual-polarized antenna at the receiver is presented and the error performance of 2-antenna SM and STBC transmission schemes are derived for this virtual MIMO system. Notice that, in [102], a SISO system is enabled with MIMO capabilities through the use of dual-polarized antennas. In this section, we present the performance of MIMO systems employing triple-polarized antennas under different correlation parameters and XPD factors over correlated Rayleigh fading channels. Performance for dual-polarized systems with antenna selection can be found in [85, 103]. In this regard, not only the transmit and receive antenna correlations and the XPD factor, but also a spatial correlation is included in the system analysis. In this chapter we evaluate the following four transmission schemes:

1. 2-antenna Alamouti

2. 2-antenna SM

3. 3-antenna STBC

4. 3-antenna SM

The error performance of these schemes are presented with simulation results. We also show the performance of such systems with the use of receive antenna selection and analyze through simulations the performance gains. Notice that this range of transmission alternatives over the same physical system allow an efficient trade-off between the diversity gain and the multiplexing gain that the overall system can achieve. Even though the results can be generalized to any number of transmit/receive antennas, throughout the chapter only a 3×3 triple-polarized antenna system is considered where it is shown to have better performance than the 3×3 unipolarized antenna systems. The use of triple-polarized antennas leads the way to achieve diversity and multiplexing gains at a high rate, when combined with the link adaptation algorithms which are envisioned for next generation wireless communication systems with MIMO capabilities such as those proposed with the IEEE 802.11n and 802.16e standards, with dual-polarized antenna technology. The channel model in this section is described earlier in Section 4.2. We add the effects of LOS and NLOS channels here. The channel matrix can now be decomposed into the sum of an average and a variable component as,

$$\mathbf{H} = \sqrt{\frac{K}{K+1}} \overline{\mathbf{H}} + \sqrt{\frac{1}{K+1}} \check{\mathbf{H}}, \tag{5.1}$$

where the elements of $\overline{\mathbf{H}}$, denoted as $\overline{h}_{i,j}$, $(ij :\in \{V, H, Z\})$, represents the fixed components of the channel matrix and the elements of $\check{\mathbf{H}}$, denoted as $\check{h}_{i,j}$, are zero-mean circularly symmetric complex Gaussian random variables whose variances depend on the propagation environment and the characteristics of the antennas at both link ends. The fixed and the variable channel components are assumed to satisfy the following conditions for both dual and triple polarized systems.

$$\begin{aligned}
\left|\overline{h}^{VV}\right|^2 = \left|\overline{h}^{HH}\right|^2 = \left|\overline{h}^{ZZ}\right|^2 &= 1 \\
\left|\overline{h}^{HV}\right|^2 = \left|\overline{h}^{VH}\right|^2 &= \alpha_f \\
\left|\overline{h}^{VZ}\right|^2 = \left|\overline{h}^{ZV}\right|^2 &= \alpha_f \\
\left|\overline{h}^{HZ}\right|^2 = \left|\overline{h}^{ZH}\right|^2 &= \alpha_f \\
E\left\{\left|\check{h}^{VV}\right|^2\right\} = E\left\{\left|\check{h}^{HH}\right|^2\right\} = E\left\{\left|\check{h}^{ZZ}\right|^2\right\} &= 1 \\
E\left\{\left|\check{h}^{HV}\right|^2\right\} = E\left\{\left|\check{h}^{VH}\right|^2\right\} &= \alpha \\
E\left\{\left|\check{h}^{VZ}\right|^2\right\} = E\left\{\left|\check{h}^{ZV}\right|^2\right\} &= \alpha \\
E\left\{\left|\check{h}^{HZ}\right|^2\right\} = E\left\{\left|\check{h}^{ZH}\right|^2\right\} &= \alpha,
\end{aligned} \tag{5.2}$$

where $0 < \alpha_f < 1$ and $0 < \alpha < 1$ are the XPD values for fixed and the variable channels respectively. The Ricean K-factor, which denotes the ratio between the power of LOS and the power of NLOS components, is defined as,

$$K_{VV} \;\; = \;\; K_{HH} = K_{ZZ} = K, \tag{5.3}$$

$$K_{HV} \quad = \quad K_{VH} = K_{HZ} = K_{ZH} = K_{VZ} = K_{ZV} = \frac{\alpha_f}{\alpha} K. \tag{5.4}$$

Some experiments [102] [104] have shown that their exists certain amount of correlation between elements of such channels. We, therefore define the various correlations as follows,

$$t \quad = \quad \frac{E\left\{\check{h}_{HH}\check{h}_{VH}^*\right\}}{\sqrt{\alpha}} = \frac{E\left\{\check{h}_{HV}\check{h}_{VV}^*\right\}}{\sqrt{\alpha}} = \frac{E\left\{\check{h}_{HH}\check{h}_{ZH}^*\right\}}{\sqrt{\alpha}} = \frac{E\left\{\check{h}_{HZ}\check{h}_{ZZ}^*\right\}}{\sqrt{\alpha}} \tag{5.5}$$

$$r \quad = \quad \frac{E\left\{\check{h}_{HH}\check{h}_{HV}^*\right\}}{\sqrt{\alpha}} = \frac{E\left\{\check{h}_{VH}\check{h}_{VV}^*\right\}}{\sqrt{\alpha}} = \frac{E\left\{\check{h}_{HH}\check{h}_{HZ}^*\right\}}{\sqrt{\alpha}} = \frac{E\left\{\check{h}_{ZH}\check{h}_{ZZ}^*\right\}}{\sqrt{\alpha}}, \tag{5.6}$$

where t is referred to as the transmit correlation coefficient, and r is the receive correlation coefficient. Recall that we assumed that $\alpha > 0$, which ensures viability of the above definitions. Experiments have shown that the correlation between the diagonal elements of the channel matrix $\check{h}_{HH}$ and $\check{h}_{VV}$, $\check{h}_{HH}$ and $\check{h}_{ZZ}$, $\check{h}_{VV}$ and $\check{h}_{ZZ}$ and the off-diagonal elements $\check{h}_{HV}$ and $\check{h}_{VH}$, $\check{h}_{HZ}$ and $\check{h}_{ZH}$, $\check{h}_{VZ}$ and $\check{h}_{ZV}$ is typically very small. For the sake of simplicity, throughout the chapter, we therefore assume them to be equal to zero. Measured values of XPD, K-factor, and correlation coefficients can be found in [104].

5.2 Data Model

For dual-polarized systems we simply send the symbols x_1, x_2 at full rate Alamouti code on the two transmit antennas. For various transmission schemes mentioned in previously we use the following 1/2-rate and 3/4-rate complex G_3 space time code as given in [105] at the three antennas of triple-polarized antenna system.

$$\mathbf{X}_2^{DP} = \begin{bmatrix} x_1 & -x_2^* \\ x_2 & x_1^* \end{bmatrix}. \tag{5.7}$$

The data model for 1/2-rate G_3 coding we send the symbols $x_1 \cdots x_4$ on three antennas over complex signal constellations and is given as follows,

$$\mathbf{X}_3^{TP} = \begin{bmatrix} x_1 & -x_2 & -x_3 & -x_4 & x_1^* & -x_2^* & -x_3^* & -x_4^* \\ x_2 & x_1 & -x_4 & -x_3 & x_2^* & x_1^* & x_4^* & -x_3^* \\ x_3 & -x_4 & x_1 & x_2 & x_3^* & -x_4^* & x_1^* & x_2^* \end{bmatrix}. \tag{5.8}$$

The data model for 3/4-rate G_3 coding we send the symbols $x_1 \cdots x_3$ on three antennas over complex signal constellations and is given as follows,

$$\mathbf{X}_3^{TP} = \begin{bmatrix} x_1 & x_2^* & x_3^* & 0 \\ -x_2 & x_1^* & 0 & -x_3^* \\ -x_3 & 0 & x_1^* & x_2^* \end{bmatrix}. \tag{5.9}$$

These symbols are mapped to the horizontal and vertical polarizations of the dual-polarized antennas and to another horizontal antenna for triple-polarized antenna system. Maximum-ratio combining is employed at the receiver in order to obtain the decision metrics [105]. Due to the orthogonality of the transmit matrices given in Equations (5.7),(5.8) and (5.9), the Maximum Likelihood (ML) detection involves a simple linear operation in the receiver and can be used to detect the transmit symbols $x_1 \cdots x_4$, assuming that the channel is static during consecutive symbol periods. For example the channel should be static for two symbol periods in Equation (5.7). Eight for Equation (5.8) and three

for Equation (5.9). The orthogonality characteristic of $\mathbf{X}$ is based on the orthogonal designs. The data model for pure spatial multiplexing schemes that maximize the spectral efficiency are shown below both for dual and triple-polarized antenna systems. Well-known schemes proposed with this focus are the Bell laboratories layered space-time (BLAST) schemes, such as the vertical-BLAST (VBLAST) and diagonal-BLAST [101]. In the VBLAST scheme, all the antennas are used to multiplex different symbols in each symbol period. In this scheme each different multiplexed symbol is defined as a layer. For instance, in the case of three transmit antennas we have three layers. In this section we use Maximum Likelihood (ML) receivers for both the transmission schemes. The transmitted signals at any time instant, considering two or three transmit antennas, can be organized in the equivalent space-time coding matrices,

$$\mathbf{X}_2^{DP} = \left[\begin{array}{c} x_1 \\ x_2 \end{array} \right], \tag{5.10}$$

$$\mathbf{X}_3^{TP} = \left[\begin{array}{c} x_1 \\ x_2 \\ x_3 \end{array} \right]. \tag{5.11}$$

5.3   Antenna Subset Selection for Capacity Maximization

We consider a Multiple-Input Single-Output (MIMO) system equipped with N_T transmit and M_R receive antennas. We suppose that the transmitter employs N_T RF chains whereas the receiver uses $l_r (\leq M_R)$ RF chains. The channel is assumed quasi-static fading. The performance of this MIMO system is calculated on the basis of maximum mutual information. Assuming the Channel State Information (CSI) is known to the receiver but unknown to the transmitter, and that the transmit power P is evenly distributed among the antennas, the instantaneous capacity [22] for a given channel realization is given by

$$C(\mathbf{H}) = \log_2 \det \left(\mathbf{I}_{M_R} + \frac{\gamma}{N_T} \mathbf{H}\mathbf{H}^\dagger \right) (\text{bits/s/Hz}), \tag{5.12}$$

where N_T is the number of transmit antennas, γ is the average SNR at each receiver branch and $\frac{P}{\sigma_n^2}$. The performance with receive antenna selection is calculated by selecting those l_r out of M_R receive antennas that maximize the Frobenius norm for a given channel realization. In other words we select those rows of the channel matrix $\mathbf{H}$ which have the maximum norm and then calculate their mutual information. Thus, the previous equation with receive antenna selection becomes

$$C(\tilde{\mathbf{H}}) = \log_2 \det \left(\mathbf{I}_{l_r} + \frac{\gamma}{N_T} \tilde{\mathbf{H}}\tilde{\mathbf{H}}^\dagger \right), \tag{5.13}$$

where $\tilde{\mathbf{H}}$ represents the selected sub matrix.

5.4   Simulation Results and Discussion

In this section, we provide simulation results demonstrating the performance of SM and the Alamouti scheme for varying channel scenarios. We simulated a system with one dual-polarized transmit and one dual-polarized receive antenna. Similarly we simulated a system with one triple-polarized transmit and

one triple-polarized receive antenna. In order to keep the data rates in both systems (SM and STBC) the same, the data symbols for SM were drawn from a 4-QAM constellation, whereas the data symbols for the Alamouti scheme were drawn from a 16-QAM constellation for dual polarized system. For triple-polarized ML decoding with perfect channel knowledge was performed. All simulation results were obtained by averaging over 1×10^5 independent Monte Carlo trials.

5.4.1   Simulation Example 1:

The first simulation example serves to demonstrate BER for SM. For $t = 0.5, r = 0.3, \alpha = 0.4$, and $\alpha_f = 0.3$, the Figure 5.1(a) shows the BER obtained using Monte Carlo simulations. At higher K values dual-polarized system behaves better compared to lower K values. This trend is opposite in triple-polarized antenna systems. Selection in triple-polarized systems does not give a very significant performance improvement compared to dual-polarized system without selection.

5.4.2   Simulation Example 2:

This simulation example shows the potential benefit of dual-polarized and triple-polarized antennas at high K-factor for systems employing SM. For high K-factor, the BER is governed primarily by the characteristics of the fixed component $\overline{\mathbf{H}}$. In Figure 5.1(b), we plot the BER as a function of α_f for $t = 0.5, r = 0.3, \alpha = 0.4$, $K = 10$ and SNR of 15dB. We note here that $\alpha_f = 1$ corresponds to the case of two and three physical uni-polarized antennas, the plot reveals that system performance improves by over an order of magnitude with the use of dual-polarized antennas or triple-polarized antennas. At $K = 0$, all the systems are decreasing functions of BER. This behavior is different for high K values. The BER is maximum at $\alpha_f = 0.5$. Antenna selection does not help in improving the performance much.

5.4.3   Simulation Example 3:

This example serves to demonstrate that provides bit error rate for the Alamouti scheme for dual-polarized system and half rate G3 code for triple-polarized system. For $t = 0.7, r = 0.1, \alpha = 0.2$, and $\alpha_f = 0.6$, Figure 5.1(c) shows the bite error rate obtained using Monte Carlo simulations. We see that the performance of a triple-polarized system with two antenna selected at the receiver performs better than the corresponding dual-polarized antenna systems with all antenna elements.

5.4.4   Simulation Example 4:

In this simulation the effect of K-factor on the coding schemes is investigated. We consider the channel with $\alpha = \alpha_f$. We know that at high K-factor, $\overline{\mathbf{H}}$ is responsible for the performance,, whereas $\check{\mathbf{H}}$ dominates at low K-factor. Figure 5.1(d) the BER for Alamouti and G3 codes as a function of K for $t = 0.5, r = 0.3, \alpha = \alpha_f = 0.6$ for an SNR of 17dB. From the figure we see that triple-polarized system with single antenna selected at the receiver has slightly better performance than full complexity dual-polarized system. The performance boosts further if another antenna is selected.
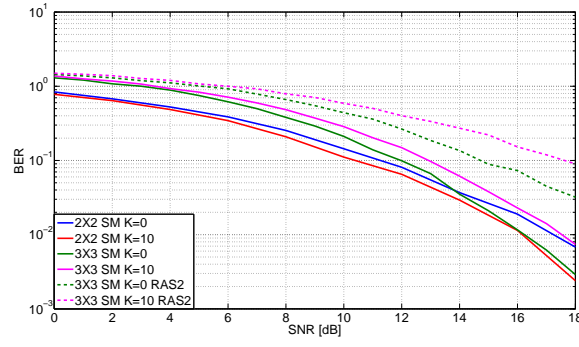
(a) Bit error ratio for spatial multiplexing as a function of SNR for varying K-factor.
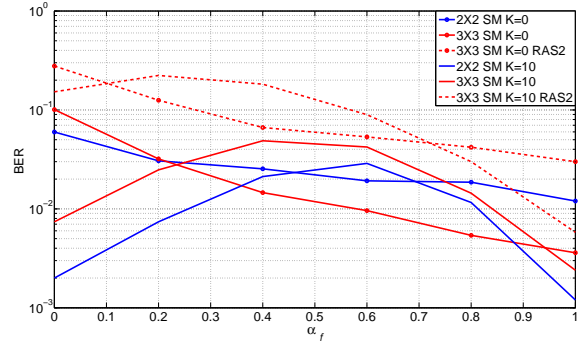
(b) Bit error ratio for spatial multiplexing as a function of α_f.
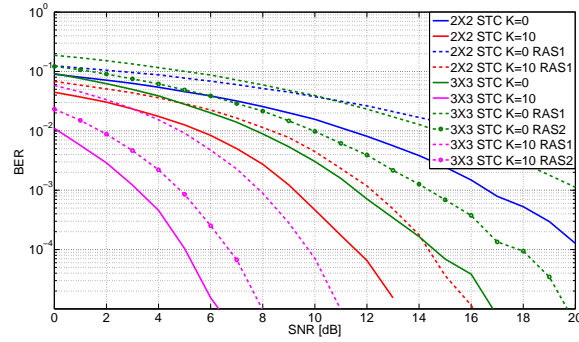
(c) Bit error ratio for the Alamouti and 1/2-rate G3 scheme as a function of SNR for varying K-factor.
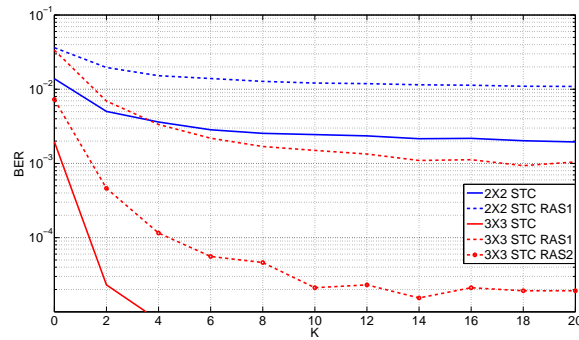
(d) Bit error ratio for the Alamouti and 1/2-rate G3 scheme as a function of K-factor.

Figure 5.1: Error performance of SM and TD MIMO with antenna selection.

5.5   Conclusions

We considered the use of multiple antenna signaling technologies, specifically Space Time Block Coding (STBC) and spatial multiplexing (SM) schemes, in MIMO communication systems employing dual polarized antennas at both ends. In our work, we consider these effects and model a 3×3 system with triple-polarized antennas for both STBC and SM cases. We also present simulation results for both multi-antenna signaling techniques together with hybrid approaches under various Cross Polarization Discrimination (XPD) and correlation scenarios. The results show a significant performance gain by joint utilization of space, time and polarization diversity in comparison to uni-polarized systems with the same number of antennas.

Selection methods applied in all the previous chapters increase in complexity as the number if antenna elements grow. In the next chapter we analyze systems with various channel parameters, in terms of convex optimization theory, to reduce computational complexity.

6

Antenna Selection with Convex Optimization

6.1 Introduction

An exhaustive search over all possible antennas for maximum output Signal to Noise Ratio (SNR) is proposed in [26], when the system uses linear receivers. Since exhaustive search is computationally expensive for large Multiple-Input Multiple-Output (MIMO) systems, several sub-optimal algorithms with lower complexity are derived at the expense of performance. A selection algorithm based on accurate approximation of the conditional error probability of quasi-static MIMO systems is derived in [106]. In [107], the authors formulate the receive antenna selection problem as a combinatorial optimization problem and relax it to a convex optimization problem. They employ an interior point algorithm, i.e., a barrier method, to solve a relaxed convex problem. However, they treat only the case of capacity maximization. An alternative approach to receive antenna selection for capacity maximization that offers near optimal performance at a complexity, significantly lower than the schemes in [22] but marginally greater than the schemes in [108], is described in [109]. In [110, 111] a new approach to antenna selection is proposed, based on the minimization of the union bound, which is the sum of the all Pairwise Error Probabilities (PEPs). In this chapter we apply convex optimization techniques on 2D and 3D antenna arrays to optimize the performance in terms of capacity. Our approach is based on formulating the selection problem as a combinatorial optimization problem and relaxing it to obtain a problem with a concave objective function and convex constraints. We follow the lines of [107] [109], and extend it to systems with both spatial and angular correlation, so-called True Polarization Diversity (TPD) [59–61] arrays. We optimize the performance of systems with such arrays of antennas which are both spatially separated and also inclined at a certain angle. A model for combined spatial and angular correlation functions is also given in [72], but we adhere to the work from Valenzuela [59–61]. We apply a simple norm based antenna selection method to a Polarization Diverse (PD) array for both 2D and 3D arrays in this chapter. Applications of receive antenna selection on polarized arrays can be found in [69] [85].

6.2 System Model

We consider a MIMO system with N_T transmit and M_R receive antennas. The channel is assumed to have frequency-flat Rayleigh fading with Additive White Gaussian Noise (AWGN) at the receiver. The received signal can thus be represented as

$$\mathbf{x}(k) = \sqrt{E_s}\mathbf{H}\mathbf{s}(k) + \mathbf{n}(k), \tag{6.1}$$

where $M_R \times 1$ vector $\mathbf{x}(k) = [x_1(k), \ldots, x_{M_R}(k)]^T$ represents the kth sample of the signals collected at the M_R receive antennas, sampled at symbol rate. The $N_T \times 1$ vector $\mathbf{s}(k) = [s_1(k), \ldots, s_{N_T}(k)]^T$ is the kth sample of the signal transmitted from the N_T transmit antennas. The symbol E_s denotes the average energy per receive antenna and per channel use, $\mathbf{n}(k) = [n_1(k), \ldots, n_{M_R}(k)]^T$ describes the noise of an AWGN channel with energy $N_0/2$ per complex dimension and $\mathbf{H}$ is the $M_R \times N_T$ channel matrix, where $H_{p,q}(p = 1, \ldots, M_R, q = 1, \ldots, N_T)$ is a scalar channel between the pth receive antenna and q^{th} transmit antenna. The entries of $\mathbf{H}$ are assumed to be Zero-Mean Circularly Symmetric Complex Gaussian (ZMCSCG), such that the covariance matrix of any two columns of $\mathbf{H}$ is a scaled identity matrix. Perfect Channel State Information (CSI) is assumed at the receiver while performing antenna subset selection. No CSI is available at the transmitter. The correlation models are taken from the work of [59–61, 72]. The array is with an aperture size of $L_r = \lambda/2$, the antennas in the array are randomly oriented in space and also separated by the spatial separation of d_r. Thus, we have $d_r = L_r/(M_R - 1)$. The inter element distance in a Uniform Linear Array (ULA) configuration depends on the radius. This limits the total number of antennas that can be stacked in a given area constraint. From [70] and [71], a practical measure for r is given to be 0.025λ. Thus, a maximum of nine antenna elements can be stacked in such configurations. The angles are represented by θ_r. The radiation patterns of all the elements in a ULA configuration are constant. But in an array of polarized antenna elements, different patterns exist due to the slant angles, hence introducing both, pattern and polarization diversity. Here, for the sake of simplicity we assume only polarization diversity and discard the effects produced by pattern diversity. The investigations of [60, 72, 112] describe the correlation models for structures with both angular as well as spatial diversity. We work on the modified model given in [72], which also is in agreement to the model presented in [60]. The spatial correlation between two consecutive identical antennas can be found in [61]. The combined spatial-polarization correlation function as given in [72] is a separable function of space d_r and angle θ_r variables, shown below

$$\varsigma(d_r, \theta_r) = \text{sinc}(kd_r)\cos\theta_r. \tag{6.2}$$

If we have a ULA configuration, $\varsigma_r = \text{sinc}(kd_r)$ and $\varsigma_a = \cos\theta_r$ for the angular separated configuration. We use these simple models in order to describe correlation values. It should be noted that effects of mutual coupling are ignored here for the sake of simplicity. We have shown a six element True Polarization Diversity (TPD) antenna array in Figure 6.1.

6.3 Capacity Maximization for RAS

We focus here on receive antenna selection for capacity maximization. The capacity of the MIMO system is given by the well known formula

$$C(H) = \max_{\text{trace}(\mathbf{R}_{ss}) \leq \text{K}} \log_2 \det\left(\mathbf{I}_{N_T} + \frac{\gamma}{N_T}\mathbf{R}_{ss}\mathbf{H}^H\mathbf{H}\right), \tag{6.3}$$
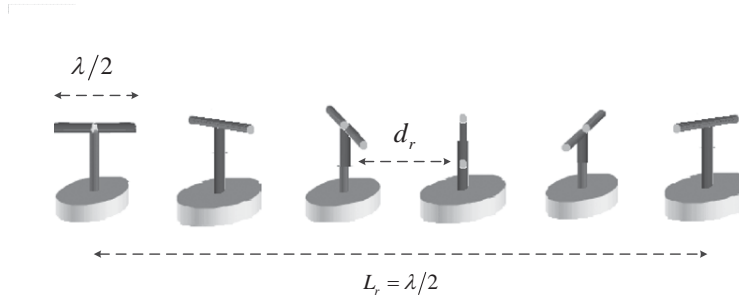
Figure 6.1: True polarization diversity antenna array with $M_R = 6$ antenna elements.

where trace($\mathbf{R_{ss}}$) is the power of the transmitted symbols, K denotes an upper bound for power which here we have taken to be equal to one. It is also defined as the maximally allowed transmit power. Applying these conditions maximizes the capacity given by,

$$C(\mathbf{H}) = \log_2 \det \left(\mathbf{I}_{N_T} + \frac{\gamma}{N_T} \mathbf{R}_{ss} \mathbf{H}^H \mathbf{H} \right),$$ (6.4)

where $\gamma = E_s/N_0$, $\mathbf{R}_{ss} = E\left(\mathbf{s}(k)\mathbf{s}(k)^H \right)$ is the covariance matrix of the transmitted signals with trace($\mathbf{R}_{ss}$) = 1. The determinant is denoted by det($\cdot$) and $\mathbf{I}_{N_T}$ represents the $N_T \times N_T$ identity matrix. However, when only $l_r < M_R$ receive antennas are used, the capacity becomes a function of the antennas chosen. If we represent the indices of the selected antennas by $\mathbf{r} = [r_1, \ldots, r_{l_r}]$, the effective channel matrix is $\mathbf{H}$ with those rows only corresponding to these indices. Denoting the resulting $M_R' \times N_T$ matrix by $\mathbf{H}_r$, the channel capacity with antenna selection is given by

$$C_r(\mathbf{H}_r) = \log_2 \det \left(\mathbf{I}_{N_T} + \frac{\gamma}{N_T} \mathbf{R}_{ss} \mathbf{H}_r^H \mathbf{H}_r \right).$$ (6.5)

In the absence of CSI at the transmitter, $\mathbf{R}_{ss}$ is chosen as $\mathbf{I}_{N_T}$. Our goal is to chose the index set $\mathbf{r}$ such that the capacity in Equation (6.5) is maximized. A closed form characterization of the optimal solution is difficult. We propose a possible selection scheme in the next section.

6.4 Optimization Algorithm for Antenna Selection in 2-D arrays

We formulate the problem of receive antenna selection as a constrained convex optimization problem [113] that can be solved efficiently using numerical methods such as interior-point algorithms [114]. Similar to [109], the $\Delta_i (i = 1, \ldots, M_R)$ is defined such that,

$$\Delta_i = \begin{cases} 1, & i^{th} \text{ receive antenna selected} \\ 0, & \text{otherwise.} \end{cases}$$ (6.6)

By definition, $\Delta_i = 1$ if $r_i \in \mathbf{r}$, and 0 else. Now, consider an $M_R \times M_R$ diagonal matrix $\mathbf{\Delta}$ that has Δ_i as its diagonal entries. Thus, the MIMO channel capacity with antenna selection can be re-written as

$$\begin{aligned} C_r(\mathbf{\Delta}) &= \log_2 \det \left(\mathbf{I}_{N_T} + \frac{\gamma}{N_T} \mathbf{H}^H \mathbf{\Delta} \mathbf{H} \right) \\ &= \log_2 \det \left(\mathbf{I}_{M_R} + \frac{\gamma}{N_T} \mathbf{\Delta} \mathbf{H} \mathbf{H}^H \right). \end{aligned}$$ (6.7)

in previous notation, $\tilde{\mathbf{H}} = \mathbf{\Delta H}$. The second euality in Equation (6.7) follows from the matrix identity

$$\det(\mathbf{I}_m + \mathbf{AB}) = \det(\mathbf{I}_n + \mathbf{BA}).$$

The capacity expression given by $C_r(\mathbf{\Delta})$ is concave in $\mathbf{\Delta}$. The proof follows from the following facts: The function $f(\mathbf{X}) = \log_2\det(\mathbf{X})$ is concave in the entries of $\mathbf{X}$ if $\mathbf{X}$ is a positive definite matrix, and the concavity of a function is preserved under an affine transformation [113]. We transform Equation (6.7) into another form that includes the correlation matrices,

$$C_r(\mathbf{\Delta}) = \log_2\det\left(\mathbf{I}_{M_R} + \frac{\gamma}{N_T}\mathbf{\Delta R}_R^{1/2}\mathbf{H R}_T^{1/2}\mathbf{R}_T^{H/2}\mathbf{H}^H\mathbf{R}_R^{H/2}\right), \tag{6.8}$$

where $\mathbf{R}_T^{1/2}$ and $\mathbf{R}_R^{1/2}$ are the normalized correlation matrices at the transmit and receive side. We assume that antennas at the transmit side are well separated to avoid any correlation. The matrix $\mathbf{R}_T^{1/2}$ would then be an identity matrix and can be ignored in the above equation. After applying rotation and simplification, Equation (6.8) can be written as,

$$C_r(\mathbf{\Delta}) = \log_2\det\left(\mathbf{I}_{M_R} + \frac{\gamma}{N_T}\mathbf{R}_R^{H/2}\mathbf{\Delta R}_R^{1/2}\mathbf{H H}^H\right). \tag{6.9}$$

We split the correlation matrix $\mathbf{R}_R^{1/2}$ into two parts: the spatial separation and the polarization of individual antenna elements and obtain,

$$C_r(\mathbf{\Delta}) = \log_2\det\left(\mathbf{I}_{M_R} + \frac{\gamma}{N_T}\mathbf{R}_S^{H/2} \cdot \mathbf{R}_P^{H/2}\mathbf{\Delta R}_P^{1/2} \cdot \mathbf{R}_S^{1/2}\mathbf{H H}^H\right), \tag{6.10}$$

where $\mathbf{R}_S^{1/2}$ is the normalized correlation matrix due to the spatial separation and $\mathbf{R}_P^{1/2}$ is the additional correlation matrix due the polarization of antenna elements. The elements of these matrices are found from Equation (6.2). The variables Δ_i are binary valued (0 or 1) integer variables, thereby rendering the selection problem NP-hard. We seek a simplification by relaxing the binary integer constraints and allowing $\Delta_i \in [0, 1]$. To make things easily tractable we divide the optimization problem into two parts. We first calculate the optimum $\mathbf{R}_P^{1/2}$ and then find the optimum $\mathbf{\Delta}$ as a separate optimization problem. Thus, the problem of receive antenna subset selection for capacity maximization is approximated by the constrained convex relaxation plus rounding schemes:

$$\text{maximize} \quad \log_2\det\left(\mathbf{I}_{M_R} + \frac{\gamma}{N_T}\mathbf{R}_S^{H/2} \cdot \mathbf{R}_P^{H/2}\mathbf{R}_P^{1/2} \cdot \mathbf{R}_S^{1/2}\mathbf{H H}^H\right) \tag{6.11a}$$

$$\text{subject to}$$

$$r_p(m, m) = 1, \quad m = 1, \ldots, M_R \tag{6.11b}$$

$$|r_p(m, n)| \leq 1, \quad m, n = 1, \ldots, M_R; m \neq n \tag{6.11c}$$

$$\mathbf{R}_S^{1/2} \cdot \mathbf{R}_P^{1/2} \leq [1]_{M_R \times M_R}, \tag{6.11d}$$

where $[1]_{M_R \times M_R}$ is a matrix of all the elements equal to one. We now suppose that $\mathbf{R}_{PD}^{1/2} = \mathbf{R}_S^{1/2} \cdot \mathbf{R}_P^{1/2}$, where $\mathbf{R}_P^{1/2}$ is the optimum correlation matrix. We use this matrix $\mathbf{R}_P^{1/2}$ obtained from Equation (6.11d), to obtain the optimum $\mathbf{\Delta}$,

$$\text{maximize} \quad \log_2\det\left(\mathbf{I}_{M_R} + \frac{\gamma}{N_T}\mathbf{R}_{PD}^{H/2}\mathbf{\Delta R}_{PD}^{1/2}\mathbf{H H}^H\right) \tag{6.12a}$$

subject to

$$0 \leq \Delta_i \leq 1, \quad i = 1, \ldots, M_R \tag{6.12b}$$

$$\text{trace}(\boldsymbol{\Delta}) = \sum_{i=1}^{M_R} \Delta_i = l_r. \tag{6.12c}$$

The objective function in Equation (6.11a) is concave because the correlation matrices defined by $\mathbf{R}_P^{1/2}$ and $\mathbf{R}_S^{1/2}$ are positive definite and hermitian. Since the constraints Equations (6.11b)-(6.11d) are linear and affine, the whole optimization algorithm Equation (6.11) is concave and can be solved efficiently using disciplined convex programming [115]. Similarly, the constraints Equation (6.12b)-(6.12c) are linear and affine, so the optimization problem Equation (6.12) is concave and can be solved using disciplined convex programming [115]. Also the diagonal matrix $\boldsymbol{\Delta}$ is positive semi-definite. From the optimum values of $\mathbf{R}_P^{1/2}$ found, we can proceed to obtain the optimum angles of polarization or orientation. From the (possibly) fractional solution obtained by solving the above problem, the l_r largest Δ_i's are chosen and the corresponding indices represent the receive antennas to be selected. The optimum capacity in Equation (6.5) is then calculated by using only the selected subset r, which is found through Equations (6.11) and (6.12). The ergodic capacity after selection now reads,

$$C(\tilde{\boldsymbol{\Delta}}) = \log_2 \det \left(\mathbf{I}_{l_r} + \frac{\gamma}{N_T} \tilde{\mathbf{R}}_{PD}^{H/2} \tilde{\boldsymbol{\Delta}} \tilde{\mathbf{R}}_{PD}^{1/2} \tilde{\mathbf{H}} \tilde{\mathbf{H}}^H \right), \tag{6.13}$$

where $(\tilde{\cdot})$ denotes a matrix, whose rows correspond to the indices given by the set r. In summary we try to compute the optimum angles θ_r's, which optimize the ergodic capacity with receive antenna selection. Practically this system is only realizable, if all the antenna elements in an array can be independently rotated around their axes. Physically realizing such system is not easy, but methods to emulate the rotating effect through the use of parasitic elements has been investigated in [116].

6.5   Results for 2-D Arrays

In this section, we evaluate the performance of the proposed antenna selection algorithm via Monte-Carlo simulations [115]. We solve the optimization algorithm using the MATLAB based tool for convex optimization called CVX [115]. We use ergodic capacity as a metric for performance evaluation, which is obtained by averaging over results, obtained from 1000 independent realizations of the channel matrix $\mathbf{H}$. For each realization, the entries of the channel matrix are uncorrelated ZMCSCG random variables. We take the example of real valued correlation matrices calculated from Equation (6.2). In Figure 6.2(a) we show the results for $l_r/6$ selection. In Figure 6.2(b) we show the results for capacity against l_r for values of N_T. In Figure 6.2(a) and 6.2(b) we also show the simulation results for systems with only vertical oriented antenna elements i.e, only separated spatially (ULA). We see clearly that the performance of these systems is substantially less than the systems which contain both spatial and angular separation. The optimization problem similar to Equation (6.14) for only spatially separated systems is given by,

$$\text{maximize}\quad \log_2 \det \left(\mathbf{I}_{M_R} + \frac{\gamma}{N_T} \mathbf{R}_S^{H/2} \boldsymbol{\Delta} \mathbf{R}_S^{1/2} \mathbf{H} \mathbf{H}^H \right) \tag{6.14a}$$

subject to

$$0 \leq \Delta_i \leq 1, \quad i = 1, \ldots, M_R \tag{6.14b}$$

$$\text{trace}(\boldsymbol{\Delta}) = \sum_{i=1}^{M_R} \Delta_i = l_r. \tag{6.14c}$$

The above stated optimization problem is now simpler because of only one matrix $\boldsymbol{\Delta}$ to be optimized with two constraints. As an example for a Polarization Diverse (PD) system, we show in Equation (6.15), the diagonal matrix $\boldsymbol{\Delta}$ for a 2/6 selection. We see that $\text{trace}(\boldsymbol{\Delta}) = \sum_{i=1}^{M_R} \Delta_i = 2$. We take the two largest elements of the vector $\text{trace}(\boldsymbol{\Delta})$ and calculate the ergodic capacity with the respective indices $(r = 2, 3)$ of the rows of the channel matrix $\mathbf{H}$. Now we show an optimum correlation matrix in Equation (6.17) $\mathbf{R}_P^{1/2}$ for a given $\mathbf{R}_S^{1/2}$, calculated for the optimum $\boldsymbol{\Delta}$, as an example. The $\tilde{\boldsymbol{\Delta}}$ matrix formed after selection, is given in Equation (6.16). We use the same indices $(r = 2, 3)$ again to select the rows and columns of correlation matrix $\mathbf{R}_P^{1/2}$. The selected correlation matrix is shown in Equation (6.18). From this matrix the corresponding angles are $\theta_r = 0, 71°$. We show more examples of selection systems with the corresponding optimum angles in Table 6.1 at 20dB SNR.

$$\boldsymbol{\Delta} = \begin{bmatrix} 0.3957 & 0 & 0 & 0 & 0 & 0 \\ 0 & 1 & 0 & 0 & 0 & 0 \\ 0 & 0 & 0.3847 & 0 & 0 & 0 \\ 0 & 0 & 0 & 0 & 0 & 0 \\ 0 & 0 & 0 & 0 & 0 & 0 \\ 0 & 0 & 0 & 0 & 0 & 0.2196 \end{bmatrix}. \tag{6.15}$$

$$\tilde{\boldsymbol{\Delta}} = \begin{bmatrix} 1 & 0 \\ 0 & 0.3957 \end{bmatrix}. \tag{6.16}$$

$$\mathbf{R}_P^{1/2} = \begin{bmatrix} 1.000 & 0.189 & 0.174 & 0.033 & 0.000 & 0.229 \\ 0.189 & 1.000 & 0.000 & 0.139 & 0.297 & 0.951 \\ 0.174 & 0.000 & 1.000 & 0.081 & 0.050 & 0.210 \\ 0.033 & 0.139 & 0.081 & 1.000 & 0.000 & 0.000 \\ 0.000 & 0.297 & 0.050 & 0.000 & 1.000 & 0.143 \\ 0.229 & 0.951 & 0.210 & 0.000 & 0.143 & 1.000 \end{bmatrix}. \tag{6.17}$$

$$\tilde{\mathbf{R}}_P^{1/2} = \begin{bmatrix} 1.000 & 0.189 \\ 0.189 & 1.000 \end{bmatrix}. \tag{6.18}$$

Table 6.1: Optimum Angles with $l_r/9$ Selection at 20dB SNR for $M_R = 1, \cdots, 5$

l_r	Indices (r)	Angles (θ_r°)
1	7	0
2	2,6	0,62
3	3,7,9	0,56,76
4	2,5,7,9	0,73,78,90
5	1,4,5,6,7	0,55,90,65,70
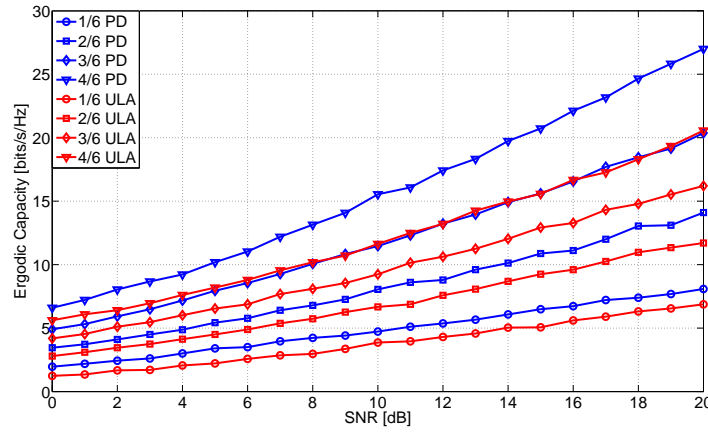
(a) Ergodic capacity v/s SNR, $M_R = 6$, $N_T = 1, 2, 3, 4$, $l_r = N_T$, for PD and ULA systems.
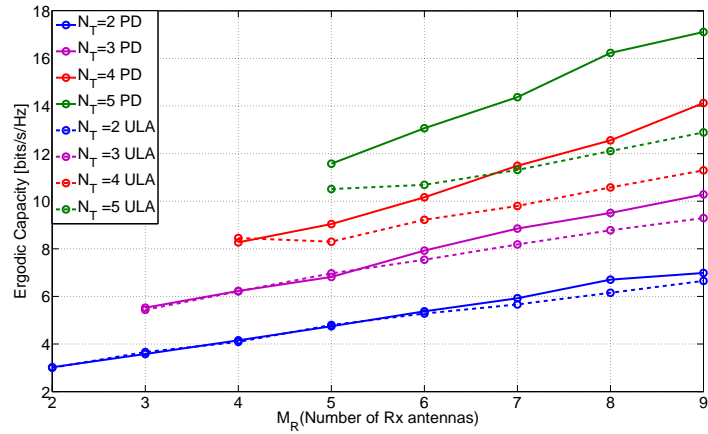
(b) Ergodic capacity v/s M_R, SNR=10dB, $N_T = 2, 3, 4, 5$, $l_r = N_T$, for PD and ULA systems.

Figure 6.2: Ergodic capacity for antenna configurations.

6.6   Convex Optimization for RAS in 3-D Polarized MIMO Transmissions

Exhaustive search based on maximum output SNR is proposed in [26], when the system uses linear receivers. Since exhaustive search is computationally expensive for large MIMO systems, several sub-optimal algorithms with lower complexity are derived at the expense of performance. A selection algorithm based on accurate approximation of the conditional error probability of quasi-static MIMO systems is derived in [106]. In [107], the authors formulate the receive antenna selection problem as a combinatorial optimization problem and relax it to a convex optimization problem. They employ an interior point algorithm based on the barrier method, to solve a relaxed convex problem. However, they treat only the case of capacity maximization. An alternative approach to receive antenna selection for capacity maximization that offers near optimal performance at a complexity, significantly lower than the schemes in [22] but marginally greater than the schemes in [108], is described in [109].

Our approach is based on formulating the selection problem as a combinatorial optimization problem

and relaxing it to obtain a problem with a concave objective function and convex constraints. We follow the lines of [107] [109], and apply this to the system of arrays with Dual-Polarized (DP) and Triple-Polarized (TP) antenna structures. Application of receive antenna selection on polarized array can be found in [69] [85]. We first model the Dual Polarized (DP) and Triple Polarized (TP) systems with respect to many channel characteristics, e.g, K-factor, channel correlations and XPD. A good investigation on the modeling of DP MIMO channels in [49]. In [103] the author models TP systems and presents the performance in terms of outage probabilities. We then compare the results with the Spatially Separated-Single Polarized (SS-SP) systems with the same channel characteristics. We extend our DP and TP systems to Spatially-Separated Dual-Polarized (SS-DP) and Triple Polarized (SS-TP) systems. These systems are a combination of both spatial and polarization domain.

6.7 Channel Model for 2-D and 3-D MIMO

The channel is modeled as a Ricean fading channel, i.e, the channel matrix can be composed of a fixed (possibly line-of-sight) part and a random (fast fading) part according to Equation (5.1) described in the previous chapter.

For a DP system, the channel matrix is described in V and H polarizations, i.e., its elements represent the input-output relation from V to V, V to H, H to H, and H to V polarized waves [49] [52],

$$\mathbf{H}_{DP} = \begin{bmatrix} \check{h}^{VV} & \check{h}^{VH} \\ \check{h}^{HV} & \check{h}^{HH} \end{bmatrix}, \tag{6.19}$$

and that for 3×3 triple-polarized channels represented as [117] [90],

$$\mathbf{H}_{TP} = \begin{bmatrix} \check{h}^{VV} & \check{h}^{VH} & \check{h}^{VZ} \\ \check{h}^{HV} & \check{h}^{HH} & \check{h}^{HZ} \\ \check{h}^{ZV} & \check{h}^{ZH} & \check{h}^{ZZ} \end{bmatrix}, \tag{6.20}$$

A 4×4 MIMO channel with two spatially separated DP antennas on each side can for example be written as,

$$\mathbf{H} = \begin{bmatrix} \check{h}^{1V,1V} & \check{h}^{1V,1H} & \check{h}^{1V,2V} & \check{h}^{1V,2H} \\ \check{h}^{1H,1V} & \check{h}^{1H,1H} & \check{h}^{1H,2V} & \check{h}^{1H,2H} \\ \check{h}^{2V,1V} & \check{h}^{2V,1H} & \check{h}^{2V,2V} & \check{h}^{2V,2H} \\ \check{h}^{2H,1V} & \check{h}^{2H,1H} & \check{h}^{2H,2V} & \check{h}^{2H,2H} \end{bmatrix} = \begin{bmatrix} \mathbf{H}_{11} & \mathbf{H}_{12} \\ \mathbf{H}_{21} & \mathbf{H}_{22} \end{bmatrix}, \tag{6.21}$$

where the scalar channel between the ith transmit antenna and the jth receive antenna is denoted by $\check{h}_{jV,iV}$ for the vertical component and $\check{h}_{jH,iH}$ for the horizontal component. The cross-components are denoted by $\check{h}_{jV,iH}$ and $\check{h}_{jH,iV}$, respectively. The channel XPD's are mentioned in the previous chapters. We have used the following normalizations,

$$E\left\{ \left| \check{h}^{VV} \right|^2 \right\} = E\left\{ \left| \check{h}^{HH} \right|^2 \right\} = 1 - \alpha \tag{6.22}$$

$$E\left\{ \left| \check{h}^{HV} \right|^2 \right\} = E\left\{ \left| \check{h}^{VH} \right|^2 \right\} = \alpha. \tag{6.23}$$

Similarly for TP array we have some additional normalizations as follows,

$$E\left\{\left|\check{h}^{VV}\right|^2\right\} = E\left\{\left|\check{h}^{HH}\right|^2\right\} = E\left\{\left|\check{h}^{ZZ}\right|^2\right\} = 1 - (\alpha_1 + \alpha_2). \tag{6.24}$$

$$E\left\{\left|\check{h}^{VH}\right|^2\right\} = E\left\{\left|\check{h}^{ZV}\right|^2\right\} = E\left\{\left|\check{h}^{HZ}\right|^2\right\} = \alpha_1 \tag{6.25}$$

$$E\left\{\left|\check{h}^{HV}\right|^2\right\} = E\left\{\left|\check{h}^{VZ}\right|^2\right\} = E\left\{\left|\check{h}^{ZH}\right|^2\right\} = \alpha_2. \tag{6.26}$$

The above normalizations are motivated by power or energy conservation arguments. That is, the channel cannot introduce more energy to the transmitted signal and with this normalization the power is conserved by subtracting from the co-polarized component the corresponding amount of power α that has leaked into the cross-polarized component. This normalization is of great importance when comparing DP to SP systems. The XPD for TP channel can then be represented by,

$$\text{XPD} = \frac{1 - (\alpha_1 + \alpha_2)}{\alpha_1 + \alpha_2}, \quad 0 < (\alpha_1 + \alpha_2) \le 1, \tag{6.27}$$

Similarly, we define the channel XPD for the fixed part of the DP channel as,

$$\text{XPD}_f = \frac{1 - \alpha_f}{\alpha_f}, \quad 0 < \alpha_f \le 1. \tag{6.28}$$

with the following normalizations

$$\left|\bar{h}^{VV}\right|^2 = \left|\bar{h}^{HH}\right|^2 = 1 - \alpha_f. \tag{6.29}$$

$$\left|\bar{h}^{HV}\right|^2 = \left|\bar{h}^{VH}\right|^2 = \alpha_f. \tag{6.30}$$

Similarly for triple polarized array we have some additional normalizations as follows,

$$\left|\bar{h}^{VV}\right|^2 = \left|\bar{h}^{HH}\right|^2 = \left|\bar{h}^{ZZ}\right|^2 = 1 - (\alpha_{1f} + \alpha_{2f}). \tag{6.31}$$

$$\left|\bar{h}^{VH}\right|^2 = \left|\bar{h}^{ZV}\right|^2 = \left|\bar{h}^{HZ}\right|^2 = \alpha_{1f} \tag{6.32}$$

$$\left|\bar{h}^{HV}\right|^2 = \left|\bar{h}^{VZ}\right|^2 = \left|\bar{h}^{ZH}\right|^2 = \alpha_{2f}. \tag{6.33}$$

$$\tag{6.34}$$

The channel XPD for the fixed part of the TP channel is given by,

$$\text{XPD}_f = \frac{1 - (\alpha_{1f} + \alpha_{2f})}{\alpha_{1f} + \alpha_{2f}}, \quad 0 < (\alpha_{1f} + \alpha_{2f}) \le 1. \tag{6.35}$$

6.7.1 Channel Correlations in Multipolarized MIMO

The elements of the Spatially Separated-Single Polarized (SS-SP) MIMO channel matrix will be correlated, when the channel is not rich enough, i.e., when there is not enough scattering to decorrelate the elements of the channel matrix and/or when the antenna spacing is too small. We define the transmit, t_s, and receive, r_s, spatial and co-polarized correlation coefficients as,

$$t_s = \frac{E\left\{\check{h}_{iV,iV}\check{h}^*_{iV,jV}\right\}}{1 - \alpha} = \frac{E\left\{\check{h}_{iH,jH}\check{h}^*_{iH,iH}\right\}}{1 - \alpha}, i \ne j, \tag{6.36}$$

$$r_s = \frac{E\left\{\tilde{h}_{iV,iV}\check{h}^*_{jV,iV}\right\}}{1-\alpha} = \frac{E\left\{\check{h}_{iH,jH}\check{h}^*_{iH,iH}\right\}}{1-\alpha}, i \neq j. \tag{6.37}$$

Similarly, we define the transmit, t_p, and receive, r_p, polarization correlation coefficients as,

$$t_p = \frac{E\left\{\check{h}_{iV,iV}\check{h}^*_{iV,iH}\right\}}{\sqrt{\alpha(1-\alpha)}} = \frac{E\left\{\check{h}_{iH,iV}\check{h}^*_{iH,iH}\right\}}{\sqrt{\alpha(1-\alpha)}}, \tag{6.38}$$

$$r_p = \frac{E\left\{\check{h}_{iV,iV}\check{h}^*_{iH,iV}\right\}}{\sqrt{\alpha(1-\alpha)}} = \frac{E\left\{\check{h}_{iV,iH}\check{h}^*_{iH,iH}\right\}}{\sqrt{\alpha(1-\alpha)}}. \tag{6.39}$$

For example, the measurements reported in [89] showed that the average envelope correlations (worst case) were all less than 0.2, and, in fact, all of the reported measurements in [118] showed that $t_p \approx r_p \approx 0$. The correlations between elements of TP structures can be shown in a straight forward manner as above.

6.7.2 Complete Channel Model

The combined channel including all the parameters is described here. A 2×2 dual-polarized MIMO channel is expressed as follows,

$$\tilde{\mathbf{H}}_{DP} = \boldsymbol{\Sigma}_{DP} \odot \left(\mathbf{C}^{1/2}_{r_p}\mathbf{W}_{2\times 2}\mathbf{C}^{1/2}_{t_p}\right), \tag{6.40}$$

$$\boldsymbol{\Sigma}_{DP} = \begin{bmatrix} \sqrt{1-\alpha} & \sqrt{\alpha} \\ \sqrt{\alpha} & \sqrt{1-\alpha} \end{bmatrix}, \tag{6.41}$$

$$\mathbf{C}_{r_p} = \begin{bmatrix} 1 & r_p \\ r^*_p & 1 \end{bmatrix}; \ \mathbf{C}_{t_p} = \begin{bmatrix} 1 & t_p \\ t^*_p & 1 \end{bmatrix}, \tag{6.42}$$

are the polarization leakage, receive and transmit correlation matrices and $\mathbf{W}$ is a complex-valued Gaussian matrix with i.i.d entries from $\mathcal{N}_C(0,1)$. A 3×3 triple-polarized MIMO channel is expressed as follows,

$$\tilde{\mathbf{H}}_{TP} = \boldsymbol{\Sigma}_{TP} \odot \left(\mathbf{C}^{1/2}_{r_p}\mathbf{W}_{3\times 3}\mathbf{C}^{1/2}_{t_p}\right), \tag{6.43}$$

where

$$\boldsymbol{\Sigma}_{TP} = \begin{bmatrix} \sqrt{1-\beta} & \sqrt{\alpha_1} & \sqrt{\alpha_2} \\ \sqrt{\alpha_2} & \sqrt{1-\beta} & \sqrt{\alpha_1} \\ \sqrt{\alpha_1} & \sqrt{\alpha_2} & \sqrt{1-\beta} \end{bmatrix}, \tag{6.44}$$

where $\beta = (\alpha_1 + \alpha_2)$ and the condition for "symmetry" is that $0 \leq \beta \leq 1$.

$$\mathbf{C}_{r_p} = \begin{bmatrix} 1 & r_p & r_p \\ r^*_p & 1 & r_p \\ r^*_p & r^*_p & 1 \end{bmatrix}; \ \mathbf{C}_{t_p} = \begin{bmatrix} 1 & t_p & t_p \\ t^*_p & 1 & t_p \\ t^*_p & t^*_p & 1 \end{bmatrix}, \tag{6.45}$$

are the polarization leakage, receive and transmit correlation matrices. Here we assume that the correlation values for each pair of polarization, in a TP structure are equal. Extension to arrays of

multiple Spatially Separated Dual Polarized (SS-DP) and Spatially Separated Triple Polarized (SS-TP) antenna arrays are straight forward and shown below as,

$$\tilde{\mathbf{H}}_{DP} = \mathbf{1}_{M_R/2 \times N_T/2} \otimes \boldsymbol{\Sigma}_{DP} \odot \left(\mathbf{C}_r^{1/2} \mathbf{W}_{M_R \times N_T} \mathbf{C}_t^{1/2} \right), \tag{6.46}$$

where M_R and N_T are the number of receive and transmit antennas respectively. They should always be multiples of two for the DP case.

$$\tilde{\mathbf{H}}_{TP} = \mathbf{1}_{M_R/3 \times N_T/3} \otimes \boldsymbol{\Sigma}_{TP} \odot \left(\mathbf{C}_r^{1/2} \mathbf{W}_{M_R \times N_T} \mathbf{C}_t^{1/2} \right), \tag{6.47}$$

where M_R and N_T should always be multiples of three for the TP case. The $\mathbf{C}_r = \mathbf{C}_{r_s} \otimes \mathbf{C}_{r_p}$ and $\mathbf{C}_t = \mathbf{C}_{t_s} \otimes \mathbf{C}_{t_p}$ are the receive correlation and transmit correlation matrices of the $M_R \times M_R$ MIMO channel with M_R spatially separated dual-polarized and triple-polarized antennas on each side. The matrix $\mathbf{1}_{M_R/2 \times N_T/2}$ and $\mathbf{1}_{M_R/3 \times N_T/3}$ are representing matrices of all elements to be one, respectively. The spatial correlation matrices are given, for example for a 2×2 SS system, as follows,

$$\mathbf{C}_{r_s} = \left[\begin{array}{cc} 1 & r_s \\ r_s^* & 1 \end{array} \right]; \; \mathbf{C}_{t_s} = \left[\begin{array}{cc} 1 & t_s \\ t_s^* & 1 \end{array} \right]. \tag{6.48}$$

6.8   Optimization Algorithm for Antenna Selection in 3-D Arrays

Receive antenna selection for capacity maximization is described in previous sections. A closed form characterization of the optimal solution is difficult. We propose a possible selection method here. We formulate the problem of receive antenna selection as a constrained convex optimization problem [113] that can be solved efficiently using numerical methods such as interior-point algorithms [119]. Similar to [109], the $\Delta_i (i = 1, \ldots, M_R)$ is defined as in Equation (6.6). By definition, $\Delta_i = 1$ if $r_i \in \mathbf{r}$, and 0 else. Now, consider an $M_R \times M_R$ diagonal matrix $\boldsymbol{\Delta}$ that has Δ_i as its diagonal entries. Thus, the achievable MIMO channel capacity with antenna selection is given by Equation (6.7). The capacity expression given by $C_r(\boldsymbol{\Delta})$ is concave in $\boldsymbol{\Delta}$. The proof follows from the following facts: The function $f(\mathbf{X}) = \log_2 \det(\mathbf{X})$ is concave in the entries of $\mathbf{X}$ if $\mathbf{X}$ is a positive definite matrix, and the concavity of a function is preserved under an affine transformation [113]. The variables Δ_i are binary valued (0 or 1) integer variables, thereby rendering the selection problem NP-hard. We seek a simplification by relaxing the binary integer constraints and allowing $\Delta_i \in [0, 1]$. Thus, the problem of receive antenna subset selection for capacity maximization is approximated by the constrained convex relaxation plus rounding schemes.

$$\text{maximize} \quad \log_2 \det \left(\mathbf{I}_{M_R} + \frac{\gamma}{N_T} \boldsymbol{\Delta} \mathbf{H} \mathbf{H}^H \right) \tag{6.49a}$$

$$\text{subject to}$$

$$0 \leq \Delta_i \leq 1, \quad i = 1, \ldots, \tag{6.49b}$$

$$\text{trace}(\boldsymbol{\Delta}) = \sum_{i=1}^{M_R} \Delta_i = l_r. \tag{6.49c}$$

where $\mathbf{H}$ is given by Equation (6.40) for DP and Equation (6.43) for TP antenna systems.

6.9 Results for 3-D Arrays

In this section we evaluate the capacity for different channel scenarios depending on parameters like correlation, XPD and K-factor. For all Ricean fading examples the fixed 2×2 channel components are given by to,

$$\bar{\mathbf{H}}_{DP} = \left[\begin{array}{cc} \sqrt{1-\alpha_f} & \sqrt{\alpha_f} \\ \sqrt{\alpha_f} & \sqrt{1-\alpha_f} \end{array} \right]. \tag{6.50}$$

Similarly for the triple-polarized case we have,

$$\bar{\mathbf{H}}_{TP} = \left[\begin{array}{ccc} \sqrt{1-\beta_f} & \sqrt{\alpha_{1f}} & \sqrt{\alpha_{2f}} \\ \sqrt{\alpha_{2f}} & \sqrt{1-\beta_f} & \sqrt{\alpha_{1f}} \\ \sqrt{\alpha_{1f}} & \sqrt{\alpha_{2f}} & \sqrt{1-\beta_f} \end{array} \right], \tag{6.51}$$

where $\beta_f = (\alpha_{1f} + \alpha_{2f})$. A nominal value of $\text{XPD}_f = \frac{1-\beta_f}{\beta_f} = 15\text{dB}$ is chosen for simulations [49]. For the SS-SP systems, we have the following matrices with fixed channel (see Equation (5.1)).

$$\bar{\mathbf{H}}_{2SS-SP} = \left[\begin{array}{cc} \sqrt{1-\alpha_f} & \sqrt{1-\alpha_f} \\ \sqrt{1-\alpha_f} & \sqrt{1-\alpha_f} \end{array} \right]. \tag{6.52}$$

Similarly for three SS-SP case we have,

$$\bar{\mathbf{H}}_{3SS-SP} = \left[\begin{array}{ccc} \sqrt{1-\alpha_f} & \sqrt{1-\alpha_f} & \sqrt{1-\alpha_f} \\ \sqrt{1-\alpha_f} & \sqrt{1-\alpha_f} & \sqrt{1-\alpha_f} \\ \sqrt{1-\alpha_f} & \sqrt{1-\alpha_f} & \sqrt{1-\alpha_f} \end{array} \right]. \tag{6.53}$$

Throughout all simulations we used typical correlation values $t_p = r_p = 0.3$ and $t_s = r_s = 0.5$ [118] [89]. We compute ergodic capacity by averaging over 100 instantaneous capacity values, varying the matrix $\mathbf{W} \in \mathcal{N}_C(0,1)$ as i.i.d complex-valued Gaussian. We compare Antenna Selection (AS) methods by selecting l_r out of M_R antennas against Non Antenna Selection (NAS) by utilizing all $l_r = M_R$ antennas. As selection method we apply Equation (6.49).

6.9.1 Effect of SNR on Capacity in Rayleigh Channels

From Figure 6.3(a) we observe that with the given channel parameters, the performance of 2SS-DP and 3SS-SP systems is almost the same for all l_r. The 3SS-TP systems has a better performance with selection for values of $l_r > 4$ as compared to 2SS-DP. We also observe in the figure that all the systems with antenna selection perform better compared to non Non Antenna Selection (NAS) systems. The 3SS-TP system has the best overall performance.

6.9.2 Effect of XPD on Capacity in Rayleigh Channels

In Figure 6.3(b), we show the impact of the XPD parameter on the ergodic capacity of the polarized systems with and without selection. We use the case of $l_r = 6$ as an example for both DP and TP systems. For a fair comparison of DP and TP systems we used $\text{XPD}_f = 15\text{dB}$ for both systems. In the simulations we used $\beta_f = (\alpha_{1f} + \alpha_{2f})$. We assumed $\alpha_{1f} = \alpha_{2f}$ in our simulations (see Equation (6.27)). The same condition is applied for the varying XPD from Equation (6.44) and the condition of symmetry is taken as $\beta = (\alpha_1 + \alpha_2)$. Again $\alpha_1 = \alpha_2$ is assumed for simulations (see Equation
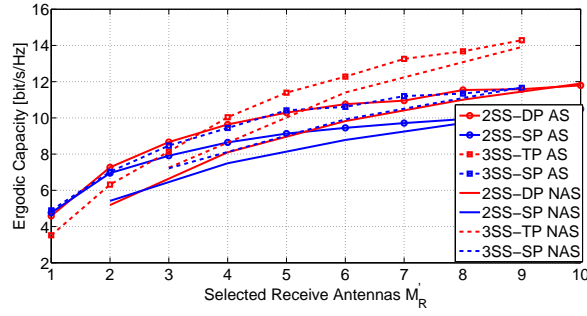
(a) Capacity vs antennas selected for dual-polarized $N_T = 2$, $M_R = 10$ and triple-polarized $N_T = 3$, $M_R = 9$ with SNR=10dB, $t_p = r_p = 0.3$, $t_s = r_s = 0.5$, Rayleigh fading $K = 0$ and XPD = 10dB.
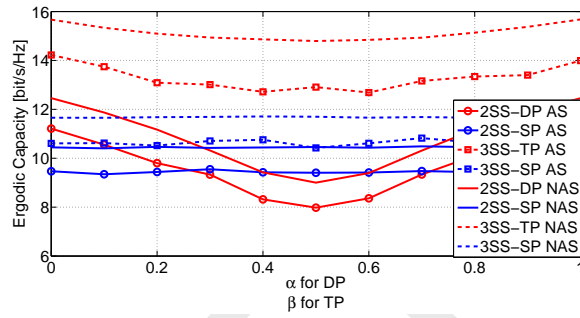
(b) Capacity vs XPD for dual-polarized $N_T = 2$, $M_R = 10$ and triple-polarized $N_T = 3$, $M_R = 9$ with $l_r = 6$, SNR=10dB, $t_p = r_p = 0.3$, $t_s = r_s = 0.5$, Rayleigh fading $K = 0$.
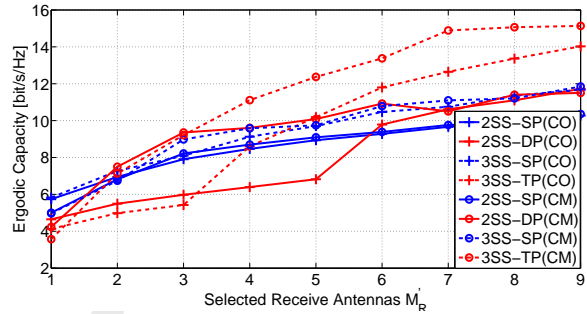
(c) Capacity vs antennas selected for dual-polarized $N_T = 2$, $M_R = 10$ and triple-polarized $N_T = 3$, $M_R = 9$ with SNR=10dB, $t_p = r_p = 0.3$, $t_s = r_s = 0.5$, Rayleigh fading $K = 0$ and XPD = 10dB. Comparison between Convex Optimization (CO) and Capacity Maximization (CM) based selection.
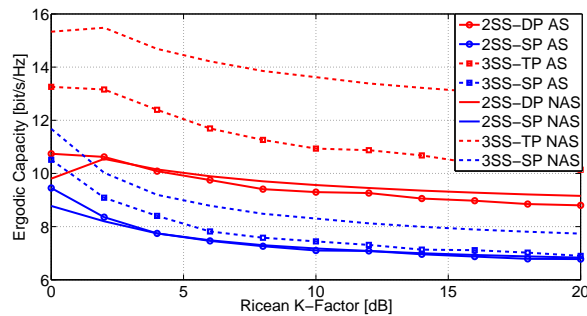
(d) Capacity vs K-factor for dual-polarized $N_T = 2$, $M_R = 10$ and triple-polarized $N_T = 3$, $M_R = 9$ with $l_r = 6$, SNR=10dB, $t_p = r_p = 0.3$, $t_s = r_s = 0.5$, and XPD = 10dB, $XPD_f = 15$dB.

Figure 6.3: Capacity of multi-polarized configurations for various channel parameters.

(6.35)). We observe that with the given channel parameters, SS-SP systems are not effected by the α values. We observe that 3SS-TP without selection has the best performance. A selection within 3SS-TP systems is far better than a selection within 2SS-DP.

6.9.3   Effect of Ricean K-factor on Capacity

In Figure 6.3(d) we show the performance in terms of Ricean K-factor. We observe that the performance gets worse when the LOS component K increases. We also observe that DP systems with or without antenna selection are effected more by the K-factor compared to TP systems. We also extract from the figure that TP systems with selection perform a lot better than all other systems except full complexity TP systems.

6.9.4   Comparison of CO and CM Selection Methods

In Figure 6.3(c) we compared the CO antenna selection method to the well known Capacity Maximization (CM) method based on exhaustive search for the maximum capacity of the selected sub-channels [1] [26]. For CM the average was taken over 10^5 channel realizations for the matrix $\mathbf{W}$. We observe that the CO method performs almost close to CM method for spatially separated systems. In DP systems, at larger values of l_r, the CO method has almost the same performance as CM method. Although in TP systems the CM method is always better than CO method at all values of l_r, for the given channel conditions.

6.10   Conclusions

In this chapter we investigated a model for dual and triple polarized MIMO channels. We used convex optimization to optimize the performance of such systems for maximizing ergodic capacity. We used the relaxation of a binary integer constraint to have a convex optimization algorithm and solved it, using disciplined convex programming. The optimization algorithm finds the best antennas for selection. We also compared the results with an array consisting of spatially separated single polarized array of linear elements. We found that by using an optimization algorithm, the performance of multiple polarized systems can be significantly enhanced. For certain channel conditions we see that triple polarized systems increase the performance significantly compared to spatially separated systems. We also observe that applying selection at the receiver only boosts the performance in NLOS channels compared to LOS channels. A comparison with the exhaustive search method of capacity maximization for selection shows that convex optimization based search method performs better for polarized MIMO systems with antenna selection. In this chapter we modified simple antenna selection problem into convex optimization problem while using mutual information as the cost function. We did not consider other cost functions like BER minimization [111] or throughput maximization for optimization. Also we could consider other constraints like power and rate for maximizing or minimizing certain cost function. Based on such optimization, optimal receiver architectures can be devised for multipolarized systems with antenna selection [107].

7

Conclusions and Future Work

In this PhD dissertation we have explored and justified the use of antenna selection mechanisms in single user MIMO wireless scenarios from a geometric point of view for antenna array structures. We first explored and investigated various antenna configurations and then applied antenna selection on such systems. We analyzed theoretically the performances in terms of capacity. We also compared the results with conventional linear arrays. While considering various configurations of arrays we emphasized on the parameters such as correlation and mutual coupling and devised novel selection algorithms for such systems. We also exploited convex optimization methods to further reduce the computational complexity on various antenna configurations. We also experimentally investigated the gains achieved by multipolarized systems through a few channel measurement campaigns. Various selection algorithms were also applied on multicarrier systems and performances were simulated.

7.1   Conclusion

After motivating this PhD thesis and giving an overview of the state of the art, in the introductory chapter we apply simple antenna selection algorithms on frequency selective channels. In broadband systems such as WiMAX (IEEE 802.16-2004), the overall channel under consideration is typically frequency selective, and flat only over the subcarrier bandwidths. We applied receive antenna subset selection schemes to a WiMAX compliant MIMO-OFDM transmission system. Simulation results in terms of average throughput and Bit Error Ratio (BER) on an adaptive modulation and coding link were shown. We found that the optimal selection for maximum throughput, does not give the best results in terms of BER performance. We concluded that the minimum BER method is not the right choice for antenna selection. We also showed through our simulations that the simple, low complex norm based selection algorithm, provided good results, close to optimal selection in frequency selective channels.

We analyzed the combined effects of array orientation/rotation and antenna cross polarization discrimination on the performance of two dimensional dual-polarized systems with receive antenna selection. We started our analysis by selecting only one receive antenna out of multiple antennas selection and extend it to multiple selected receive antennas. We derived numerical expressions for the effective channel gains for all such systems. We found these expressions for small values of antenna elements, and approximately valid for higher values. We concluded from our analysis that the maximum effective channel gain can be attained if the number of selected antennas are at least half of the total antennas available. We then compared co-located antenna array structures with their spatial counterpart while deploying receive antenna selection. To this purpose, the performance in terms of MIMO maximum mutual information was presented. We derived some explicit numerical expressions for the effective channel gains. Further a comparison in terms of power imbalance between antenna elements was presented. We concluded that angularly separated compact antenna arrays with a few simple monopoles, if used with antenna selection can provide a better performance compared to a conventional Uniform Linear Array (ULA). We also showed that co-located structures are robust to power imbalance and orientation variations compared to a ULA. We then examined the performance of a typical antenna selection strategy in such systems and under various scenarios of antenna spacing and mutual coupling with varying antenna elements. We compared a linear array with an NSpoke co-located antenna structure. We further improved the performance of such systems by a new selection approach which terminates the non-selected antenna elements with a short circuit. We observed that this methodology, improved the performance considerably. We presented analytical bounds for capacity with receive antenna selection. We found that NSpoke structures perform better than side-by-side systems with receive antenna selection with few number of antennas even in the presence of strong mutual coupling effects.

From 2-D antenna structures we moved forward to 3-D structures. We investigated orthogonal multipolarized antenna structures. We theoretically analyze the impact of cross-polar discrimination on the achieved antenna selection gain for both dual and triple-polarized MIMO for non line of sight channels. We proceeded to derive the outage probabilities and observe that these systems achieve significant performance gains for compact configurations with only a nominal increase in complexity. We observed that at higher cross polarization discrimination and lower transmit signal to noise ratio, the outage performance for a dual-polarized system is almost the same as triple-polarized system with joint transmit/receive antenna selection. With selection at only one end of the link, we also observed that the triple-polarized system performs better than dual-polarized counterpart at higher values of transmit

SNRs. We then considered the use of multiple antenna signaling technologies, specifically Space Time Block Coding (STBC) and Spatial Multiplexing (SM) schemes, on such 3D multipolarized antenna arrays. We consider the effects of correlation and XPD on the performance. We presented simulation results for both multi-antenna signaling techniques. The results show a significant performance gain by joint utilization of space, time and polarization diversity in comparison to uni-polarized systems with the same number of antennas. We observed that dual and triple polarized systems have different performances at various channel scenarios. Antenna selection performs better for systems with space time coding and boosts the performance more in triple-polarized MIMO compared to its dual-polarized counterpart.

The computational complexity increases with the number of selected antennas and the total number of antennas. We presented a low complexity approach to receive antenna selection for capacity maximization, based on the theory of convex optimization. By relaxing the antenna selection variables from discrete to continuous, we arrived at a convex optimization problem. We showed via extensive Monte-Carlo simulations that the proposed algorithm provides performance very close to that of optimal selection based on exhaustive search. We consecutively optimize not only the selection of the best antennas but also the angular orientation of individual antenna elements in the array for a so-called true polarization diversity system. We then used the same convex techniques and applied on 3-D polarized systems. We also included channel parameters like transmit and receive correlations, XPD. We compared our results with the Spatially Separated (SP) MIMO with and without selection by performing extensive Monte-Carlo simulations. We found that by using convex optimization algorithm, the performance of multiple polarized systems can be significantly enhanced. For certain channel conditions we observed that triple polarized systems increase the performance significantly compared to dual-polarized and spatially separated systems. We observed that applying selection at the receiver only boosts the performance in Non Line of Sight (NLOS) channels compared to Line of Sight (LOS) channels.

7.2   Future Work

The work presented in this PhD dissertation can be extended as follows:

- To take into account more realistic channels, possibly considering users fading statistics.

- To apply antenna joint antenna selection with various pre-coding techniques.

- To perform practical antenna selection system design with realistic switching.

- To extend physical layer design to cross-layer perspective.

- To apply selection schemes on Planar and conformal arrays with beam synthesis.

- To perform selection techniques on Cooperative MIMO with network coding.

As for the specific problems addressed in each chapter, some interesting topics to be addressed are the following

- In Chapter 2, various selection algorithms can be applied on OFDM based LTE physical layer simulator. The performance can be compared by incorporating various antenna structures. The performance can also be calculated in terms of complexity and receiver architecture.

- In Chapter 3, a possible extension would be the analytical evaluation of the proposed approach by deriving performance bounds in terms of capacity, through put and BER. Joint transmit/receive antenna selection can be applied as well. Impairments in the feedback channel should be considered in order to derive a more robust joint antenna selection procedure. To consider more types of antenna arrays specially conformal antenna array structures considering all the coupling effects.

- In Chapter 4, extension could be towards analytically calculating capacity bounds with all the impairments with antenna selection for multipolarized systems. Channel measurements for various channel conditions with a practical antenna selection system, can also be a pert of future work. Various receiver can be designed for such multipolarized system as well. The effects of mutual coupling can be included and bounds can be calculated for selection systems.

- In Chapter 5, various performance bounds can be calculated for SM and diversity techniques for multi-polarized systems and some optimum receiver structures can be devised.

- In Chapter 6, possibly the work could be extended into designing performance constraints for optimization problem based on bit error and throughput.

Bibliography

[1] A. F. Molisch and M. Z. Win, "MIMO systems with antenna selection," *IEEE Microwave Magazine*, vol. 5, no. 1, pp. 46–56, 2004.

[2] S. Sanayei and A. Nosratinia, "Antenna selection in MIMO systems," *IEEE Communications Magazine*, vol. 42, no. 10, pp. 68–73, 2004.

[3] D. A. Gore and A. J. Paulraj, "MIMO antenna subset selection with space-time coding," *IEEE Transactions on Signal Processing*, vol. 50, no. 10, pp. 2580–2588, 2002.

[4] W. Jakes, *Microwave Mobile Communications*. John Wiley & Sons, 1974.

[5] J. H. Winters, "Smart antennas for wireless systems," *IEEE Personal Communications*, vol. 5, no. 1, pp. 23–27, 1998.

[6] S. Caban, C. Mehlführer, M. Rupp, and M. Wrulich, *HSDPA Antenna Spacing Measurements, in Evaluation of HSDPA and LTE: From Testbed Measurements to System Level Performance*. John Wiley & Sons, Ltd, Chichester, UK., 2011, chapter 7.

[7] J. H. Winters, "Switched diversity with feedback for DPSK mobile radio systems," *IEEE Transactions on Vehicular Technology*, vol. 32, no. 1, pp. 134–150, 1983.

[8] M. Z. Win, G. Chrisikos, and J. H. Winters, "Error probability for M-ary modulation using hybrid selection/maximal-ratio combining in Rayleigh fading," in *Proc. IEEE Military Communications MILCOM 1999*, vol. 2, 1999, pp. 944–948.

[9] M. Z. Win and J. H. Winters, "Analysis of hybrid selection/maximal-ratio combining in Rayleigh fading," *IEEE Transactions on Communications*, vol. 47, no. 12, pp. 1773–1776, 1999.

[10] ——, "Virtual branch analysis of symbol error probability for hybrid selection/maximal-ratio combining in Rayleigh fading," *IEEE Transactions on Communications*, vol. 49, no. 11, pp. 1926–1934, 2001.

[11] A. F. Molisch, M. Z. Win, and J. H. Winters, "Reduced-complexity transmit/receive-diversity systems," in *Proc. VTC 2001 Spring Vehicular Technology Conf. IEEE VTS 53rd*, vol. 3, 2001, pp. 1996–2000.

[12] ——, "Reduced-complexity transmit/receive-diversity systems," *IEEE Transactions on Signal Processing*, vol. 51, no. 11, pp. 2729–2738, 2003.

[13] Z. Chen, "Asymptotic performance of transmit antenna selection with maximal-ratio combining for generalized selection criterion," *IEEE Communications Letters*, vol. 8, no. 4, pp. 247–249, 2004.

[14] X. N. Zeng and A. Ghrayeb, "Performance bounds for space-time block codes with receive antenna selection," *IEEE Transactions on Information Theory*, vol. 50, no. 9, pp. 2130–2137, 2004.

[15] B. Badic, P. Fuxjaeger, and H. Weinrichter, "Performance of quasi-orthogonal space-time code with antenna selection," *Electronics Letters*, vol. 40, no. 20, pp. 1282–1284, 2004.

[16] B. Badic, M. Rupp, and H. Weinrichter, "Adaptive channel-matched extended alamouti space-time code exploiting partial feedback," *ETRI Journal*, vol. 26, no. 5, pp. 443–451, October 2004.

[17] A. Sanei, A. Ghrayeb, Y. Shayan, and T. M. Duman, "Antenna selection for space-time trellis codes in fast fading," in *Proc. 15th IEEE Int. Symp. Personal, Indoor and Mobile Radio Communications (PIMRC'04)*, vol. 3, 2004, pp. 1623–1627.

[18] D. A. Gore, R. U. Nabar, and A. Paulraj, "Selecting an optimal set of transmit antennas for a low rank matrix channel," in *Proc. IEEE Int. Conf. Acoustics, Speech, and Signal Processing (ICASSP'00)*, vol. 5, 2000, pp. 2785–2788.

[19] T. Cover and J. Thomas, *Elements of Information Theory*.   John Wiley & Sons, 1991.

[20] S. Sandhu, R. U. Nabar, D. A. Gore, and A. Paulraj, "Near-optimal selection of transmit antennas for a MIMO channel based on shannon capacity," in *Proc. Conf Signals, Systems and Computers Record of the Thirty-Fourth Asilomar Conf*, vol. 1, 2000, pp. 567–571.

[21] A. Gorokhov, "Antenna selection algorithms for MEA transmission systems," in *Proc. IEEE Int Acoustics, Speech, and Signal Processing (ICASSP'02) Conf*, vol. 3, 2002.

[22] A. Gorokhov, D. A. Gore, and A. J. Paulraj, "Receive antenna selection for MIMO spatial multiplexing: Theory and algorithms," *IEEE Transactions on Signal Processing*, vol. 51, no. 11, pp. 2796–2807, 2003.

[23] M. Gharavi-Alkhansari and A. B. Gershman, "Fast antenna subset selection in MIMO systems," *IEEE Transactions on Signal Processing*, vol. 52, no. 2, pp. 339–347, 2004.

[24] A. Gorokhov, M. Collados, D. Gore, and A. Paulraj, "Transmit/receive MIMO antenna subset selection," in *Proc. IEEE Int. Conf. Acoustics, Speech, and Signal Processing (ICASSP '04)*, vol. 2, 2004.

[25] L. Zheng and D. N. C. Tse, "Diversity and multiplexing: A fundamental tradeoff in multiple-antenna channels," *IEEE Transactions on Information Theory*, vol. 49, no. 5, pp. 1073–1096, 2003.

[26] J. Heath, R. W., S. Sandhu, and A. Paulraj, "Antenna selection for spatial multiplexing systems with linear receivers," *IEEE Communications Letters*, vol. 5, no. 4, pp. 142–144, 2001.

[27] D. A. Gore, J. Heath, R. W., and A. J. Paulraj, "Transmit selection in spatial multiplexing systems," *IEEE Communications Letters*, vol. 6, no. 11, pp. 491–493, 2002.

[28] I. Berenguer, X. Wang, and I. J. Wassell, "Transmit antenna selection in linear receivers: Geometrical approach," *Electronics Letters*, vol. 40, no. 5, pp. 292–293, 2004.

[29] J. P. Kermoal, L. Schumacher, K. I. Pedersen, P. E. Mogensen, and F. Frederiksen, "A stochastic MIMO radio channel model with experimental validation," *IEEE Journal on Selected Areas in Communications*, vol. 20, no. 6, pp. 1211–1226, 2002.

[30] W. Weichselberger, M. Herdin, H. Ozcelik, and E. Bonek, "A stochastic MIMO channel model with joint correlation of both link ends," *IEEE Transactions on Wireless Communications*, vol. 5, no. 1, pp. 90–100, 2006.

[31] Z. Xu, S. Sfar, and R. S. Blum, "On the importance of modeling the mutual coupling for antenna selection for closely-spaced arrays," in *Proc. 40th Annual Conf. Information Sciences and Systems*, 2006, pp. 1351–1355.

[32] C. Mehlführer, S. Caban, and M. Rupp, "Cellular system physical layer throughput: How far off are we from the shannon bound?" *IEEE Wireless Communications Magazine*, vol. 18, no. 6, pp. 54–63, 2011.

[33] IEEE, "IEEE standard for information technology–telecommunications and information exchange between systems–local and metropolitan area networks–specific requirements part 11: Wireless LAN medium access control (MAC) and physical layer (PHY) specifications amendment 5: Enhancements for higher throughput."

[34] G. M. Rebeiz and J. B. Muldavin, "RF MEMS switches and switch circuits," *IEEE Microwave Magazine*, vol. 2, no. 4, pp. 59–71, 2001.

[35] G. M. Rebeiz, "RF MEMS for low power wireless communications," in *Proc. Int MEMS, NANO and Smart Systems Conf*, 2005.

[36] H. Zhang and H. Dai, "Fast transmit antenna selection algorithms for MIMO systems with fading correlation," in *60th IEEE Proc. Vehicular Technology Conf. (VTC'04-Fall)*, vol. 3, 2004, pp. 1638–1642.

[37] H. Zhang, A. F. Molisch, and J. Zhang, "Applying antenna selection in WLANs for achieving broadband multimedia communications," *IEEE Transactions on Broadcasting*, vol. 52, no. 4, pp. 475–482, 2006.

[38] A. Hottinen, O. Tirkkonen, and R. Wichman, *Multi-Antenna Transceiver Techniques for 3G and Beyond.* Wiley, 2003.

[39] 3GPP, "Technical specification group radio access network: Spatial Channel Model for Multiple Input Multiple Output (MIMO) simulations (release 8). 3GPP TS 25.996 v8.0.0," Dec 2008.

[40] A. Wilzeck and T. Kaiser, "Antenna subset selection for cyclic prefix assisted MIMO wireless communications over frequency selective channels," *EURASIP Journal on Advances in Signal Processing*, vol. 2008, p. 14, 2008.

[41] X. Shao, J. Yuan, and P. Rapajic, "Antenna selection for MIMO-OFDM spatial multiplexing system," in *Proc. IEEE Int Information Theory Symp*, 2003.

[42] A. Forenza, A. Pandharipande, H. Kim, and J. Heath, R. W., "Adaptive MIMO transmission scheme: exploiting the spatial selectivity of wireless channels," in *Proc. VTC 2005-Spring Vehicular Technology Conf. 2005 IEEE 61st*, vol. 5, 2005, pp. 3188–3192.

[43] C. Mehlführer, S. Caban, and M. Rupp, "Experimental evaluation of adaptive modulation and coding in MIMO WiMAX with limited feedback," *EURASIP Journal on Advances in Signal Processing*, vol. 2008, 2008.

[44] A. Narasimhamurthy and C. Tepedelenlioglu, "Antenna selection for mimo-ofdm systems with channel estimation error," *Vehicular Technology, IEEE Transactions on*, vol. 58, no. 5, pp. 2269 –2278, jun 2009.

[45] T. Gucluoglu and E. Panayirci, "Performance of transmit and receive antenna selection in the presence of channel estimation errors," *Communications Letters, IEEE*, vol. 12, no. 5, pp. 371 –373, may 2008.

[46] Q. Ma and C. Tepedelenlioglu, "Antenna selection for space-time coded systems with imperfect channel estimation," *Wireless Communications, IEEE Transactions on*, vol. 6, no. 2, pp. 710 –719, feb. 2007.

[47] T. Ramya and S. Bhashyam, "Using delayed feedback for antenna selection in mimo systems," *Wireless Communications, IEEE Transactions on*, vol. 8, no. 12, pp. 6059 –6067, december 2009.

[48] Q. Zhou and H. Dai, "Joint antenna selection and link adaptation for mimo systems," *Vehicular Technology, IEEE Transactions on*, vol. 55, no. 1, pp. 243 – 255, jan. 2006.

[49] M. Coldrey, "Modeling and capacity of polarized MIMO channels," in *Proc. IEEE Vehicular Technology Conf. VTC Spring 2008*, 2008, pp. 440–444.

[50] 3GPP, "Technical specification group radio access network: Evolved Universal Terrestrial Radio Access (E-UTRA).3GPP TS 25.996 v8.0.0," Mar 2008.

[51] W. Lee and Y. Yeh, "Polarization diversity system for mobile radio," *IEEE Transactions on Communications*, vol. 20, no. 5, pp. 912–923, 1972.

[52] C. Oestges, B. Clerckx, M. Guillaud, and M. Debbah, "Dual-polarized wireless communications: From propagation models to system performance evaluation," *IEEE Transactions on Wireless Communications*, vol. 7, no. 10, pp. 4019–4031, 2008.

[53] M. Shafi, M. Zhang, A. L. Moustakas, P. J. Smith, A. F. Molisch, F. Tufvesson, and S. H. Simon, "Polarized MIMO channels in 3-D: Models, measurements and mutual information," *IEEE Journal on Selected Areas in Communications*, vol. 24, pp. 514–527, 2006.

[54] F. Quitin, C. Oestges, F. Horlin, and P. De Doncker, "Analytical model and experimental validation of cross polar ratio in polarized MIMO channels," in *Proc. IEEE 19th Int. Symp. Personal, Indoor and Mobile Radio Communications (PIMRC'08)*, 2008, pp. 1–5.

[55] V. R. Anreddy and M. A. Ingram, "Capacity of measured Ricean and Rayleigh indoor MIMO channels at 2.4 GHz with polarization and spatial diversity," in *Proc. IEEE Wireless Communications and Networking Conf. (WCNC'06) 2006*, vol. 2, 2006, pp. 946–951.

[56] L. Jiang, L. Thiele, and V. Jungnickel, "Polarization rotation evaluation for macrocell MIMO channel," in *Proc. 6th Int. Symp. Wireless Communication Systems (ISWCS'09) 2009*, 2009, pp. 21–25.

[57] V. R. Anreddy and M. A. Ingram, "Antenna selection for compact dual-polarized MIMO systems with linear receivers," in *Proc. IEEE Global Telecommunications Conf. GLOBECOM '06*, 2006, pp. 1–6.

[58] S.-Y. Lee and C. Mun, "Transmit antenna selection of dual polarized MIMO systems applying SCM," in *Proc. VTC-2006 Fall Vehicular Technology Conf. 2006 IEEE 64th*, 2006, pp. 1–5.

[59] J. F. Valenzuela-Valdes, M. A. Garcia-Fernandez, A. M. Martinez-Gonzalez, and D. Sanchez-Hernandez, "The role of polarization diversity for MIMO systems under Rayleigh-fading environments," *IEEE Antennas and Wireless Propagation Letters*, vol. 5, no. 1, pp. 534–536, 2006.

[60] J. F. Valenzuela-Valdes, A. M. Martinez-Gonzalez, and D. Sanchez-Hernandez, "Estimating combined correlation functions for dipoles in Rayleigh-fading scenarios," *IEEE Antennas and Wireless Propagation Letters*, vol. 6, pp. 349–352, 2007.

[61] J. F. Valenzuela-Valdes, A. M. Martinez-Gonzalez, and D. A. Sanchez-Hernandez, "Accurate estimation of correlation and capacity for hybrid spatial-angular MIMO systems," *IEEE Transactions on Vehicular Technology*, vol. 58, no. 8, pp. 4036–4045, 2009.

[62] D. G. Landon and C. M. Furse, "Recovering handset diversity and MIMO capacity with polarization-agile antennas," *IEEE Transactions on Antennas and Propagation*, vol. 55, no. 11, pp. 3333–3340, 2007.

[63] X. Li and Z.-P. Nie, "Effect of array orientation on performance of MIMO wireless channels," *Antennas and Wireless Propagation Letters, IEEE*, vol. 3, pp. 368–371, 2004.

[64] A. Pal, B. S. Lee, P. Rogers, G. Hilton, M. Beach, and A. Nix, "Effect of antenna element properties and array orientation on performance of MIMO systems," in *Proc. 1st Int Wireless Communication Systems Symp*, 2004, pp. 120–124.

[65] C. Waldschmidt, C. Kuhnert, S. Schulteis, and W. Wiesbeck, "Compact MIMO arrays based on polarization-diversity," in *Proc. IEEE Antennas and Propagation Society Int. Symp*, vol. 2, 2003, pp. 499–502.

[66] T. Svantesson, "On capacity and correlation of multi-antenna systems employing multiple polarizations," in *Proc. IEEE Antennas and Propagation Society Int. Symp*, vol. 3, 2002.

[67] R. Bhagavatula, C. Oestges, and R. W. Heath, "A new double-directional channel model including antenna patterns, array orientation, and depolarization," *IEEE Transactions on Vehicular Technology*, vol. 59, no. 5, pp. 2219–2231, 2010.

[68] H. Li, G. Zhaozhi, M. Junfei, J. Ze, L. ShuRong, and Z. Zheng, "Analysis of mutual coupling effects on channel capacity of MIMO systems," in *Proc. IEEE Int. Conf. Networking, Sensing and Control ICNSC 2008*, 2008, pp. 592–595.

[69] A. Habib, C. Mehlführer, and M. Rupp, "Receive antenna selection for polarized antennas," in *Proceedings of 18th IEEE International Conference on Systems, Signals and Image Processing*, Sarajevo, Bosnia, June 2011.

[70] R. S. Elliott, *Antenna theory and design.* Wiley, 2003.

[71] J. Kraus and R. Marhefka, *Antenna: For all Applications*, 3rd, Ed. The Mc Graw Hill Companies, 2006.

[72] V. Dehghanian, J. Nielsen, and G. Lachapelle, "Combined spatial-polarization correlation function for indoor multipath environments," *IEEE Antennas and Wireless Propagation Letters*, vol. 9, pp. 950–953, 2010.

[73] J. Zhao, Y. Li, and G. Sun, "Analysis of antenna mutual coupling in the X-type polarization diversity system," in *Proc. 5th Int. Conf. Wireless Communications, Networking and Mobile Computing WiCom '09*, 2009, pp. 1–4.

[74] S. Lu, H. T. Hui, and M. Bialkowski, "Optimizing MIMO channel capacities under the influence of antenna mutual coupling," *IEEE Antennas and Wireless Propagation Letters*, vol. 7, pp. 287–290, 2008.

[75] J. Sahaya, K. Raj, and C. Poongodi, "Echelon, collinear, H-shaped and V-shaped dipole arrays for MIMO systems," in *Proc. Asia-Pacific Microwave Conf. APMC 2007*, 2007, pp. 1–4.

[76] C. Poongodi, K. Dineshkumar, D. Deenadhayalan, and A. Shanmugam, "Capacity of echelon, H-shaped, V-shaped and printed dipole arrays in MIMO system," in *Proc. Int Communications and Signal Processing (ICCSP) Conf*, 2011, pp. 100–104.

[77] J. Zhao, Y. Li, and G. Sun, "The effect of mutual coupling on capacity of 4-element squared antenna array MIMO systems," in *Proc. 5th Int. Conf. Wireless Communications, Networking and Mobile Computing WiCom '09*, 2009, pp. 1–.

[78] S. Durrani and M. E. Bialkowski, "Effect of mutual coupling on the interference rejection capabilities of linear and circular arrays in CDMA systems," *IEEE Transactions on Antennas and Propagation*, vol. 52, no. 4, pp. 1130–1134, 2004.

[79] R. Fallahi and M. Roshandel, "Investigation of mutual coupling effect on the interference rejection capability of linear patch array in CDMA systems," in *Proc. Int Microwave, Antenna, Propagation and EMC Technologies for Wireless Communications Symp*, 2007, pp. 205–208.

[80] A. Gorokhov, "Capacity of multiple-antenna Rayleigh channel with a limited transmit diversity," in *Proc. IEEE Int Information Theory Symp*, 2000.

[81] Z. Xu, S. Sfar, and R. Blum, "Receive antenna selection for closely-spaced antennas with mutual coupling," *IEEE Transactions on Wireless Communications*, vol. 9, no. 2, pp. 652–661, 2010.

[82] Y. Yang, S. Sfar, and R. S. Blum, "A simulation study of antenna selection for compact MIMO arrays," in *Proc. 42nd Annual Conf. Information Sciences and Systems CISS 2008*, 2008, pp. 57–61.

[83] D. Lu, D. K. C. So, and A. K. Brown, "Receive antenna selection scheme for V-BLAST with mutual coupling in correlated channels," in *Proc. IEEE 19th Int. Symp. Personal, Indoor and Mobile Radio Communications PIMRC 2008*, 2008, pp. 1–5.

[84] L. Dai, S. Sfar, and K. B. Letaief, "Optimal antenna selection based on capacity maximization for MIMO systems in correlated channels," *IEEE Transactions on Communications*, vol. 54, no. 3, pp. 563–573, 2006.

[85] A. Habib, C. Mehlführer, and M. Rupp, "Performance of compact antenna arrays with receive selection," in *Proceedings of 7th IEEE International Conference on Wireless Advanced 2011*, London, U.K, June 2011.

[86] J.-S. Jiang and M. A. Ingram, "Spherical-wave model for short-range MIMO," *IEEE Journal on Selected Areas in Communications*, vol. 53, no. 9, pp. 1534–1541, 2005.

[87] C.-Y. Chiu, J.-B. Yan, and R. D. Murch, "Compact three-port orthogonally polarized MIMO antennas," *IEEE Antennas and Wireless Propagation Letters*, vol. 6, pp. 619–622, 2007.

[88] G. Gupta, B. Hughes, and G. Lazzi, "On the degrees of freedom in linear array systems with tri-polarized antennas," *IEEE Transactions on Wireless Communications*, vol. 7, no. 7, pp. 2458–2462, 2008.

[89] V. Erceg, P. Soma, D. S. Baum, and S. Catreux, "Multiple-input multiple-output fixed wireless radio channel measurements and modeling using dual-polarized antennas at 2.5 GHz," *IEEE Transactions on Wireless Communications*, vol. 3, no. 6, pp. 2288–2298, 2004.

[90] F. Quitin, F. Bellens, A. Panahandeh, J.-M. Dricot, F. Dossin, F. Horlin, C. Oestges, and P. De Doncker, "A time-variant statistical channel model for tri-polarized antenna systems," in *Proc. IEEE 21st Int Personal Indoor and Mobile Radio Communications (PIMRC'10) Symp*, 2010, pp. 64–69.

[91] P. Kyritsi and D. C. Cox, "Propagation characteristics of horizontally and vertically polarized electric fields in an indoor environment: Simple model and results," in *Proc. VTC 2001 Fall Vehicular Technology Conf. IEEE VTS 54th*, vol. 3, 2001, pp. 1422–1426.

[92] X. Zhao, S. Geng, L. Vuokko, J. Kivinen, and P. Vainikainen, "Polarization behaviours at 2, 5 and 60 GHz for indoor mobile communications," *Wireless Personal Communications*, vol. 27, pp. 99–115, 2003.

[93] A. J. Paulraj, R. Nabar, and D. A. Gore, *Introduction to Space-Time Wireless Communications*, 2nd ed. Cambridge University Press, 2003.

[94] C. Oestges, "Channel correlations and capacity metrics in mimo dual-polarized rayleigh and ricean channels," in *Vehicular Technology Conference, 2004. VTC2004-Fall. 2004 IEEE 60th*, vol. 2, sept. 2004, pp. 1453 – 1457 Vol. 2.

[95] D. Hammarwall, M. Bengtsson, and B. Ottersten, "Acquiring partial CSI for spatially selective transmission by instantaneous channel norm feedback," *IEEE Transactions on Signal Processing*, vol. 56, no. 3, pp. 1188–1204, 2008.

[96] L. H. Ozarow, S. Shamai, and A. D. Wyner, "Information theoretic considerations for cellular mobile radio," *IEEE Transactions on Vehicular Technology*, vol. 43, no. 2, pp. 359–378, 1994.

[97] Y.-C. Ko, M.-S. Alouini, and M. K. Simon, "Outage probability of diversity systems over generalized fading channels," *IEEE Transactions on Communications*, vol. 48, no. 11, pp. 1783–1787, 2000.

[98] N. Balakrishnan and A. Cohen, *Order Statistics and Inference: Estimation Methods*, 2nd ed. Academic Press Inc., 1991.

[99] S. M. Alamouti, "A simple transmit diversity technique for wireless communications," *IEEE Journal on Selected Areas in Communications*, vol. 16, no. 8, pp. 1451–1458, 1998.

[100] V. Tarokh, N. Seshadri, and A. R. Calderbank, "Space-time codes for high data rate wireless communication: performance criterion and code construction," *IEEE Transactions on Information Theory*, vol. 44, no. 2, pp. 744–765, 1998.

[101] G. J. Foschini, "Layered space-time architecture for wireless communication in a fading environment when using multi-element antennas," *Bell Labs Technical Journal*, vol. 1, p. 4159, 1996.

[102] R. U. Nabar, H. Bolcskei, V. Erceg, D. Gesbert, and A. J. Paulraj, "Performance of multiantenna signaling techniques in the presence of polarization diversity," *IEEE Transactions on Signal Processing*, vol. 50, no. 10, pp. 2553–2562, 2002.

[103] A. Habib, "Multiple polarized MIMO with antenna selection," in *18th IEEE Symposium on Communications and Vehicular Technology (SCVT'11), Belgium, Nov. 2011*.

[104] D. S. Baum, D. Gore, R. Nabar, S. Panchanathan, K. V. S. Hari, V. Erceg, and A. J. Paulraj, "Measurement and characterization of broadband MIMO fixed wireless channels at 2.5 GHz," in *Proc. IEEE Int Personal Wireless Communications Conf*, 2000, pp. 203–206.

[105] V. Tarokh, H. Jafarkhani, and A. R. Calderbank, "Space-time block coding for wireless communications: performance results," *IEEE Journal on Selected Areas in Communications*, vol. 17, no. 3, pp. 451–460, 1999.

[106] F. Kharrat-Kammoun, S. Fontenelle, S. Rouquette, and J. J. Boutros, "Antenna selection for MIMO systems based on an accurate approximation of QAM error probability," in *Proc. IEEE 61st Vehicular Technology Conf. (VTC Spring'05)*, vol. 1, 2005, pp. 206–210.

[107] F. Sun, J. Liu, H. Xu, and P. Lan, "Receive antenna selection using convex optimization for MIMO systems," in *Proc. Third Int. Conf. Communications and Networking in China (ChinaCom'08)*, 2008, pp. 426–430.

[108] G. Zhang, L. Tian, and L. Peng, "Fast antenna subset selection for MIMO wireless systems," in *Proc. Punta del Este Information Theory Workshop (ITW '06)*, 2006, pp. 493–496.

[109] A. Dua, K. Medepalli, and A. J. Paulraj, "Receive antenna selection in MIMO systems using convex optimization," *IEEE Transactions on Wireless Communications*, vol. 5, no. 9, pp. 2353–2357, 2006.

[110] K. T. Phan and C. Tellambura, "Receive antenna selection based on union-bound minimization using convex optimization," *IEEE Signal Processing Letters*, vol. 14, no. 9, pp. 609–612, 2007.

[111] ——, "Receive antenna selection for spatial multiplexing systems based on union-bound minimization," in *Proc. IEEE Wireless Communications and Networking Conf. (WCNC'07)*, 2007, pp. 1286–1289.

[112] T. W. C. Brown, S. R. Saunders, and B. G. Evans, "Analysis of mobile terminal diversity antennas," *IEE Proceedings -Microwaves, Antennas and Propagation*, vol. 152, no. 1, pp. 1–6, 2005.

[113] S. Boyd and L. Vandenberghe, *Convex Optimization.* Cambridge University Press, 2004.

[114] Y. Nesterov and A. Nemirovsky, "Interior-point polynomial methods in convex programming," *Studies in Applied Mathematics*, vol. 13, 1994.

[115] M. Grant and S. Boyd, "CVX: Matlab software for disciplined convex programming, version 1.21," http://cvxr.com/cvx, Apr. 2011.

[116] R. Bains and R. R. Muller, "Using parasitic elements for implementing the rotating antenna for MIMO receivers," *IEEE Transactions on Wireless Communications*, vol. 7, no. 11, pp. 4522–4533, 2008.

[117] F. Quitin, C. Oestges, F. Horlin, and P. De Doncker, "Multipolarized MIMO channel characteristics: Analytical study and experimental results," *IEEE Transactions on Antennas and Propagation*, vol. 57, no. 9, pp. 2739–2745, 2009.

[118] H. Asplund, J.-E. Berg, F. Harrysson, J. Medbo, and M. Riback, "Propagation characteristics of polarized radio waves in cellular communications," in *Proc. 66th Fall Vehicular Technology Conf. (VTC Fall'07)*, 2007, pp. 839–843.

[119] A. Habib, B. Krasniqi, and M. Rupp, "Antenna selection in polarization diverse MIMO transmissions with convex optimization," in *18th IEEE Symposium on Communications and Vehicular Technology (SCVT'11), Belgium, Nov. 2011*.